Struct Bond (2012) 144: 43–104
DOI: 10.1007/430_2011_65

Published online: 3 March 2012

Second-Order Nonlinear Optical Materials Based on Metal Iodates, Selenites, and Tellurites

Fang Kong, Chuan-Fu Sun, Bing-Ping Yang, and Jiang-Gao Mao

Abstract In this chapter, the syntheses, structures, and Second Harmonic Generation (SHG) properties of metal iodates, selenites, and tellurites all of which contain a lone pair cation in an asymmetric coordination geometry were reviewed. A second asymmetric building unit such as distorted octahedra of the d^0 transition-metal (TM) cations such as V^{5+}, Mo^{6+}, other cations with a stereochemically active lone pair such as Pb^{2+} and Bi^{3+}, and tetrahedral groups such as BO_4^{5-} and PO_4^{3-}, can be introduced into metal iodates, selenites, and tellurites. The combination of d^0 transition-metal cations with the iodate groups afforded a large number of new metal iodates, a number of which display excellent SHG properties due to the additive effects of polarizations from both types of the asymmetric units. Introducing other lone-pair cations such as Pb^{2+} and Bi^{3+} into the metal iodates is also an effective strategy to design new SHG materials. With respect to the metal selenite or tellurite systems, many compounds in the alkali or alkaline earth-d^0 TM–Se(IV)/Te(IV)–O systems can also exhibit excellent SHG properties due to the additive effects of polarizations from both types of asymmetric units. Lanthanide or posttransition metal main group element-d^0 TM–Se(IV)/Te(IV)–O compounds are usually structurally centrosymmetric and not SHG active, but they can also display abundant structural diversities and interesting magnetic or luminescent properties. Metal tellurites and selenites containing tetrahedral groups of the main group elements such as BO_4 and PO_4 may also form NCS structures with excellent SHG properties.

F. Kong, C.-F. Sun, B.-P. Yang, and J.-G. Mao (✉)
State Key Laboratory of Structural Chemistry, Fujian Institute of Research on the Structure of Matter, Chinese Academy of Sciences, Fuzhou 350002, People's Republic of China
e-mail: mjg@fjirsm.ac.cn

Keywords Iodates · Lone pairs · Noncentrosymmetric structures · Second harmonic generation · Selenites · Tellurites

Contents

1 Introduction

The search for new Second Harmonic Generation (SHG) or Second-Order Non-Linear Optical (NLO) materials is of current interest and great importance due to their applications in photonic technologies, such as laser frequency conversion, optical parameter oscillator (OPO), and signal communication [1–4]. At present, the most widely used and commercially manufactured such materials are mainly inorganic materials based on borates such as α-BaB_2O_4 (BBO) and LiB_3O_5 (LBO), phosphates such as KH_2PO_4 (KDP) and $KTiOPO_4$ (KTP), niobates such as $LiNbO_3$, iodates such as $LiIO_3$, and metal chalcogenides such as $AgGaS_2$ and $AgGaSe_2$ [5–10]. As we all know, an important prerequisite for a material to be SHG active is that it should be structurally noncentrosymmetric (NCS). In inorganic materials, the macroscopic acentricity is often a manifestation of the asymmetric coordination environments of the cations. The above four types of most widely used inorganic NLO oxides contain four different types of asymmetric units that are responsible for their NCS structures: π-conjugated planar (e.g., BO_3^{3-}) [10–12], rigid tetrahedral groups (e.g., PO_4^{3-}, BO_4^{5-}, BeO_4^{4-}) [13–15], d^0 transition-metal (TM) cations in an octahedral geometry (e.g., Nb^{5+}, V^{5+}, Mo^{6+}) [16, 17], and cations with a stereochemically active lone pair (e.g., SeO_3^{2-}, IO_3^{3-}, Pb^{2+}, Bi^{3+}) [18–21]. The last two types of cations are both susceptible to Second-Order Jahn–Teller (SOJT) distortion which will be discussed in more details later. During the early days, lots of efforts have been made to explore Second-Order NLO materials just containing one type of asymmetric building unit. Such compounds often exhibit simple structural features, which allow us to synthesize and grow large their single crystals easily. However, with the fast developments of the science and technique, they also

have various shortcomings. Firstly, the possibilities to discover new SHG materials in such systems are rather limited. Furthermore, many of the NLO materials that are in current use still have shortcomings of one kind or another and improvements should be made. For example, KDP shows a low SHG effect and it is also very moisture sensitive, and it is still a great challenge to grow high-quality large-single crystals of $KBe_2BO_3F_2$ (KBBF) [22]. Therefore, searching for better SHG materials is still a hot research topic and a great challenge. It has been demonstrated that the combination of two or more types of asymmetric inorganic building units into a same compound is an effective synthetic route for new inorganic solids with excellent SHG properties if polarizations of those asymmetric units can be properly aligned [15, 17].

SOJT distortion is a very important concept in second order NLO materials, it occurs in two different types of cations: d^0 transition metals (Mo^{6+}, W^{6+}, etc) in an octahedral coordination geometry and cations with stereoactive lone pairs (I^{5+}, Se^{4+}, Te^{4+}, etc). The d^0 transition metal cation can be distorted toward either a face (local C_3 direction), an edge (local C_2 direction), or a corner (local C_4 direction) of the MO_6 octahedron [7]. The situation with the lone-pair cations is more complex. The structural distortion and polarization was thought to be through the mixing of the metal cation *s* and *p* orbitals. Recently, it is believed that the oxide anion also plays an important role in the lone-pair formation. The interaction of the *s* and *p* orbitals of the metal cation with the oxide anion *p* states is critical for lone-pair formation. No matter how the lone pair is created, its structural consequences are profound, as the lone pair "pushes" the oxide ligands toward one side of the cation, resulting in a highly asymmetric coordination environment [14].

Metal iodates are one class of very important materials [18–20]. Many of them such as α-$LiIO_3$ [10] and α-$Cs_2I_4O_{11}$ [19], have been reported to be promising new SHG materials with wide transparent wavelength regions, large SHG coefficients and high optical-damage thresholds as well as high thermal stabilities. Furthermore, it is reported when iodate anion is combined with a transition metal ion with d^0 electronic configuration such as Mo^{6+} and W^{6+}, the chances to obtain materials with noncentrosymmetric structures and excellent SHG properties can be greatly increased due to the "constructive" addition of the polarizations from both types of asymmetric units [23–30].

Likewise, metal selenites and tellurites are also able to form a diversity of unusual structures because of the presence of the stereochemically active lone-pair electrons which could serve as a structure-directing agent [13, 14]. The asymmetric coordination polyhedron of the Se(IV) or Te(IV) atom caused by the so-called SOJT distortion may also result in noncentrosymmetric (NCS) structures with consequent interesting physical properties, such as SHG. Transition metal ions with d^0 electronic configuration such as V^{5+}, W^{6+}, Mo^{6+}, etc. have been also introduced into the selenite or tellurite systems to obtain new SHG materials by means of the additive polarizations of both types of bonds [31–33]. Most of these research efforts have been focused on alkali, alkaline earth, and NH_4^+ compounds which show potential application in SHG materials because of their broad

Table 1 Metal iodates with NCS structures and SHG properties

Compounds	Space group	SHG efficiency	Ref.
α-HIO_3	$P2_12_12_1$	300 × α-SiO_2	[19]
α-$LiIO_3$	$P6_3$	300 × α-SiO_2	[19, 20]
NaI_3O_8	$P\bar{4}$	300 × α-SiO_2	[10]
$Cs_2I_4O_{11}$	$P6_3$	300 × α-SiO_2	[19]
$La(IO_3)_3$	Cc	400 × α-SiO_2	[42]
$NaY(IO_3)_4$	Cc	300 × α-SiO_2	[42]
$K_2Zn(IO_3)_4(H_2O)_2$	$I2$	2.3 × KDP	[43]
$K_2Mg(IO_3)_4(H_2O)_2$	$I2$	1.4 × KDP	[43]
$K_2Co(IO_3)_4(H_2O)_2$	$I2$	0.3 × KDP	[43]
α-$K_3In(IO_3)_6$	$Fdd2$	1 × KDP	[44]
$BaPd(IO_3)_4$	$P1$	0.4 × KTP	[45]
$La_3Pb_3(IO_3)_{13}(\mu^3$-O)	$R3c$	2 × KDP	[46]
$Pr_3Pb_3(IO_3)_{13}(\mu^3$-O)	$R3c$	1 × KDP	[46]
$Nd_3Pb_3(IO_3)_{13}(\mu^3$-O)	$R3c$	0.8 × KDP	[46]
$Li_2Ti(IO_3)_6$	$P6_3$	500 × α-SiO_2	[26]
$Na_2Ti(IO_3)_6$	$P6_3$	400 × α-SiO_2	[27]
$NaVO_2(IO_3)_2(H_2O)$	$P2_1$	20 × KDP	[29]
$K(VO)_2O_2(IO_3)_3$	$Ima2$	3.6 × KTP	[30]
$LaVO_2(IO_3)_4{\cdot}H_2O$	$P2_1$	0.2 × KDP	[47]
$Cs(VO)_2O_2(IO_3)_3$	$Ima2$	500 × α-SiO_2	[24]
$BaNbO(IO_3)_5$	Cc	14 × KDP	[28]
$ThCrO_4(IO_3)_2$	$P2_12_12_1$	1 × α-SiO_2	[48]
$LiMoO_3(IO_3)$	$P2_1$	4 × KDP	[49]
$RbMoO_3(IO_3)$	$Pna2_1$	400 × α-SiO_2	[23]
$CsMoO_3(IO_3)$	$Pna2_1$	400 × α-SiO_2	[23]
$NdMoO_2(OH)(IO_3)_4$	$P2_1$	350 × α-SiO_2	[25]

transparency range and high transmittance in the ultraviolet and visible region [34–39]. Recently, similar phases of transition metal as well as the posttransition metal main group cations have also been prepared [40, 41]. Furthermore, boroselenites which contain both borate anion and selenium(IV) with a lone pair may also possess good SHG properties due to the presence of two types of SHG active groups. So far, such compounds are still rather scarce and $B_2Se_2O_7$ prepared by our group represents the only example. Its structure is built from B_2O_7 dimers composed of two corner-sharing BO_4 tetrahedra and SeO_3^{2-} groups. It exhibits a SHG efficiency of about 2.3 times that of KDP [13].

Our group and others have been exploring new NCS compounds in these systems during the past few years (Tables 1 and 2). In this chapter, our discussions will be mainly focused on metal iodates, selenites, or tellurites that contain d^0 transition metal (TM) ions; or additional lone-pair cations such as Pb^{2+}, Bi^{3+} etc, or tetrahedral groups of main group elements such as GeO_4 and PO_4. A brief description of some ternary compounds that exhibit SHG response will also be given when necessary. The discussions on metal selenites and tellurites will be mainly focused on those reported after 2008 since we had reviewed them in 2008 [14].

Table 2 Metal selenites or tellurites show NCS structures and SHG properties

Compounds	Space group	SHG efficiency	Ref.
TeO_2	$P4_12_12$	5 × α-SiO_2	[32]
Te_2O_5	$P2_1$	400 × α-SiO_2	[32]
$TeSeO_4$	Ia	400 × α-SiO_2	[31, 32]
Te_2SeO_7	$Pmn2_1$	200 × α-SiO_2	[32]
Bi_2TeO_5	$Abm2$	300 × α-SiO_2	[33]
$K(VO_2)_3(SeO_3)_2$	$P6_3$	45 × α-SiO_2	[50]
$Tl(VO_2)_3(SeO_3)_2$	$P6_3$	50 × α-SiO_2	[51]
$A(VO_2)_3(SeO_3)_2$(A = NH_4, Rb, Cs)	$P6_3$	40 × α-SiO_2	[50, 51]
$Cs(VO_2)_3(TeO_3)_2$	$P6_3$	40 × α-SiO_2	[50, 52]
$Rb_2(MoO_3)_3(SeO_3)$	$P6_3$	300 × α-SiO_2	[50]
$Cs_2(MoO_3)_3(SeO_3)$	$P6_3$	350 × α-SiO_2	[53]
$Tl_2(MoO_3)_3(SeO_3)$	$P31c$	400 × α-SiO_2	[50]
$(NH_4)_2(MoO_3)_3(SeO_3)$	$P6_3$	400 × α-SiO_2	[53]
$A_2(MoO_3)_3(TeO_3)$ (A = NH_4, Cs)	$P6_3$	400 × α-SiO_2	[54]
$A_2(WO_3)_3(SeO_3)$ (A = NH_4, Cs)	$P6_3$	200 × α-SiO_2	[55]
$Rb_2W_3TeO_{12}$	$P31c$	200 × α-SiO_2	[56]
$Cs_2W_3TeO_{12}$	$P6_3$	400 × α-SiO_2	[56]
$Na_2Mo_3Te_3O_{16}$	$I2$	500 × α-SiO_2	[57]
$Ag_2Mo_3Te_3O_{16}$	$I2$	8.0 × KDP	[58]
$(NH_4)_2WTe_2O_8$	$P2_1$	250 × α-SiO_2	[59]
Na_2MoSeO_6	$P2_13$	10 × α-SiO_2	[60]
$Na_2W_2TeO_9$	Ia	500 × α-SiO_2	[39]
$BaMo_2TeO_9$	$P2_1$	600 × α-SiO_2	[34]
BaW_2TeO_9	$P2_1$	500 × α-SiO_2	[34]
$Cd_4V_2Te_3O_{15}$	$P2_12_12_1$	1.4 × KDP	[61]
$Zn_2(MoO_4)(SeO_3)$	$P2_1$	100 × α-SiO_2	[62]
$Zn_2(MoO_4)(TeO_3)$	$P2_1$	80 × α-SiO_2	[62]
$TlSeVO_5$	$Pna2_1$	40 × α-SiO_2	[63]
$TlTeVO_5$	$Pna2_1$	40 × α-SiO_2	[63]
$InVSe_2O_8$	Pm	30 × α-SiO_2	[64]
$Te_2O(PO_4)_2$	Cc	50 × α-SiO_2	[65]
$Mn(MoO_3)(SeO_3)(H_2O)$	$Pmc2_1$	3.0 × KDP	[66]
α-$Ga_2(TeO_3)_3$	I-43d	1.0 × KDP	[67]
$B_2Se_2O_7$	$P2_12_12_1$	2.2 × KDP	[13]

2 Metal Iodates Containing d^0 Transition Metal Ions or Other Lone-Pair Cations

Metal iodates are a very important class of SHG materials. Even simple alkali metal iodates such as $LiIO_3$, have become standard materials exploited for laser frequency-doubling applications [10]. Metal iodates that display SHG properties are listed in Table 1. In this section, our discussion will be focused on two systems: combination of d^0 transition metal (TM) ions or other lone pair-containing cations with iodate anions.

Metal iodates containing IIIA group elements such as In(III) and divalent metal ions such as Pd^{2+}, Mn^{2+}, Co^{2+}, Zn^{2+}, and Mg^{2+} will also be described.

2.1 Combination of d^0 Transition Metal Ions with Iodate Group

A large number of compounds with abundant structural types have been reported in this system, many of which exhibit excellent SHG properties (Table 1). The transition metals with d^0 electronic configuration are mostly Mo(VI) and V(V) ions but there are also some examples involving Ti(IV), Zr(IV), Nb(V) and Cr(VI). The counterions include alkali(I), alkaline earth(II), lanthanide(III), and silver(I).

2.1.1 Mo(VI)–I(V)–O System

Such types of compounds are dominantly alkali(I) and silver(I) compounds but some alkaline earth(II) and lanthanide(III) compounds are also reported. Studies revealed that the ionic size of the counterions has also a great influence on the compositions, structures, and SHG properties of the materials formed.

Eight compounds, namely, $A_2MoO_2(IO_3)_4$ ($A = K^+$, Ag^+), $Rb_2Mo(IO_3)_6$, α- and β-$KMoO_3(IO_3)$, $LiMoO_3(IO_3)$ and $AMoO_3(IO_3)$ ($A = Rb^+$, Cs^+) were reported in A(I)–Mo(VI)–I(V)–O systems [23, 49, 68–70]. They exhibit six different structural types.

Colorless rhombohedra $K_2MoO_2(IO_3)_4$ crystals were obtained by hydrothermal reactions of MoO_3 (0.731 mmol), KIO_4 (1.46 mmol), NH_4Cl (1.10 mmol), and 1 mL H_2O at 180°C. $Ag_2MoO_2(IO_3)_4$ was synthesized by heating a mixture of $AgNO_3$ (1.0 mmol), MoO_3 (0.50 mmol), I_2O_5 (3.0 mmol), and 2 mL H_2O at 200°C. $A_2MoO_2(IO_3)_4$ ($A = Ag^+$, K^+) are isostructural and crystallized in the centrosymmetric (CS) space group *C*2/c [68, 69]. Their structures exhibit a zero-dimensional (0D) $[MoO_2(IO_3)_4]^{2-}$ anionic unit consisting of a Mo^{6+} cation bonded to two terminal oxo and four iodate anions, with the K^+ or Ag^+ cations acting as spacers to keep charge balance.

Orange rhombohedral crystals of $Rb_2Mo(IO_3)_6$ were prepared by hydrothermal reactions of MoO_3 (0.597 mmol), H_5IO_6 (1.202 mmol), Rb_2CO_3 (0.602 mmol), and 1 mL H_2O at 200°C. Its structure (*R*-3, CS) exhibits a 0D $[Mo(IO_3)_6]^{2-}$ anionic unit consisting of a nondistorted d^0-TM cation linked to six IO_3^- anions. These 0D anionic units are separated by the Rb^+ cations [70].

Colorless rods of β-$KMoO_3(IO_3)$ were obtained in a similar method to that of $K_2MoO_2(IO_3)_4$ by using more amount of MoO_3 [69]. Crystals of α-$KMoO_3(IO_3)$, $AMoO_3(IO_3)$ ($A = Rb^+$, Cs^+) can be produced in high yield with a 1:2 molar ratio of MoO_3:AIO_4 (A = K, Rb, Cs) in the absence of NH_4Cl [23]. Very pale yellow plate-like crystals of $LiMoO_3(IO_3)$ were synthesized by heating a mixture of MoO_3

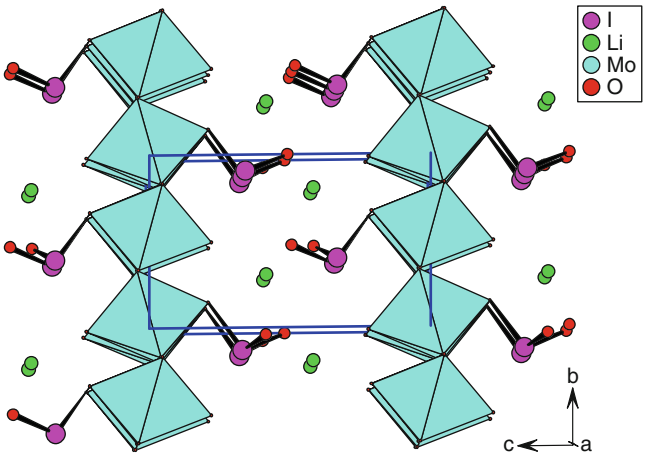

Fig. 1 View of the structure of $LiMoO_3(IO_3)$ along the *a*-axis

(2.529 mmol), H_5IO_6 (2.518 mmol), Li_2CO_3 (1.245 mmol), and 2 mL H_2O at 170°C [49]. Although α-$KMoO_3(IO_3)$, β-$KMoO_3(IO_3)$, $LiMoO_3(IO_3)$, and $AMoO_3(IO_3)$ ($A = Rb^+$, Cs^+) have a similar chemical formula, their structures are totally different. α-$KMoO_3(IO_3)$ (*P*bca) and β-$KMoO_3(IO_3)$ ($P2_1/n$) are centrosymmetric. Their structures exhibit a similar 2D $[MoO_3(IO_3)]^-$ anionic layer composed of the 1D chains of corner sharing MoO_6 octahedra further bridged by the iodate anions. The K^+ cations are located at the interlayer region to maintain the charge balance. The difference between these two compounds is that the $[MoO_3(IO_3)]^-$ layers in the α-phase are corrugated whereas those in the β-phase are regular.

$LiMoO_3(IO_3)$ [49] and $AMoO_3(IO_3)$ ($A = Rb^+$, Cs^+) [23] are NCS and SHG-active. $LiMoO_3(IO_3)$ ($P2_1$, NCS) exhibits a layered structure composed of $[MoO_3(IO_3)]^-$ anionic layers that are separated by Li^+ cations. Such a $[MoO_3(IO_3)]^-$ layer is totally different from those described above. Within the layer, the MoO_6 octahedra are interconnected into a WO_3-type sheet via corner-sharing with quadrangular windows along *c*-axis. The unidentate IO_3 groups are appended on both sides of the 2D layer (Fig. 1). Each Mo^{6+} cation undergoes intraoctahedral distortion toward a face (local C_3 direction), resulting in three short and three long Mo–O bonds, but the polarizations from neighboring MoO_6 octahedra are partially cancelled out. The large dipole moment of the compound is produced by IO_3^- groups because all of the lone pairs of the iodate groups are almost aligned in the same direction. SHG measurements revealed that $LiMoO_3(IO_3)$ shows a large SHG response of about 4×KDP [49].

$AMoO_3(IO_3)$ ($A = Rb^+$, Cs^+) are isostructural and crystallized in the polar space group $Pna2_1$. Their structures feature a three-dimensional (3D) network composed of 1D chains of corner-sharing MoO_6 octahedra that are bridged by iodate groups with the Rb^+ or Cs^+ cations filling in the voids of the structure and keeping charge

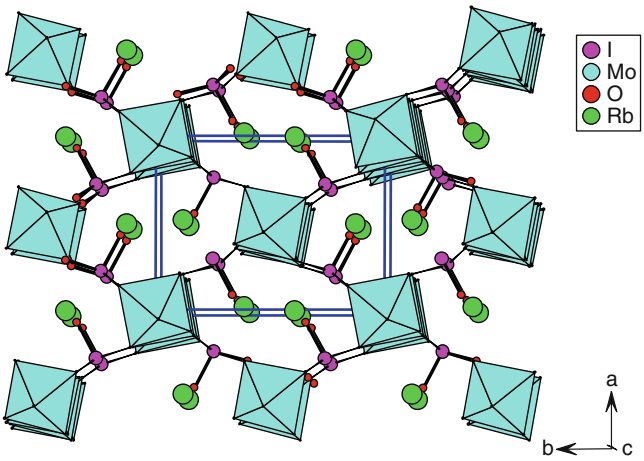

Fig. 2 View of the structure of $RbMoO_3(IO_3)$ along the *a*-axis

balance (Fig. 2). Each Mo^{6+} cation is octahedrally coordinated by two bridging and two terminal oxoanions as well as two unidentate iodate groups, displaying two short, two long, and two normal Mo–O bonds. Therefore the MoO_6 octahedron is distorted toward an edge (local C_2 direction). The polarizations of neighboring MoO_6 octahedra are partially cancelled out whereas those of the iodate groups are almost aligned along the *c*-axis to produce a large net dipole moment. SHG measurements reveal that $AMoO_3(IO_3)$ ($A = Rb^+$, Cs^+) display strong SHG responses of about 400 × α-SiO_2 and they are phase-matchable [23].

Only two alkaline earth molybdenum(VI) iodates were reported, namely, $BaMoO_2(IO_3)_4(H_2O)$ and $Ba(MoO_2)_6(IO_4)_2O_4(H_2O)$ [71, 72]. $BaMoO_2(IO_3)_4(H_2O)$ was synthesized by hydrothermal reactions of a mixture of $Ba(OH)_2{\cdot}8H_2O$ (1.58 mmol), MoO_3 (3.47 mmol), and HIO_3 (28.4 mmol) in 10 mL of H_2O at 230°C whereas $Ba(MoO_2)_6(IO_4)_2O_4(H_2O)$ was obtained by reactions of a mixture of MoO_3 (0.599 mmol) and BaH_3IO_6 (0.371 mmol) in 1 mL H_2O at 180°C. Both of them crystallized in centrosymmetric space groups. $BaMoO_2(IO_3)_4(H_2O)$ ($P2_1/n$, CS) exhibits a 0D $[MoO_2(IO_3)_4]^{2-}$ anionic unit consisting of a Mo^{6+} cation linked to four IO_3^- groups and two terminal oxoanions, such anionic units are separated by water molecules and Ba^{2+} cations. The structure of $Ba(MoO_2)_6(IO_4)_2O_4(H_2O)$ ($C2/c$, CS) consists of 2D $[(MoO_2)_3(IO_4)O_2]^-$ layers that are separated by Ba^{2+} cations and water molecules. There are three crystallographically unique Mo(VI) and one unique I(V) atoms in its asymmetric unit. Two $Mo(1)O_6$ octahedra form a $[Mo(1)_2O_{10}]$ dimer via edge sharing, likewise $[Mo(3)_2O_{10}]$ dimers. The above two types of dimers are further condensed into a 1D chain along *a*-axis via corner sharing, and neighboring 1D chains are further bridged by $Mo(2)O_6$ octahedra via corner sharing into a 2D layer with 1D tunnels of 6 MRs along *a*-axis. The IO_4^{3-} group are located at above tunnels and each forming six I–O–Mo bridges with five Mo(VI) centers.

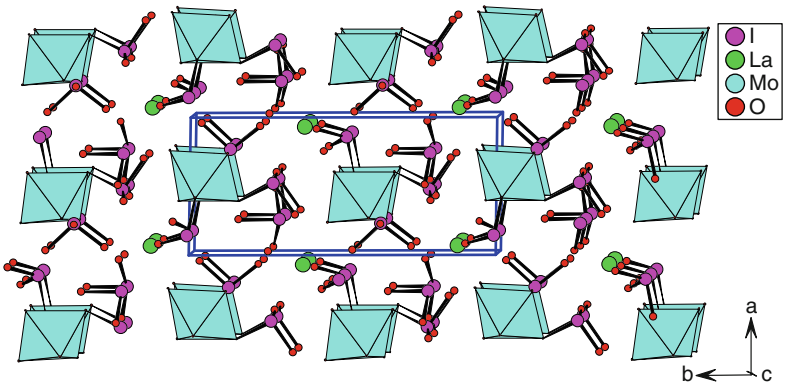

Fig. 3 View of structure of $LaMoO_2(OH)(IO_3)_4$ down the *c*-axis

$LnMoO_2(OH)(IO_3)_4$ (Ln = La, Nd, Sm, Eu) are the only lanthanide molybdenum (VI) iodates reported [25, 73]. They are isostructural and crystallized in the polar space group $P2_1$. $LaMoO_2(OH)(IO_3)_4$ was synthesized by heating a mixture of $La(NO_3)_3{\cdot}6H_2O$ (0.734 mmol), MoO_3 (1.480 mmol), H_5IO_6 (2.198 mmol), and I_2O_5 (1.474 mmol) in 9 mL H_2O at 170°C, whereas $LnMoO_2(OH)(IO_3)_4$ (Ln = Sm, Eu) were isolated by hydrothermal reactions of a mixture of MoO_3 (0.490 mmol), I_2O_5 (0.490 mmol), and $Ln(IO_3)_3$ (0.245 mmol) (Ln = Sm, Eu) in 1.0 mL H_2O at 200°C. For $NdMoO_2(OH)(IO_3)_4$, the loads are different: MoO_3 (0.616 mmol), I_2O_5 (0.616 mmol), $Ln(IO_3)_3$ (0.308 mmol), and 1.5 mL H_2O. Their structures feature a 0D $[MoO_2(OH)(IO_3)_3]^{2-}$ anionic unit composed of a Mo^{6+} cation linked to one hydroxyl, two terminal oxoanions, and three unidentate IO_3^- groups, these anionic units are separated by the Ln^{3+} cations and other "isolated" IO_3^- anions (Fig. 3). The Mo^{6+} cation undergoes an out-of-center distortion toward a face (local C_3 direction), exhibiting three short and three long Mo–O bonds. The Nd(III) compound displays a large SHG efficiency of about 350 × α-SiO_2 and it is also phase matchable.

2.1.2 V(V)–I(V)–O System

Such compounds are mostly focused in the A(I)–V(V)–I(V)–O system besides one Ba(II) and three La(III) compounds. Only six compounds were reported before our group's work in A(I)–V(V)–I(V)–O system, namely, $LiVO_2(IO_3)_2$, $KVO_2(IO_3)_2$, $RbVO_2(IO_3)_2$, $A(VO)_2O_2(IO_3)_3$ (A = NH_4^+, Rb^+, Cs^+) [24, 74]. Seven new compounds, namely, $NaVO_2(IO_3)_2(H_2O)$, α-$KVO_2(IO_3)_2(H_2O)$, β-$KVO_2(IO_3)_2(H_2O)$, $K_4[(VO)(IO_3)_5]_2(HIO_3)(H_2O)_2{\cdot}H_2O$, $K(VO)_2O_2(IO_3)_3$, $Ag_2VO_2(IO_3)_3$, and $Ag_2(V_2O_4)(IO_3)_4$, were prepared in our group through hydrothermal syntheses [29, 30, 68].

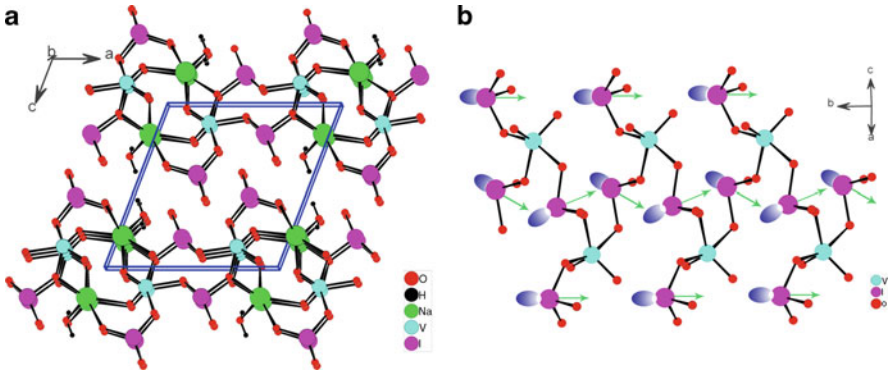

Fig. 4 (**a**) View of structure of $NaVO_2(IO_3)_2(H_2O)$ down the *b*-axis; (**b**) a 1D helical anionic chain with the macroscopic polarity indicated by *small green arrows* in $NaVO_2(IO_3)_2(H_2O)$

Yellow block-like crystals of $LiVO_2(IO_3)_2$ were obtained by heating a mixture of Li_2CO_3 (0.487 mmol), V_2O_5 (0.489 mmol), I_2O_5 (0.983 mmol), and H_2O (2 mL) at 170°C. $LiVO_2(IO_3)_2$ crystallized in the centrosymmetric space group $P2_1/c$ and its structure exhibits a 2D $[VO_2(IO_3)_2]^-$ anionic layer consisting of VO_6 octahedra bridged by IO_3 groups with the Li^+ cations being located at the interlayer space [74]. Bright yellow prisms of $KVO_2(IO_3)_2$ and yellow prisms of $RbVO_2(IO_3)_2$ were prepared by the hydrothermal reactions of a mixture of V_2O_5, KIO_4, I_2O_5, and 1 mL H_2O at 180°C. The loads are: V_2O_5 (0.51 mmol), KIO_4 (1.02 mmol), and I_2O_5 (0.51 mmol) for $KVO_2(IO_3)_2$; V_2O_5 (0.47 mmol), $RbIO_4$ (0.94 mmol), and I_2O_5 (0.47 mmol) for $RbVO_2(IO_3)_2$. Both $KVO_2(IO_3)_2$ ($P2_1/n$, CS) and $RbVO_2(IO_3)_2$ (P-1, CS) contain 1D $[VO_2(IO_3)_2]^-$ chains that are separated by K^+ or Rb^+ cations. These 1D chains are constructed by distorted VO_5 square pyramids interconnected by bidentate bridging $I(1)O_3$ groups with the $I(2)O_3$ groups being attached unidentately on the same side of the 1D chain. The difference is that the chains in $KVO_2(IO_3)_2$ are running down the *b*-axis, whereas the chains in $RbVO_2(IO_3)_2$ are along the *a*-axis [24]. We are awared that although $AVO_2(IO_3)_2$ ($A = Li^+, K^+, Rb^+$) have similar chemical formulae, their structures are very different.

Single crystals of $NaVO_2(IO_3)_2(H_2O)$ were synthesized by the hydrothermal reactions of a mixture of $NaVO_3{\cdot}2H_2O$ (1 mmol), I_2O_5 (3 mmol), Ga_2O_3 (0.25 mmol), and 5 mL of water at 200°C. It crystallized in the polar space group $P2_1$, and its structure features a unique 2D layer, which is composed of 1D right-handed helical $[VO_2(IO_3)_2]^-$ chains further bridged by Na^+ ions (Fig. 4a). The vanadium(V) cation is in a strongly distorted trigonal bipyramidal geometry, coordinated with two terminal oxoanions and three iodate anions, resulting in two short and three elongated V–O bonds. Both I(V) cations are in the asymmetric coordination environment, coordinated with three oxygen atoms in a distorted trigonal-pyramidal geometry. The VO_5 polyhedra are interconnected by the bidentate bridging $I(1)O_3$ groups into a 1D right-handed helical chain with $I(2)O_3$

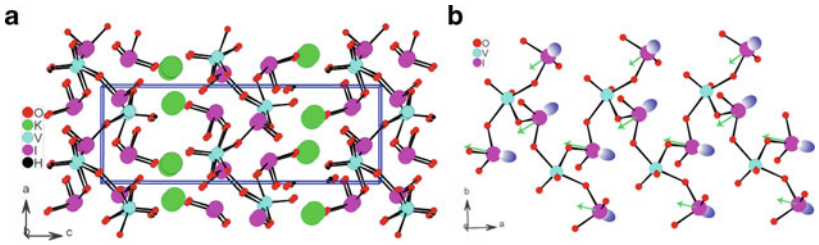

Fig. 5 (**a**) View of structure of β-$KVO_2(IO_3)_2(H_2O)$ down the *b*-axis; (**b**) a 1D $[VO_2(IO_3)_2]^-$ right-handed helical anionic chain with the macroscopic polarity indicated by *small green arrows* in β-$KVO_2(IO_3)_2(H_2O)$

groups being grafted unidentately on both sides of the helical chain. Within the 1D helical chain, all of the lone pairs of the IO_3 groups are aligned in the same direction to produce a large net dipole moment along the *b*-axis (Fig. 4b). SHG measurements revealed that $NaVO_2(IO_3)_2(H_2O)$ displays a very large SHG response of about 20 ×KDP and it is also phase matchable [29].

Yellow needle-shaped α-$KVO_2(IO_3)_2(H_2O)$ crystals were prepared by hydrothermal reactions of a mixture of K_2CO_3 (0.75 mmol), V_2O_5 (0.50 mmol), I_2O_5 (2.00 mmol), and H_2O (2.0 mL) at 155°C whereas yellow plate-shaped β-$KVO_2(IO_3)_2(H_2O)$ crystals were obtained by reactions of a mixture of K_2CO_3 (0.50 mmol), V_2O_5 (0.25 mmol), I_2O_5 (2.00 mmol), Bi_2O_3 (0.01 mmol), and H_2O (3.0 mL) at 230°C. When the reactions were carried out in the absence of Bi_2O_3, only unknown amorphous phase could be isolated. It is still not clear what kind of role Bi_2O_3 played in the formation of β-$KVO_2(IO_3)_2(H_2O)$.

α-$KVO_2(IO_3)_2(H_2O)$ (*P*bca, CS) exhibits a novel 2D layered structure composed of 1D $[VO_2(IO_3)_2]^-$ anionic chains bridged by K^+ cations. β-$KVO_2(IO_3)_2(H_2O)$ crystallizes in the chiral space group $P2_12_12_1$ and its structure features 1D $[VO_2(IO_3)_2]^-$ right-handed helical anionic chains along the *a*-axis which are separated by K^+ cations (Fig. 5a). In β-$KVO_2(IO_3)_2(H_2O)$, the V(V) cations are in a strongly distorted trigonal bipyramidal geometry composed of two terminal oxide anions and three iodate groups, resulting in two short and three long V–O bonds. Neighboring VO_5 polyhedra are further interconnected by bidentate bridging I(2)O_3 groups into a 1D right-handed helical chain along the *a*-axis with the I(1)O_3 groups being attached unidentately on both sides of the helical chain, which is similar to that in $NaVO_2(IO_3)_2(H_2O)$. Within a $[VO_2(IO_3)_2]^-$ helical chain, all of the lone pairs on the IO_3 groups are almost aligned in the same direction, producing a large dipole moment toward the *a*-axis (Fig. 5b). However, the lone pairs of the IO_3 groups from two neighboring helical chains are nearly aligned in opposite directions; hence, their local dipole moments are mostly cancelled out, which is confirmed by a very weak SHG response detected for the compound [30].

Orange brick-shaped $K_4[(VO)(IO_3)_5]_2(HIO_3)(H_2O)_2{\cdot}H_2O$ crystals were obtained by hydrothermal reactions of a mixture of K_2CO_3 (1.50 mmol), V_2O_5 (0.50 mmol),

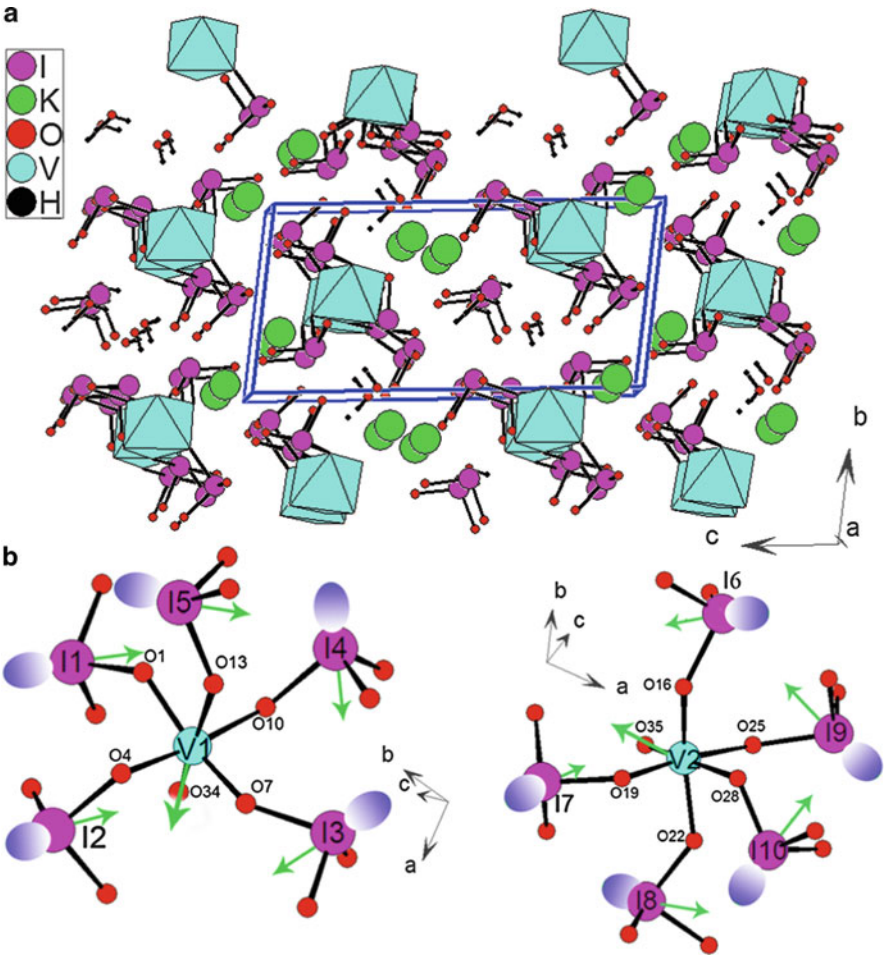

Fig. 6 (**a**) View of structure of $K_4[(VO)(IO_3)_5]_2(HIO_3)(H_2O)_2{\cdot}H_2O$ down the *a*-axis; (**b**) two 0D $[(VO)(IO_3)_5]^{2-}$ anions in the asymmetric unit showing the lone pairs (*purple ellipsoids*) and local moments (*green arrows*). VO_6 octahedra are shaded in *cyan*

I_2O_5 (9.00 mmol), and H_2O (5.0 mL) at 160°C. $K_4[(VO)(IO_3)_5]_2(HIO_3)(H_2O)_2{\cdot}H_2O$ crystallizes in the polar space group *P*1 and its structure features novel 0D $[(VO)(IO_3)_5]^{2-}$ anionic units composed of one VO_6 octahedron corner sharing with five IO_3 groups (Fig. 6a). The K^+ cations, water molecules, and "isolated" HIO_3 groups are located in-between these 0D units. Both V(V) cations in the asymmetric unit undergo an intraoctahedral distortion toward the terminal oxoanions, that is, local C_4 distortion, exhibiting one short, one long, and four normal V–O bonds. Although the 0D $[(VO)(IO_3)_5]^{2-}$ units in the asymmetric unit are polar, the polarization directions of VO_6 and IO_3 groups in the 0D units are almost opposite each other

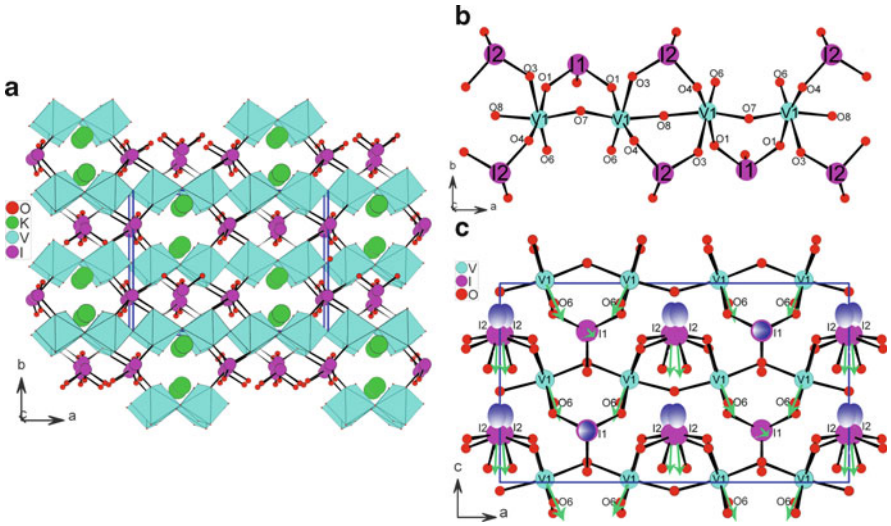

Fig. 7 (**a**) View of structure of $K(VO)_2O_2(IO_3)_3$; (**b**) a 1D $[(VO)_2O_2(IO_3)_3]^-$ chain along the *a*-axis; (**c**) 1D $[(VO)_2O_2(IO_3)_3]^-$ chains along the *a*-axis showing the lone pairs (*purple ellipsoids*) and local moments (*green arrows*)

(Fig. 6b), resulting in partial cancellation of the local dipole moments, which is also confirmed by its very weak SHG response [30].

Red brick-shaped crystals of $K(VO)_2O_2(IO_3)_3$ were prepared by heating a mixture of K_2CO_3 (0.40 mmol), V_2O_5 (0.50 mmol), I_2O_5 (2.00 mmol), and H_2O (2.0 mL) at 160°C, whereas $A(VO)_2O_2(IO_3)_3$ ($A = Rb^+, Cs^+, NH_4^+$) were prepared from the hydrothermal reactions of V_2O_5, AIO_4 ($A = Rb^+, Cs^+, NH_4^+$), and I_2O_5 at 180°C. $A(VO)_2O_2(IO_3)_3$ ($A = K^+, Rb^+, Cs^+, NH_4^+$) are isostructural and crystallized in the polar space group *I*ma2. Their structures features a 1D $[(VO)_2O_2(IO_3)_3]^-$ chain formed by 1D corner-sharing VO_6 octahedral chain which is further decorated by the bidentate bridging IO_3 groups from both sides (Fig. 7). These 1D chains are separated by the alkali or ammonium cations. The V(V) cation is distorted toward a corner (local C_4 direction), resulting in one long, one short, and four normal V–O bonds. Within the 1D chain, the lone pairs from $I(1)O_3$ groups are nearly aligned in the opposite directions, which makes their polarizations cancelled out. The polarizations of these compounds mainly come from $I(2)O_3$ groups and VO_6 octahedra. As shown in Fig. 7c, the polarizations of $I(2)O_3$ groups and VO_6 octahedra are almost aligned along the *c*-axis. Hence, the polarizations associated with $I(2)O_3$ and VO_6 octahedra constructively add, resulting in a large net dipole moment. SHG measurements showed that all four compounds display strong SHG responses, corresponding to 3.6, 2.2, 1.3, and 0.4 times of KTP ($KTiOPO_4$) for the potassium, rubidium, cesium, and ammonium phases, respectively. It is apparent that the SHG responses follow a sequence of K> Rb> Cs> NH_4. The SHG response of $K(VO)_2O_2(IO_3)_3$ is the strongest one,

being about 1.6 times as large as that of the rubidium phase. It is concluded that the different ionic sizes of K^+, Rb^+, Cs^+, and NH_4^+ produce different net polarizations for the four materials, and eventually led to different SHG responses [24, 30].

$Ag_2VO_2(IO_3)_3$ (*P*bca, CS) and $Ag_2(V_2O_4)(IO_3)_4$ (*P*ccn, CS) exhibit 1D $[VO_2(IO_3)_2]^{2-}$ and $[(V_2O_4)(IO_3)_3]^{2-}$ anionic chains, respectively, both based on 1D chains of corner-sharing VO_6 octahedra. Such 1D anionic chains are separated by the Ag^+ cations and "isolated" IO_3 groups. The IO_3 groups in the 1D $[VO_2(IO_3)_2]^{2-}$ chains are attached on both sides of the 1D vanadium oxide chain in unidentate or bidentate fashions, whereas all the IO_3 groups in $[(V_2O_4)(IO_3)_3]^{2-}$ anionic chains are grafted from both sides of the 1D vanadium oxide chain in a bidentate bridging fashion. Both compounds were prepared by heating a mixture of $AgNO_3$, V_2O_5, I_2O_5 in water at 200°C. The loaded compositions are $AgNO_3$, (1 mmol), V_2O_5 (0.3 mmol), and I_2O_5 (3.0 mmol) in 2 mL of H_2O for $Ag_2(VO_2)(IO_3)_3$; and $AgNO_3$ (0.25 mmol), V_2O_5 (0.25 mmol), and I_2O_5 (1.0 mmol) in 1 mL of H_2O (1 mL) for $Ag_2(V_2O_4)(IO_3)_4$ [68].

$Ba_2VO_2(IO_3)_5$ was prepared by heating a mixture of $Ba(OH)_2{\cdot}8H_2O$ (1.58 mmol), V_2O_5 (1.10 mmol), HIO_3 (28.4 mmol), and 10 mL H_2O at 230°C. It crystallized in CS space group $P2_1/c$, its structure features a 0D $[VO_2(IO_3)_4]^{3-}$ anionic unit that consists of a V^{5+} cation bonded to two terminal oxoanions and four IO_3 groups. These 0D anions are separated by the Ba^{2+} cations and "noncoordination" IO_3 groups [71].

Three compounds in the La(III)–V(IV)/V(V)–I(V)–O systems, namely, $LaVO^{IV}(IO_3)_5$, $LaV_2O_6(IO_3)$, and $LaVO_2(IO_3)_4{\cdot}H_2O$ were prepared by our group [47]. Green needle-shaped crystals of $LaVO(IO_3)_5$ were obtained by heating a mixture of La_2O_3 (0.25 mmol), V_2O_5 (0.75 mmol), and I_2O_5 (4.0 mmol) and H_2O (2 mL) at 250°C. It was found that V^{5+} ion was reduced to V^{4+} ion during the reactions. Yellow needle-shaped crystals of $LaV_2O_6(IO_3)$ were prepared by the hydrothermal reactions of $La(NO_3)_3{\cdot}6H_2O$ (0.45 mmol), V_2O_5 (0.25 mmol), I_2O_5 (1.5 mmol), and H_2O (2 mL) at 250°C. Orange brick-shaped single crystals of $LaVO_2(IO_3)_4{\cdot}H_2O$ were obtained by heating a mixture of $La(NO_3)_3{\cdot}6H_2O$ (0.35 mmol), VO_2 (0.5 mmol), I_2O_5 (2.0 mmol), and H_2O (2 mL) at 180°C. V^{4+} ion was oxidized to V^{5+} ion during the reactions.

$LaV^{IV}O(IO_3)_5$ ($P2_1/n$, CS) contains a 0D $[VO(IO_3)_5]^{3-}$ anionic unit in which a VO_6 octahedron is corner sharing with five IO_3 groups. Such 0D units are separated by the La^{3+} ions. $LaV_2O_6(IO_3)$ (*P*bcm, CS) exhibits a unique 1D ladder-like $[V_2O_6]^{2-}$ anionic chain which is not directly connected to any IO_3 groups, the La^{3+} ions and the "isolated" iodate groups are located between these anionic chains. $LaVO_2(IO_3)_4{\cdot}H_2O$ ($P2_1$) is isostructural with $LnMoO_2(IO_3)_4(OH)$ (Ln = La, Nd, Sm, Eu) and its structure contains a 0D $[VO_2(IO_3)_4]^{3-}$ anionic unit in which the V^{5+} cation is octahedrally coordinated by four unidentate IO_3 groups and two terminal oxoanions, and such anionic units are separated by La^{3+} cations and lattice water molecules (Fig. 8). The V^{5+} cation undergoes a SOJT distortion toward an edge (local C_2 direction), displaying two short, two normal, and two long V–O bonds. $LaVO_2(IO_3)_4{\cdot}H_2O$ displays a weak SHG response of 0.2 ×KDP since the polarizations from VO_6 octahedra and iodate groups have been largely cancelled out.

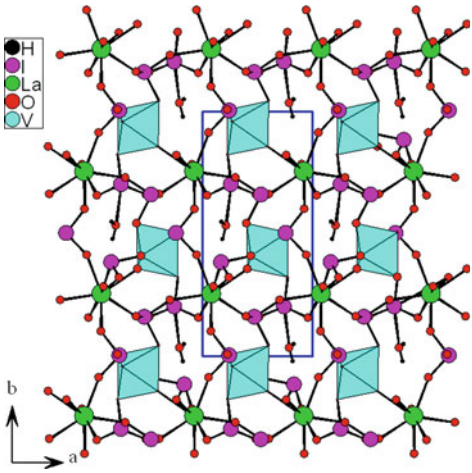

Fig. 8 View of the structure of $LaVO_2(IO_3)_4{\cdot}H_2O$ down the *c*-axis

2.1.3 Other d^0-TM–I(V)–O Systems

So far, only three Ti(IV), one Zr(IV), one Nb(IV), and two Cr(VI) iodates have been reported.

$A_2Ti(IO_3)_6$ ($A = Li^+$, Na^+) (space group $P6_3$) are isostructural and NCS. They revealed very strong SHG responses of about 500 and 400 × α-SiO_2, respectively, and both are phase matchable [26, 27]. $A_2Ti(IO_3)_6$ ($A = K^+$, Rb^+, Cs^+, Tl^+, Ag^+), $BaTi(IO_3)_6$, and $A_2Zr(IO_3)_6$ ($A = Rb^+$, Cs^+) are isostructural and crystallize in the centrosymmetric (CS) space group *R*-3; hence, they are not SHG active [27, 68, 70, 71].

$A_2Ti(IO_3)_6$ ($A = Li^+$, Na^+, K^+, Rb^+, Cs^+, Tl^+) were synthesized by hydrothermal reactions of a mixture of A_2CO_3 ($A = Li^+$, Na^+, K^+, Rb^+, Cs^+, Tl^+), TiO_2, and HIO_3 in 10 mL water at 230°C for 4 days [26, 27]. The loads are: for $Li_2Ti(IO_3)_6$, Li_2CO_3 (4.06 mmol), TiO_2 (3.76 mmol), and HIO_3 (28.4 mmol); for $Na_2Ti(IO_3)_6$, Na_2CO_3 (4.7 mmol), TiO_2 (3.8 mmol), and HIO_3 (28 mmol); for $K_2Ti(IO_3)_6$, K_2CO_3 (1.7 mmol), TiO_2 (1.3 mmol), and HIO_3 (17 mmol); for $Rb_2Ti(IO_3)_6$, Rb_2CO_3 (1.7 mmol), TiO_2 (1.3 mmol), and HIO_3 (17 mmol); for $Cs_2Ti(IO_3)_6$, Cs_2CO_3 (1.4 mmol), TiO_2 (1.3 mmol), and HIO_3 (17 mmol); for $Tl_2Ti(IO_3)_6$, Tl_2CO_3 (1.4 mmol), TiO_2 (1.3 mmol), and HIO_3 (28 mmol). $Ag_2Ti(IO_3)_6$ was obtained by heating a mixture of $AgNO_3$ (0.5 mmol), TiO_2 (0.25 mmol), I_2O_5 (1.0 mmol), and 1 mL water at 200°C. $BaTi(IO_3)_6$ was prepared by heating $Ba(OH)_2{\cdot}8H_2O$ (1.58 mmol), TiO_2 (2.50 mmol), HIO_3 (28.4 mmol), and 10 mL H_2O at 230°C. $A_2Zr(IO_3)_6$ ($A = Rb^+$, Cs^+) were synthesized by hydrothermal reactions of a mixture of AIO_4 ($A = Rb^+$, Cs^+), I_2O_5, $ZrOCl_2$, and 1.5 mL H_2O at 200°C. The loaded compositions are: $RbIO_4$ (0.829 mmol), I_2O_5 (0.414 mmol), and $ZrOCl_2$ (0.425 mmol) for $RbZr(IO_3)_6$; $CsIO_4$ (0.772 mmol), I_2O_5 (0.380 mmol), and $ZrOCl_2$ (0.382 mmol) for $CsZr(IO_3)_6$. These compounds mentioned above are topologically similar and exhibit a 0D $[Ti(IO_3)_6]^{2-}$ or $[Zr(IO_3)_6]^{2-}$ anionic unit consisting of a nondistorted d^0-TM cation linked to six IO_3^- anions (Fig. 9). These 0D anionic units are separated by the A^+ cations. In $A_2Ti(IO_3)_6$ ($A = Li^+$, Na^+), all of

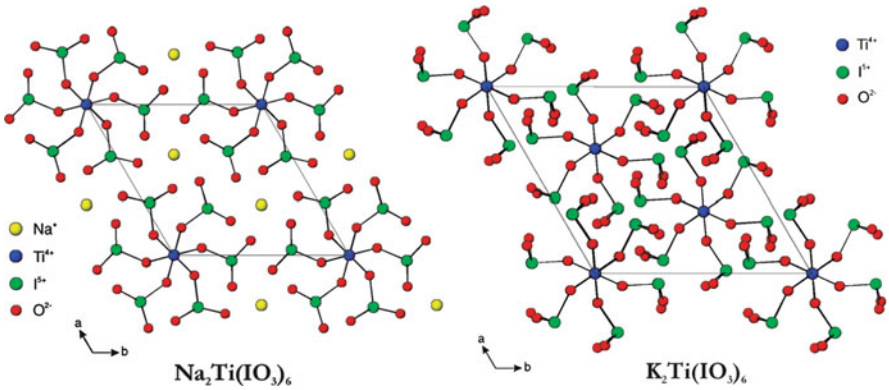

Fig. 9 View of the structure of $Na_2Ti(IO_3)_6$ and $K_2Ti(IO_3)_6$ along *c*-axis

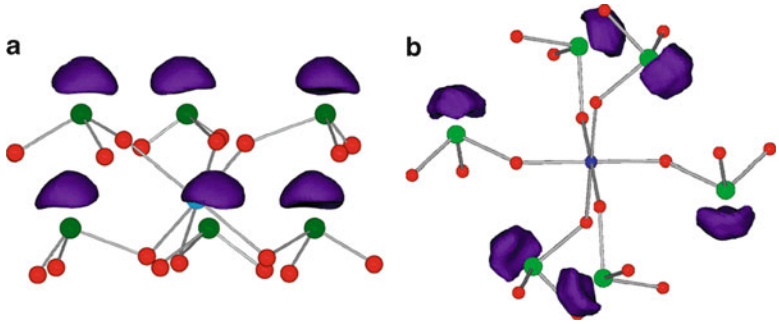

Fig. 10 A 0D $[Ti(IO_3)_6]^{2-}$ unit for $A_2Ti(IO_3)_6$ (A = Li^+, Na^+) (**a**) and $A_2Ti(IO_3)_6$ (A = K^+, Rb^+, Cs^+, Tl^+, Ag^+) (**b**)

the lone pairs on the I^{5+} cations are aligned in a parallel manner, producing a macroscopic dipole moment and thereby creating a polar material (Fig. 10a). In other compounds, the lone pairs on the I^{5+} cations are located *trans* to each other, which resulted in cancellation of the local dipole moments and they are nonpolar (Fig. 10b). It is obvious that the different ionic radii of A cations have a strong effect on the structures and properties of the materials formed.

$LaTiO(IO_3)_5$ was obtained by hydrothermal reactions of La_2O_3 (0.921 mmol), TiO_2 (2.50 mmol), and HIO_3 (28.4 mmol) in 10 mL of H_2O at 230°C. $LaTiO(IO_3)_5$ ($P2_1/n$) represents the third structural type in this system and its structure features a 0D $[TiO(IO_3)_5]^{3-}$ anionic unit composed of a Ti^{4+} ion surrounded by five IO_3 anions and one terminal oxoanion. Such 0D units are separated by the La^{3+} ions [71]. Each Ti^{4+} cation is in a distorted octahedral environment with one short, four normal, and one elongated Ti–O bonds; therefore, the Ti^{4+} undergoes an out-of-center distortion toward a corner of the octahedron (C_4 distortion).

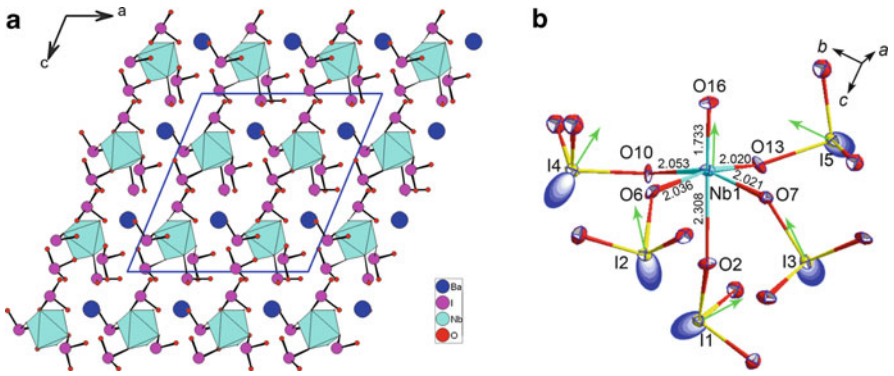

Fig. 11 (**a**) Ball-and-stick packing diagram of $BaNbO(IO_3)_5$ down the *b*-axis, NbO_6 octahedra are shaded in blue; (**b**) ORTEP drawing showing the 0D $[NbO(IO_3)_5]^{2-}$ anion, lone pairs (*blue ellipsoids*) as well as the local moments (*green arrows*)

$BaNbO(IO_3)_5$ was synthesized by the hydrothermal reaction of $Ba(IO_3)_2{\cdot}H_2O$ (1.0 mmol), Nb_2O_5 (0.6 mmol), and I_2O_5 (9 mmol) in 5 mL of water at 230°C for 4 days. $BaNbO(IO_3)_5$ is the only niobium(V) iodate reported. It crystallizes in the polar space group *Cc* and its structure features a 0D $[NbO(IO_3)_5]^{2-}$ anionic unit composed of a Nb^{5+} ion linked to five iodate groups and one terminal oxoanion (Fig. 11a) [28]. The Ba^{2+} cations act as spacers between these anionic units. Both the Nb^{5+} and I^{5+} cations are in asymmetric coordination environments attribute to SOJT effects. The Nb^{5+} cation undergoes intraoctahedral distortion toward the terminal oxide ligand, that is, a corner (C_4) distortion, resulting in one short, one long, and four normal Nb–O bonds. More interestingly, the polarizations associated with IO_3 and NbO_6 polyhedra are almost toward the same direction and therefore constructively add, resulting in a large local dipole moment (Fig. 11b). $BaNbO(IO_3)_5$ displays a very large SHG response of about 14 × KDP. Furthermore, it is phase matchable.

$KCrIO_6$ was prepared by reactions of 7.5 g $K_2Cr_2O_7$ dissolved in 40 mL H_2O and 6.5 g HIO_3. $KCrIO_6$ ($P2_1/c$, CS) can also be formulated as $KCrO_3(IO_3)$ and its structure features a 0D $[CrO_3(IO_3)]$ anionic unit composed of a CrO_4 tetrahedron corner sharing with an IO_3 group. These 0D units are separated by the K^+ cations [75]. $ThCrO_4(IO_3)_2$ was obtained by the hydrothermal reactions of $Th(NO_3)_4{\cdot}xH_2O$ (0.435 mmol), H_5IO_6 (0.451 mmol), $Cr(NO_3)_3{\cdot}9H_2O$ (0.451 mmol), and 1.0 mL of water at 200°C. $ThCrO_4(IO_3)_2$ crystallizes in the NCS space group $P2_12_12_1$ and its structure contains "isolated" IO_3 groups and CrO_4 tetrahedra; that is, the CrO_4 tetrahedron is not directly connected to any IO_3 groups. Each Th(IV) center is connected to six IO_3 and three CrO_4 groups. The SHG efficiency of $ThCrO_4(IO_3)_2$ is very weak and comparable to that of α-SiO_2 [48].

No Hf(IV), Ta(V) and W(VI) iodates has been reported; therefore, still a lot of synthetic explorations are needed. Furthermore, there are also many opportunities and challenges to find new phases in the A–Ti(IV)/Zr(IV)/Nb(V)/Cr(VI)–I(V)–O

systems, especially the Zr(IV), Nb(V), and Cr(VI) iodates. Studies also revealed that the size of the counterions has also a great influence on the compositions, structures, and SHG properties of the materials formed.

2.2 Combination of Other Lone-Pair Cations with Iodate Groups

So far, little is known about the metal iodates that contain two different types of lone pair cations. Such metal iodates reported are limited to bismuth(III), lead(II), or thallium(I) iodates, including $Tl^{I}IO_3$, $Tl_2{}^{I}Tl^{III}(IO_3)_6$, $Bi(IO_3)_3$, $Bi(IO_3)_3(H_2O)_2$, $Pb(IO_3)_2$, $Pb_3(IO_3)_2Cl_4$, and $Pb_3(IO_3)OCl_3$ [76–82]. Our recent research efforts in such systems afford four new lanthanide(III) lead(II) iodates, namely, $Ln_3Pb_3(IO_3)_{13}(\mu^3\text{-O})$ (Ln = La–Nd) [46].

$Tl^{I}IO_3$ crystallizes in the polar space group *R*3m and its structure contains isolated IO_3 groups separated by Tl^+ cations. The polarity in these structures is imparted by the alignment of the stereochemically active lone pairs of the iodate anions along the *c*-axis [76]. $Tl_4(IO_3)_6$ (*P*-1, CS) features a 0D $[Tl^{III}(IO_3)_6]^{2-}$ anions composed of a TlO_6 octahedron connected with six unidentate IO_3 groups. These 0D units are separated by the Tl^+ cations [77].

$Bi(IO_3)_3$ ($P2_1/n$, CS) exhibits a layered structure in which the Bi^{3+} cation is coordinated by seven unidentate iodate groups and each BiO_7 polyhedron is further interconnected to six neighboring ones by bridging iodate groups into a 2D layer [78]. $Bi(IO_3)_3(H_2O)_2$ (*P*-1, CS) also exhibits a layered structure in which the Bi^{3+} cation is eight coordinated by seven iodate groups in a unidentate fashion and an aqua ligand, one BiO_8 polyhedron is further connected with five neighboring ones by bridging iodate groups into a 2D layer [79]. The structure of $Pb(IO_3)_2$ (*P*bcn, CS) features a 1D chain in which neighboring asymmetric PbO_4 polyhedra are further interconnected by edge sharing into a chain with the iodate groups attached on both sides of the chain in a unidentate fashion [80].

$Pb_3(IO_3)_2Cl_4$ (*C*2/c, CS) exhibits a 3D network structure constructed by $[Pb_3Cl_4]^{2+}$ layers further interconnected by bridging iodate groups [81]. $Pb_3(IO_3)OCl_3$ crystallizes in NCS space group *C*mm2 and its structure features a thick quadruple layer composed of one $[IO_2]^+$, one $[Pb_2IO_4Cl_2]^-$, one $[Pb_3O_2Cl_3]^-$, and one $[Pb_4IO_4Cl_4]^+$ layers. It should be mentioned that the I^{5+} cation of the $[IO_2]^+$ layer is coordinated by four oxygen atoms in a square planar geometry, whereas the remaining I^{5+} cations are also four coordinated with a square pyramidal environment [82].

Single crystals of $Ln_3Pb_3(IO_3)_{13}(\mu^3\text{-O})$ (Ln = La–Nd) were prepared by the hydrothermal reactions of a mixture of lanthanide(III) oxide or nitrate (for the Ce compound), $PbCl_2$, and I_2O_5 in 10 mL (for La and Ce phases) or 4 mL (for Pr and Nd phases) H_2O in a 23 mL Teflon-lined stainless steel vessel at 200°C for 4 (for the La and Pr compounds) or 5 (for the Ce and Nd compounds) days. The loaded

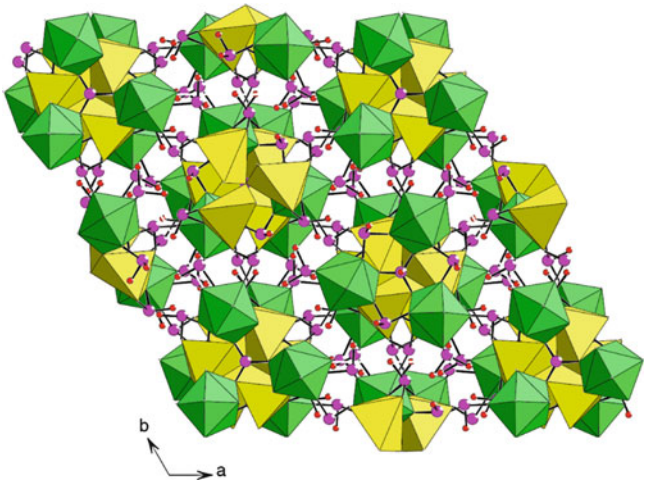

Fig. 12 View of the structure of $Ln_3Pb_3(IO_3)_{13}(\mu^3\text{-}O)$ (Ln = La–Nd) down the *c*-axis. LaO9 and PbO6 polyhedra are shaded in *green* and *yellow*, respectively. I and O atoms are drawn as *pink* and *red circles*, respectively

compositions are: La_2O_3 (0.613 mmol), $PbCl_2$ (0.719 mmol), I_2O_5 (2.4 mmol) for La compound; $Ce(NO_3)_3{\cdot}6H_2O$ (0.645 mmol), $PbCl_2$ (0.576 mmol), I_2O_5 (1.25 mmol) for Ce compound; Pr_2O_3 (0.303 mmol), $PbCl_2$ (0.719 mmol), I_2O_5 (1.35 mmol) for Pr compound; Nd_2O_3 (0.297 mmol), $PbCl_2$ (0.719 mmol), I_2O_5 (1.35 mmol) for Nd compound.

$Ln_3Pb_3(IO_3)_{13}(\mu^3\text{-}O)$ (Ln = La–Nd) crystallized in the polar space group *R*3c and their structures exhibit a complicated 3D network structure composed of LnO_9, asymmetric PbO_6 and IO_3 polyhedra that are interconnected via corner- or/and edge sharing (Fig. 12) [46]. SHG measurements revealed that $Ln_3Pb_3(IO_3)_{13}(\mu^3\text{-}O)$ (Ln = La, Pr, Nd) display SHG responses that about 2.0, 1.0, and 0.8 times of KDP, respectively. The SHG signal for the cerium compound is very weak. On the basis of structural data, the polarizations from the Pb(II) ions and $I(1)O_3$, $I(2)O_3$, and $I(4)O_3$ groups are expected to be small since their dipole moments are mainly aligned in the *ab* plane and cancelled each other. The main contributions are from $I(3)O_3$ and $I(5)O_3$ groups since their dipole moments are aligned in the same direction (along the *c*-axis).

For the metal iodates containing other lone-pair cations, there are also several opportunities and challenges. So far, there is no metal iodates with lone pair-containing Sb(III), Se(IV), Te(IV), or Sn(II) reported, and little is known about the bismuth iodates except centrosymmetric $Bi(IO_3)_3$ and $Bi(IO_3)_3(H_2O)_2$. The greatest challenge is that Sb(III), Se(IV), Te(IV), and Sn(II) are very apt to be oxidized by the I(V) cations and then the stereochemically active lone pairs may be lost.

2.3 Other Mixed Metal Iodates

From the above discussions, the combination of two types of asymmetric units (d^0 TM and iodate groups, other lone-pair cations, and iodate groups) affords many NCS compounds with rich structural types and excellent SHG properties. But it is still a great challenge to summarize the relationships between structures or chemical compositions of the materials and their second-order NLO properties. To better understand the relationships between the structures and SHG properties, we have also made a systematic exploration in the alkali metal indium iodates, palladium(II) iodates, and mixed metal iodates in the K–M(II)–IO_3 system.

Seven alkali metal indium iodates were reported in the alkali metal indium iodates, namely, $AIn(IO_3)_4$ (A = Li, Na), α-$K_3In(IO_3)_6$, β-$K_3In(IO_3)_6$, $Rb_3In(IO_3)_6$, and $A_2HIn(IO_3)_6$ (A = Rb, Cs). The seven compounds except the two potassium compounds were synthesized by a similar method of alkali metal salts In_2O_3 and H_5IO_6 in water at 200°C for 4 days. α-$K_3In(IO_3)_6$ was synthesized from a mixture containing KIO_4(1.5 mmol), $In(NO_3)_3{\cdot}20.5H_2O$ (1 mmol), 2,2′-bipy (0.5 mmol), and 0.4 mL of HCl (38%) in the presence of water (5 mL) at 120°C for 4 days, whereas β-$K_3In(IO_3)_6$ was synthesized from a mixture containing KIO_4 (1 mmol), $In(NO_3)_3{\cdot}20.5H_2O$ (1 mmol), imidazole (1 mmol), 0.4 mL of HCl (38%), and water (5 mL) at 100°C for 7 days [44, 83].

Although $LiIn(IO_3)_4$ (*P*-1, CS) and $NaIn(IO_3)_4$ ($P2_1/c$, CS) are not isostructural, both of them feature 1D $[In(IO_3)_4]^-$ chains that are separated by Li^+ or Na^+ cations. The In^{3+} ion is in a slightly distorted octahedral geometry, being coordinated by six iodate anions in a unidentate fashion. These InO_6 octahedra are further interconnected by bridging iodate groups into a 1D chain with the remaining iodate groups, which are attached monodentately on both sides of the 1D chain. The chains in $LiIn(IO_3)_4$ are propagated along the *a*-axis, whereas the chains in $NaIn(IO_3)_4$ are along the *b*-axis.

$Rb_3In(IO_3)_6$ is isostructural to α-$K_3In(IO_3)_6$ and crystallized in the CS space group *P*-1. Its structure features a 0D isolated $[In(IO_3)_6]^{3-}$ anion consisting of a InO_6 octahedron corner sharing with six iodate groups. These isolated anions are separated by Rb^+ cations. In these structures, the polarizations of IO_3 groups have cancelled out each other; hence, these three compounds are non-polar.

$A_2HIn(IO_3)_6$ (A = Rb^+, Cs^+) (*P*-1, CS) are isostructural and their structures also exhibit isolated $[In(IO_3)_6]^{3-}$ anions as in $A_3In(IO_3)_6$ (A = K^+, Rb^+). However, one of three alkali metal cations lying on an inversion center is replaced by a proton. Since the lone pairs on IO_3 polyhedra are oriented *trans* to each other, their local dipole moments cancelled out each other. Hence, these materials are nonpolar [83].

β-$K_3In(IO_3)_6$ crystallized in the polar space group *F*dd2 and exhibits a 0D isolated $[In(IO_3)_6]^{3-}$ anion consisting of a slightly distorted InO_6 octahedron corner sharing with six iodate groups. These isolated anionic units are separated by K^+ cations. Different from that in α-$K_3In(IO_3)_6$, the isolated $[In(IO_3)_6]^{3-}$ anion in β-$K_3In(IO_3)_6$ is polar and β-$K_3In(IO_3)_6$ displays an SHG efficiency of about 1 × KDP. Hence, the local asymmetric environment is a necessary, but not a sufficient condition for creating macroscopic NCS structures. In other words,

once the local acentric units are aligned in an antiparallel fashion, a material may crystallize in a centrosymmetric structure and is nonpolar [44].

Only four palladium(II) iodates have been reported so far, namely, $Pd(IO_3)_2$, $K_{2.5}Pd(IO_3)_4(H_{0.5}IO_3)$, $AgPd(IO_3)_3$, and $BaPd(IO_3)_4$ [45, 84]. Red plate-shaped crystals of $Pd(IO_3)_2$ were obtained by the hydrothermal reactions of aqueous solution of $Pd(NO_3)_2{\cdot}2H_2O$ (0.10 mmol), I_2O_5 (2.00 mmol), and H_2O (2.0 mL) with Li_2CO_3 (0.50 mmol) used as the pH adjuster at 200°C. Dark orange plates of $K_{2.5}Pd(IO_3)_4(H_{0.5}IO_3)$ were prepared by hydrothermal reactions of $Pd(NO_3)_2{\cdot}2H_2O$ (0.397 mmol), KIO_4 (1.236 mmol), and 0.5 mL H_2O at 200°C. Red plate-shaped crystals of $AgPd(IO_3)_3$ were synthesized by heating a mixture of Ag_2O (0.05 mmol), $Pd(CH_3COO)_2$ (0.102 mmol), I_2O_5 (2.00 mmol), and H_2O (2.0 mL) at 200°C. Red block-shaped crystals of $BaPd(IO_3)_4$ were obtained by the hydrothermal reactions of $BaCO_3$ (0.10 mmol), $Pd(CH_3COO)_2$ (0.103 mmol), I_2O_5 (2.00 mmol), and H_2O (2.0 mL) at 200°C.

$Pd(IO_3)_2$ (*P*bca, CS) exhibits a 2D layered structure in which each PdO_4 square is further interconnected with four neighboring ones through four bridging iodate groups. The Pd^{2+} ion is bonded to four iodate anions in a slightly distorted square planar environment. The lone pairs of IO_3 groups are aligned *trans* to each other (oriented in opposite directions), resulting in the cancellation of their local dipole moments; hence, $Pd(IO_3)_2$ is nonpolar [45].

The structure of $K_{2.5}Pd(IO_3)_4(H_{0.5}IO_3)$ (*C*2/m, CS) features a 0D $[Pd(IO_3)_4]^{2-}$ anionic unit which is composed of a PdO_4 square unit corner sharing with four iodate groups; such anionic units are separated by the K^+ cations and "isolated" HIO_3 groups. It is interesting to note that all of the four iodate anions in the $[Pd(IO_3)_4]^{2-}$ anionic unit are aligned on the same side of the PdO_4 square plane; therefore, such anionic unit is polar [84]. However, there is no macroscopic polarization for the overall structure since the polarizations of neighboring $[Pd(IO_3)_4]^{2-}$ units cancelled out each other due to its centrosymmetric space group.

$AgPd(IO_3)_3$ crystallizes in the space group *P*-1 and its structure features 1D $[Pd(IO_3)_3]^-$ anionic chains along the *c*-axis which are separated by Ag^+ cations. The Pd^{2+} cation is also in a slightly distorted square planar geometry, being coordinated by four iodate groups. The PdO_4 squares are further interconnected by bridging I(1)O_3 groups into a 1D chain with I(2)O_3 and I(3)O_3 groups alternately attached on both sides of the chain in a unidentate fashion, forming a 1D $[Pd(IO_3)_3]^-$ anionic chain. Similar to those in $Pd(IO_3)_2$, the lone pairs of the IO_3 groups are aligned *trans* to each other, resulting in the cancellation of the local dipole moments and rendering the $[Pd(IO_3)_3]^-$ chain nonpolar [45].

$BaPd(IO_3)_4$ is isostructural with $KAu(IO_3)_4$ and crystallized in polar space group *P*1. Their structures contain a 0D $[TM(IO_3)_4]^{2-}$ (TM = Au, Pd) consisting of a TMO_4 square corner sharing with four unidentate iodate groups, with the K^+ or Ba^{2+} cations acting as the spacers. The MO_4 square plane is much more distorted than those in $Pd(IO_3)_2$ and $AgPd(IO_3)_3$. All four iodate groups in the $[M(IO_3)_4]$ unit are aligned on the same side of the square plane; hence, all of the lone pairs of I(V) cations are almost oriented toward the same direction (Fig. 13). Such a special

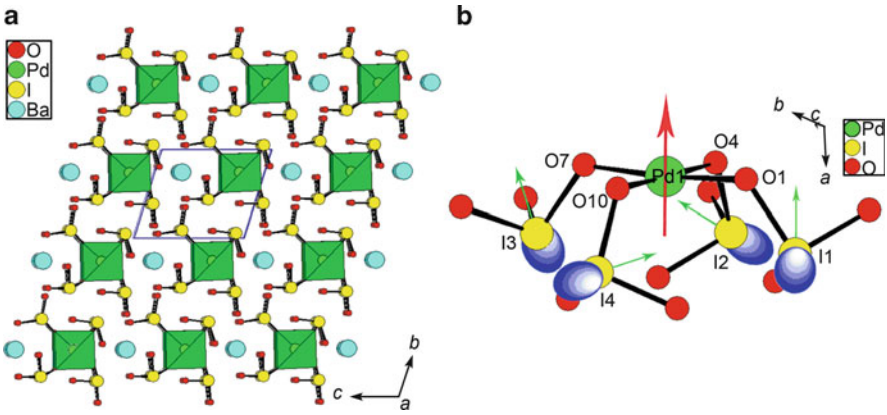

Fig. 13 (**a**) View of structure of $BaPd(IO_3)_4$ down the *a*-axis. PdO_4 squares are shaded in *green*; (**b**) a 0D $[Pd(IO_3)_4]^{2-}$ unit of $BaPd(IO_3)_4$

arrangement resulted in a large net dipole moment. SHG measurements on a 2.05 μm Q-switch laser revealed that $BaPd(IO_3)_4$ displays a moderate SHG efficiency of about 0.4 × KTP. So far, little is known about the gold(III) and platinum (II) iodates in which the metal ions may also have a square-planar geometry [45].

Most of the compounds reported in the alkali–M(II)–IO_3 system are mostly centrosymmetric except for $K_2M(IO_3)_4(H_2O)_2$ ($M = Mn^{2+}$, Co^{2+}, Zn^{2+}, Mg^{2+}) [43]. These four compounds were hydrothermally synthesized by the hydrothermal reactions of a mixture containing hexahydrated metal chloride (for Co and Mg compounds) or metal acetate (for Mn and Zn compounds) and potassium iodate in 10 mL of distilled water at 100°C. The K/M molar ratios are equal to 4/1 (5/1 for the Mn compound) for $K_2M(IO_3)_4(H_2O)_2$ ($M = Co^{2+}$, Zn^{2+}, Mg^{2+}). Furthermore, $NH_4H_2PO_4$ was used during the growth of the single crystals for $K_2Mn(IO_3)_4(H_2O)_2$.

These four compounds are isostructural and crystallized in the space group *I*2. Their structures feature 0D $[M(IO_3)_4(H_2O)_2]^{2-}$ ($M = Mn^{2+}$, Co^{2+}, Zn^{2+}, Mg^{2+}) anions that are separated by K^+ cations. The central transitional metal or Mg^{2+} cation is in a slightly distorted octahedral geometry composed of four unidentate iodate groups and two aqua ligands. The polarizations of the $I(2)O_3$ groups almost cancelled out each other, whereas those of $I(1)O_3$ groups are aligned in a parallel manner which produces a net dipole moment along the *b*-axis (Fig. 14). Neighboring 0D $[TM(IO_3)_4(H_2O)_2]^{2-}$ anions are packed in such a way that they produce a large macroscopic dipole moment along the *b*-axis. SHG measurements revealed that $K_2TM(IO_3)_4(H_2O)_2$ ($TM = Co^{2+}$, Zn^{2+}, Mg^{2+}) display SHG responses of 0.3, 2.3, and 1.4 times that of KDP, respectively, whereas no obvious SHG signal was detected for the Mn phase. Furthermore, the Zn and Mg compounds are found to be phase matchable.

One compound in the A–Ln(II)–IO_3 system is reported by Prof. Halasyamani, namely, $NaY(IO_3)_4$ [42]. Colorless crystals of $NaY(IO_3)_4$ were obtained by the reactions of Na_2CO_3 (2 mmol), Y_2O_3 (1 mmol), and HIO_3 (22.7 mmol) combining

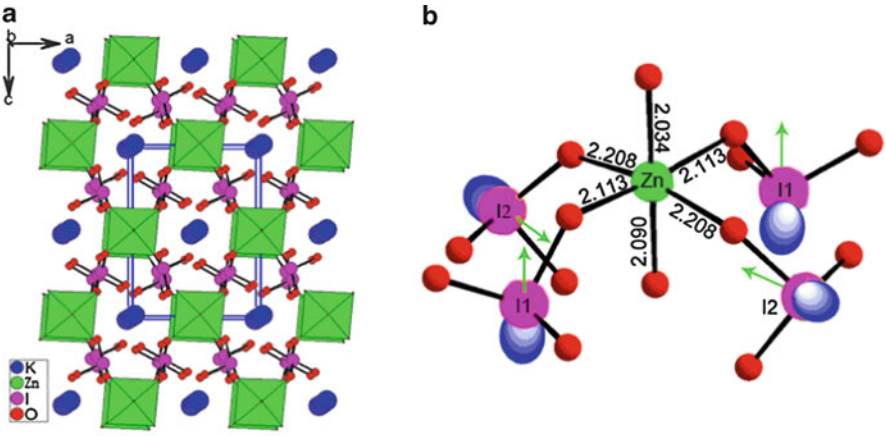

Fig. 14 (**a**) View of structure of $K_2Zn(IO_3)_4(H_2O)_2$ down the *b*-axis; (**b**) a 0D $[Zn(IO_3)_4(H_2O)_2]^{2-}$ unit, lone pairs (*blue ellipsoids*) as well as the local moments (*green arrows*), ZnO_6 octahedra are shaded in *green*

with 10 mL of H_2O at 220°C for 4 days. $NaY(IO_3)_4$ crystallizes in polar space group *Cc* and exhibits a two-dimensional (2D) layered structure consisting of YO_8 polyhedra linked to asymmetric IO_3 and IO_4 polyhedra. The connectivity of YO_8 and iodate polyhedra within each 2D layer generates 1D tunnels of eight-membered-ring (8-MRs) along the [010] direction which are occupied by the Na^+ cations. SHG measurements indicate that $NaY(IO_3)_4$ shows a large SHG response of about 300 × α-SiO_2.

Compounds with just IO_3 groups as the asymmetric inorganic building unit can also afford new NLO materials with SHG properties, but they trend to display a weak SHG response and most of such compounds are more prone to be centrosymmetric.

3 Selenites or Tellurites Containing d^0 Transition Metal Ions or Halogen Anions or Tetrahedral Groups of Main Group Elements

Metal selenites and tellurites are also a class of very important compounds, especially in nonlinear optical applications [34, 39]. Metal selenites and tellurites that display SHG properties are listed in Table 2. Recently, Tao and Halasyamani groups have also grown the large single crystals for several metal tellurites [35, 36, 85, 86]. In this part, our discussion will be focused on three systems: metal selenites and tellurites containing either d^0 transition metal (TM) ions, or halogen anions, or tetrahedral units of p-block main group elements.

3.1 Combination of d^0 Transition Metal Ions with Selenites or Tellurites

The number of compounds in these systems is much more than that of corresponding metal iodates. Different from metal iodates, the counterions in these compounds have much stronger effects on the SHG properties of the compounds formed. For example, alkali (or alkaline earth) compounds can display excellent second order NLO properties but lanthanide(III) compounds are usually not SHG active due to the high coordination number of Ln(III) ions. Hence, we will classify these compounds in terms of the counterions [15].

3.1.1 Alkali (or Alkaline Earth)-d^0 TM–Se(IV)/Te(IV)–O System

A large number of compounds in the Alkali (or Alkaline Earth)-d^0 TM–Se(IV)/Te(IV)–O systems were reported, some of which possess good SHG properties (Table 2). The transition metal ions with d^0 electronic configuration are mostly Mo^{6+}, W^{6+}, and V^{5+}, although some examples of Nb^{5+} and Ta^{5+} have also been isolated.

Seven compounds with five different structural types were reported in alkali metal-molybdenum(VI)–selenium(IV) oxide systems, A_2MoSeO_6 (A = Na^+, K^+, Rb^+), and $A_2(MoO_3)_3(SeO_3)$ (A = NH_4^+, Cs^+, Rb^+ and Tl^+) [50, 53, 60].

Colorless crystals of the first three compounds were synthesized by solid-state reactions of stoichiometric amounts of SeO_2 and A_2MoO_4 (A = Na^+, K^+, or Rb^+) at 370°C for 1 day. Na_2MoSeO_6 crystallized in an NCS space group $P2_13$, its structure features a 3D anionic network based on alternative linkage of MoO_6 octahedra (distorted toward a face) and SeO_3 groups, forming tunnels of Mo_2Se_2 four-member rings, and Mo_4Se_4 eight-member rings. The sodium cations are located at the larger tunnels. Na_2MoSeO_6 revealed a weak SHG intensity of about 10 × α-SiO_2. The SHG intensity can be attributed to the polarizations from the SeO_3 and MoO_6 groups. K_2MoSeO_6 ($P2_1/c$) and Rb_2MoSeO_6 ($Pnma$) crystallized in CS space group and are not SHG active [60].

Light yellow crystals of $A_2(MoO_3)_3(SeO_3)$ (A = NH_4^+ Cs^+, Rb^+ and Tl^+) were obtained by hydrothermal reactions of $(NH_4)_6Mo_7O_{24}{\cdot}4H_2O$ and SeO_2 at 200°C or Cs_2CO_3 (or Rb_2CO_3, Tl_2CO_3), SeO_2 and MoO_3 at 230°C for 2–3 days. $A_2(MoO_3)_3(SeO_3)$ (A = NH_4^+ Cs^+ and Rb^+) ($P6_3$, NCS) and $Tl_2(MoO_3)_3(SeO_3)$ ($P3_1c$, NCS) are polar and their structures all feature a 2D hexagonal tungsten bronze-like anionic layer of MoO_6 octahedra capped on one side by SeO_3^{2-} anions (Fig. 15). The lone pairs of the selenite groups are aligned in the same direction to produce a large macroscopic dipole moment along the *c*-axis. SHG measurements revealed that $A_2(MoO_3)_3(SeO_3)$ (A = NH_4^+ Cs^+, Rb^+, and Tl^+) display a large SHG response of about 400, 350, 300, and 400 × α-SiO_2, respectively [50, 53].

Five compounds with three different structural types have been isolated in the alkali metal–molybdenum(VI)–tellurium(IV) oxide systems, namely, $Na_2Mo_3Te_3O_{16}$, $A_2Mo_3TeO_{12}$ (A = NH_4, Cs), and $A_4Mo_6Te_2O_{24}{\cdot}6H_2O$ (A = Rb, K) [54, 57]. Colorless bar-shaped crystals of $Na_2Mo_3Te_3O_{16}$ were synthesized hydrothermally from a

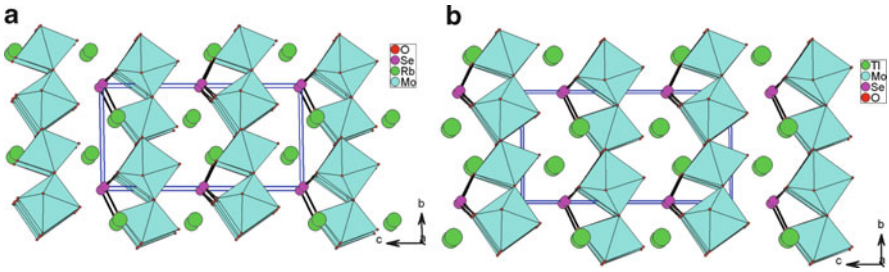

Fig. 15 View of structure of $Rb_2(MoO_3)_3(SeO_3)$ (**a**) and $Tl_2(MoO_3)_3(SeO_3)$ (**b**) along *a*-axis

mixture of Na_2TeO_3 and MoO_3 in H_2O at 220°C for 2 days. $Na_2Mo_3Te_3O_{16}$ crystallized in *NCS* space group *I*2 and its structure exhibits a quasi-one-dimensional crystal structure. Within the chain Mo_3O_{14} trimers composed of three edge-shared MoO_6 octahedra are interconnected by $Te_3O_8^{4-}$ anions each consisted of one TeO_4 group corner-sharing with two TeO_3 groups (Scheme 1a). Both Mo^{6+} and Te^{4+} cations are in the asymmetric coordination environments attributable to SOJT effects. The Mo^{6+} cations are distorted toward an edge of the MoO_6 octahedron (local C_2 direction). The polarization directions of the two TeO_3 groups are opposite but the lone pairs of the TeO_4 groups are aligned in the same direction to produce a large macroscopic dipole moment along the *b*-axis (Fig. 16). SHG measurements revealed that $Na_2Mo_3Te_3O_{16}$ displays a very large SHG response of about 500 × α-SiO_2 and is phase matchable. The strong SHG efficiency is maintained up to the melting temperature (around 450°C) [57].

Use of other alkali metal ions led to the discovery of two other structural types. $A_2Mo_3TeO_{12}$ (A = NH_4^+ and Cs^+) and $A_4Mo_6Te_2O_{24}{\cdot}6H_2O$ (A = Rb, K) were obtained by hydrothermal reactions of $(NH_4)_6Mo_7O_{24}{\cdot}4(H_2O)$ (or K_2CO_3, Rb_2CO_3, Cs_2CO_3, and MoO_3) and TeO_2 at 225°C. $A_2Mo_3TeO_{12}$ (A = NH_4^+ and Cs^+) ($P6_3$, NCS) are isostructural to $A_2(MoO_3)_3(SeO_3)$ (A = NH_4^+ and Cs^+), and their structures feature a 2D hexagonal tungsten oxide related $(Mo_3TeO_{12})^{2-}$ anionic layers that are separated by NH_4^+ or Cs^+ ions. The TeO_3 groups caps on the same side of the anionic layer in the same direction, resulting in a large macroscopic dipole moment along the *c*-axis. SHG measurements revealed that they display a large SHG response of about 400 × α-SiO_2 [54]. It is worthy to mention that large single crystals of $Cs_2Mo_3TeO_{12}$ with dimensions up to 20 × 20 × 16 mm^3 were grown successfully through a top-seeded solution growth (TSSG) method using a TeO_2–MoO_3 mixture as a self-flux by Tao's group [85]. $A_4Mo_6Te_2O_{24}{\cdot}6H_2O$ (A = Rb and K) ($P2_1/c$, CS) composed of discrete centrosymmetric $(Mo_6Te_2O_{24})^{4-}$ anionic aggregates and alkali metal ions. The hexamolybdoditellurite anion is centrosymmetric and formed by six edge-sharing MoO_6 octahedra further capped by two tellurite groups from both sides [87].

Three types of compounds were found in the alkali metal–tungsten(VI)–tellurium (IV) oxide systems, namely, $(NH_4)_2WTe_2O_8$ [59], $Na_2W_2TeO_9$ [39], and $A_2W_3TeO_{12}$ (A = K^+, Rb^+ and Cs^+) [56]. These compounds were synthesized hydrothermally from a mixture of AOH (A = NH_4, Na, K, Rb, or Cs), WO_3, and TeO_2 at 230 or 470°C.

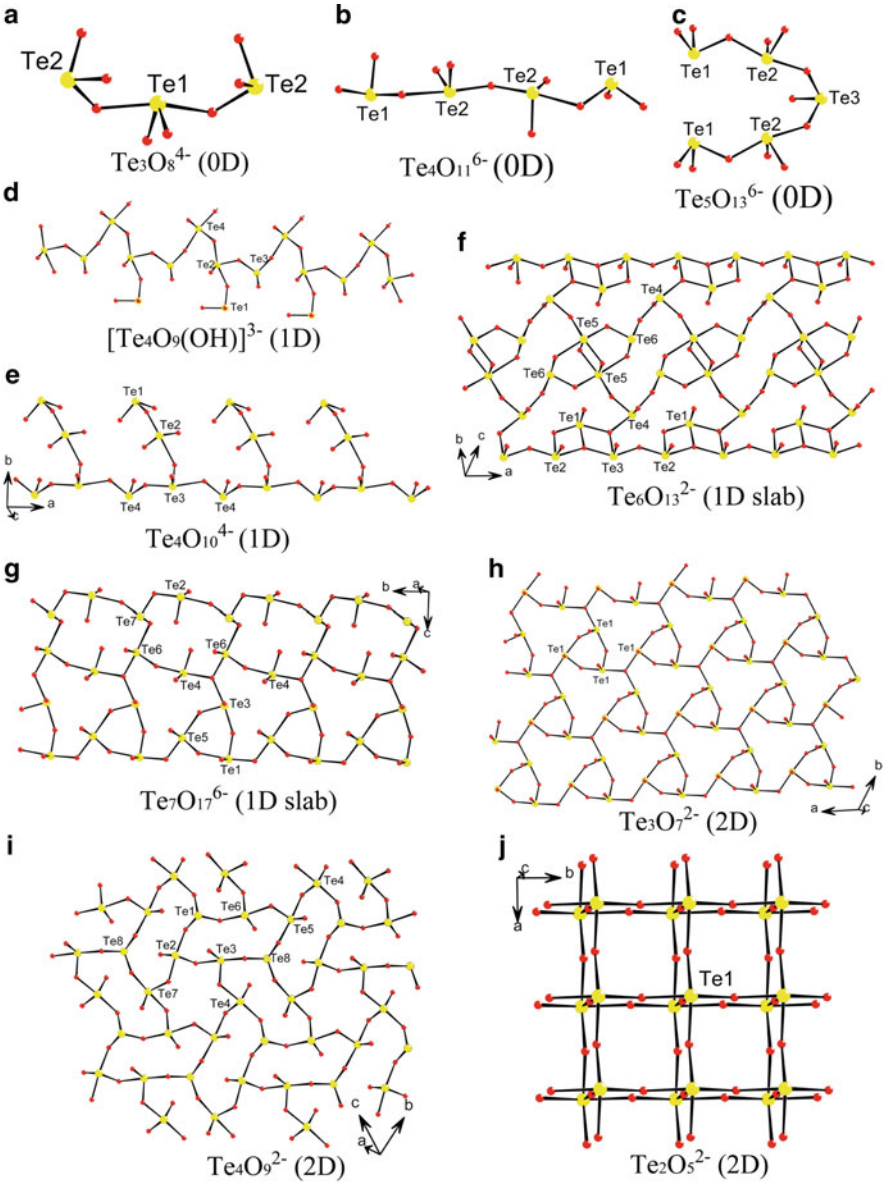

Scheme 1 Selected examples of tellurium(IV) oxide anions with polynuclear cluster units or extended structures

$(NH_4)_2WTe_2O_8$ crystallizes in the NCS polar space group $P2_1$. It exhibits a 2D layered structure consisting of WO_6 octahedra and TeO_4 polyhedra with the ammonium cations located at the interlayer region. Within the structure, the polarizations of

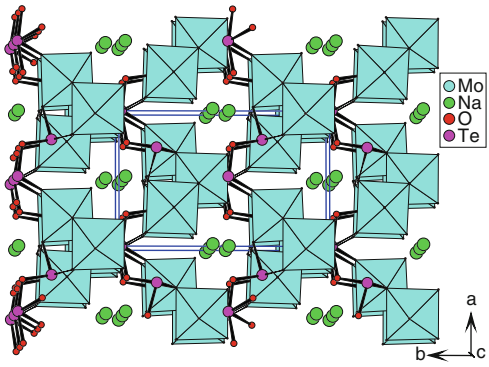

Fig. 16 View of structure of $Na_2Mo_3Te_3O_{16}$ along *c*-axis

$Te(1)O_4$ groups are toward almost opposite directions and cancel out each other but those of $Te(2)O_4$ and WO_6 polyhedra are almost aligned along the *b*-axis to produce a large net dipole moment. SHG measurements revealed that $(NH_4)_2WTe_2O_8$ displays a moderate SHG efficiency of approximately 250 × α-SiO_2 [59].

The NCS $Na_2W_2TeO_9$ (space group *Ia*) exhibits a 3D structure comprising distorted WO_6 octahedra linked by asymmetric TeO_3 groups (Fig. 17). The WO_6 octahedra form a corrugated 2D tungsten oxide layer through corner sharing, and these layers are further interconnected by bridging TeO_3 groups. Both Te(IV) and W(VI) cations are in local acentric environments attributable to the SOJT effects. Powder SHG measurements on polycrystalline $Na_2W_2TeO_9$ revealed a strong SHG intensity of approximately 500 × α-SiO_2 and the material is also phase matchable (Type I) [39].

$Cs_2W_3TeO_{12}$ ($P6_3$, NCS) is isostructural with $Cs_2Mo_3TeO_{12}$ [54]. Although $K_2W_3TeO_{12}$ ($P2_1/n$, CS) and $Rb_2W_3TeO_{12}$ ($P3_1c$, NCS) have a similar chemical formula to $Cs_2W_3TeO_{12}$, their structures are somehow different. All three compounds feature a same 2D tungsten oxide layer of corner-sharing WO_6 octahedra with W_3 and W_6 rings. The TeO_3 groups in $K_2W_3TeO_{12}$ act as interlayer linkers to form a 3D structure. In Rb and Cs phases, the TeO_3 groups only cap on the same side of the W_3 rings; therefore, they remain 2D. In the structure of $Rb_2W_3TeO_{12}$, the polarization directions of TeO_3 groups are almost aligned along the *c*-axis to produce a large net

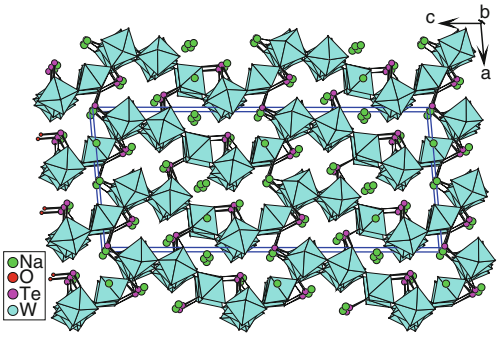

Fig. 17 View of structure of $Na_2W_2TeO_9$ along *b*-axis

dipole moment. SHG measurements revealed that the Rb and Cs compounds display strong SHG efficiencies of 200 and 400 × α-SiO_2, respectively [56]. Two tungsten (VI) selenite analog of $Cs_2W_3TeO_{12}$ were also reported, namely, $A_2(WO_3)_3(SeO_3)$ (A = NH_4, Cs), both of which show strong SHG efficiency of 200 × α-SiO_2 [55].

The Ae^{2+}–Mo^{6+}(W^{6+})–Se^{4+}(Te^{4+})–O systems are still less explored. Two compounds in the Ba–Mo(VI)–Se(IV)–O system were reported, namely, $BaMoO_3(SeO_3)$ and $BaMo_2O_5(SeO_3)_2$ [88]. Both compounds were synthesized hydrothermally from a solution of $BaCO_3$ or $Ba(OH)_2{\cdot}8H_2O$, MoO_3, and SeO_2 at 180°C for 4–5 days. $BaMoO_3(SeO_3)$ ($P2_1/c$, CS) exhibits a layered structure in which MoO_6 octahedra (distorted toward a face) are bridged by SeO_3 groups, forming Mo_2Se_2 four-member rings and Mo_3Se_3 six-member rings. $BaMo_2O_5(SeO_3)_2$ is polar ($Cmc2_1$) and features a 3D network composed of pairs of corner-sharing MoO_6 octahedra bridged by SeO_3 groups. The MoO_6 octahedron is distorted toward an edge (the local C_2 direction). Although $BaMo_2O_5(SeO_3)_2$ crystallizes in a polar space group, the polarizations from SeO_3 and MoO_6 polyhedra are almost cancel out each other [88].

$BaMo_2TeO_9$ and BaW_2TeO_9 were synthesized by solid-state reactions of stoichiometric amounts of Ba_2CO_3, MoO_3 (or WO_3), and TeO_2 at 560 or 760°C [34]. The two compounds are isostructural and crystallized in the polar space group $P2_1$. Their structures feature an anionic layer composed of MO_6 octahedra linked by the asymmetric TeO_3 polyhedra (Fig. 18). The MoO_6 octahedra in $BaMo_2TeO_9$ are distorted toward a face (along the local C_3 direction) with three short and three long Mo–O distances, whereas the WO_6 octahedra in BaW_2TeO_9 exhibit two types of distortions: toward a face as discussed above as well as toward an edge with two short, two normal, and two long W–O bonds. A pairs of MO_6 octahedra form a dimer via an M–O–M bridge and such dimeric units are further interconnected by TeO_3 groups via M–O–Te bridges. $BaMo_2TeO_9$ and BaW_2TeO_9 revealed extremely strong SHG responses of 600 and 500 × α-SiO_2, respectively [34]. Large crystals of $BaTeMo_2O_9$ with size up to 30 × 23 × 18 mm^3 and good optical quality were grown from the TeO_2–MoO_3 flux system, and their physical properties such as refractive indices, the principal thermal expansion, and thermal conductivity coefficients have been measured by the Tao's group [35, 36].

Several phases were reported in A–V^{5+}–Se^{4+}–O system, namely, $A(VO_2)_3(SeO_3)_2$ (A = K^+, Rb^+, Cs^+, Tl^+, NH_4^+), $AVSeO_5$ (A = Rb, Cs) and a V^{5+}/V^{4+} mixed valent

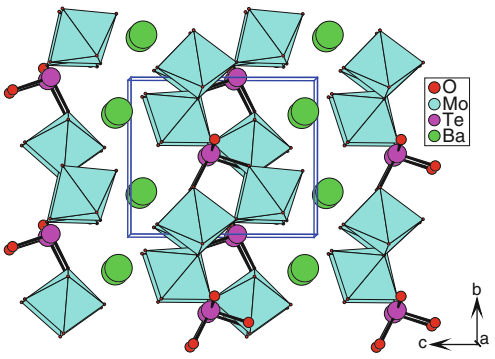

Fig. 18 View of structure of $BaMo_2TeO_9$ along *a*-axis

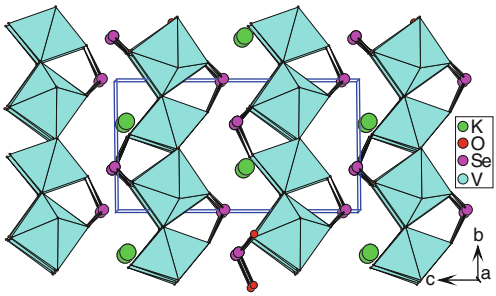

Fig. 19 View of structure of $K(VO_2)_3(SeO_3)_2$ along *a*-axis

KV_2SeO_7 [51, 89–91]. All of them were obtained by hydrothermal reactions. $A(VO_2)_3(SeO_3)_2$ ($A = K^+$, Rb^+, Cs^+, Tl^+, NH_4^+) ($P6_3$, NCS) are isostructural and exhibit layered hexagonal tungsten oxide (HTO)-type topologies consisting of corner-shared VO_6 octahedra that are capped by SeO_3 polyhedra on both sides [51, 89, 90]; such HTO layers are similar to those in $A_2(MoO_3)_3(SeO_3)$ ($A = NH_4^+$, Rb^+ and Cs^+) [53]. However, the 2D layer in the latter only capped by the SeO_3 groups on one side of the layer. Furthermore, the interlayer distances in the vanadium phases are much shorter than those of the corresponding molybdenum(VI) compounds due to the fact that much fewer countercations are needed to balance the charge. Different from those in the Mo(VI) selenites, the polarization directions of the SeO_3 groups in $A(VO_2)_3(SeO_3)_2$ ($A = K^+$, Rb^+, Cs^+, NH_4^+) are almost opposite each other and their local moments are mostly cancelled out (Fig. 19). SHG measurement revealed that $A(VO_2)_3(SeO_3)_2$ ($A = K^+, Rb^+, Cs^+, NH_4^+$) display weak SHG efficiencies of about 45, 40, 40, and 40 × α-SiO_2, respectively [50]. Only one tellurite analog of $A(VO_2)_3(SeO_3)_2$ was also reported, namely, $Cs(VO_2)_3(TeO_3)_2$, which shows a weak SHG efficiency of 40 × α-SiO_2 [50, 52].

The structure of the polar $AVSeO_5$ (A = Rb, Cs) (space group $P2_1$) is a 3D anionic network formed by alternative linkage of VO_5 square pyramids and SeO_3 groups via corner sharing, forming two types of helical tunnels along *b*-axis composed of four-member rings and eight-member rings, respectively. The alkali metal ions are located at the large tunnels. KV_2SeO_7 contains both V^{5+} and V^{4+} ions, with an octahedral and tetrahedral coordination environment, respectively. Its structure features a double layer of $\{V_2SeO_7\}^-$ composed of corner-sharing VO_6 octahedra, VO_4 tetrahedra, and SeO_3 groups [91].

Only three compounds were reported for the alkaline earth–V(V)–Se(IV)/Te(IV)–O family before our group's further explorations of these systems, namely, BaV_2TeO_8 [92], $Ba_{2.5}(VO_2)_3(SeO_3)_4{\cdot}3H_2O$ [93], and $Ba(VO_2)(SeO_3)_2(HSeO_3)$ [94]. Our efforts in alkaline earth–V^V/V^{IV}–Se^{IV}/Te^{IV}–O systems afforded six new compounds, namely, $Sr_2(VO)_3(SeO_3)_5$, $Sr(V_2O_5)(TeO_3)$, $Sr_2(V_2O_5)_2(TeO_3)_2(H_2O)$, $Ba_3(VO_2)_2(SeO_3)_4$, $Ba_2(VO_3)Te_4O_9(OH)$, $Ba_2V_2O_5(Te_2O_6)$ [95]. They exhibit six different types of structures.

The six alkaline earth metal vanadium selenites or tellurites were prepared by hydrothermal reactions of $SrCO_3$ (or $Ba(OH)_2{\cdot}8H_2O$ or $BaCO_3$), SeO_2 (or TeO_2), and V_2O_5 in different molar ratios at 230°C. During the preparation of

$Sr_2(VO)_3(SeO_3)_5$, the V^{5+} ion in V_2O_5 was reduced to an oxidation state of +4 by excess SeO_2. The structure of $Sr_2(VO)_3(SeO_3)_5$ (*P*nma, CS) features a 3D anionic network of $[(VO)_3(SeO_3)_5]^{4-}$ with 1D 8-MR tunnels along the *b*-axis, half of which are filled by Sr^{2+} ions. Within the structure, both $V(1)O_6$ and $V(2)O_6$ octahedra are distorted toward a corner (local C_4 direction) resulting one "short," four "normal," and one "long" V–O bonds. Neighboring $V(1)O_6$ octahedra are bridged by the $Se(2)O_3$ group via edge- and corner-sharing into a 1D zigzag chain along the *c*-axis, whereas two neighboring $V(2)O_6$ octahedra are bridged by a pair of $Se(1)O_3$ groups via corner sharing into a 1D chain along the *b*-axis with the $Se(3)O_3$ hanging on the chain. The intergrowth of the above two types of 1D chains resulted in a 3D anionic framework with two types of 1D 8-MR tunnels running along the *b*-axis. Half of these tunnels are occupied by the lone pairs of Se(IV) atoms, whereas the remaining tunnels are filled by Sr^{2+} ions.

Single crystals of $Sr(V_2O_5)(TeO_3)$ (as minor phase) and $Sr_2(V_2O_5)_2(TeO_3)_2(H_2O)$ (as main phase) were isolated from the same reaction. The structure of $Sr(V_2O_5)(TeO_3)$ (*P*-1, CS) features novel vanadium(V) tellurite chains in which V_2O_7 and V_2O_8 dimers are bridged by both TeO_4 and TeO_3 groups. Such structure differs from that of BaV_2TeO_8 with a similar chemical formula. BaV_2TeO_8 features a 1D chain composed of VO_4 tetrahedra and dimers of edge-sharing VO_5 square pyramids bridged by solely TeO_4 groups, forming 1D tunnels of 8-MRs each composed of two VO_4 tetrahedra, two VO_5 square pyramids, and four TeO_4 groups. The structure of $Sr_2(V_2O_5)_2(TeO_3)_2(H_2O)$ (*C*2/c, CS) features a 2D layer consisting of linear $[V_4O_{14}]$ tetramers bridged by TeO_3^{2-} anions with Sr^{2+} ions and water molecules located at the interlayer space. A pair of the $V(1)O_5$ form a V_2O_8 dimer via edge sharing. The V_2O_8 dimer is further attached by a $V(2)O_4$ tetrahedron via corner sharing on each side so as to form a linear $[V_4O_{14}]$ tetramer. Neighboring $[V_4O_{14}]$ clusters are bridged by TeO_3^{2-} groups via V–O–Te bridges into a 2D layer parallel to the *bc* plane. The structures of $Sr(V_2O_5)(TeO_3)$ and $Sr_2(V_2O_5)_2(TeO_3)_2(H_2O)$ are totally different; therefore, we failed to convert $Sr_2(V_2O_5)_2(TeO_3)_2(H_2O)$ into $Sr(V_2O_5)(TeO_3)$ by removal of a H_2O molecule.

When $Ba(OH)_2{\cdot}8H_2O$ (or $BaCO_3$) was used instead of $SrCO_3$ as the counter ions, three barium vanadium selenites or tellurites were isolated. $Ba_3(VO_2)_2(SeO_3)_4$ was obtained by hydrothermal reactions of $Ba(OH)_2{\cdot}8H_2O$ (1.0 mmol), V_2O_5 (0.4 mmol), and SeO_2 (1.0 mmol) at 230°C for 4 days. The structure of $Ba_3(VO_2)_2(SeO_3)_4$ ($P2_1$/n, CS) exhibits 0D $[(VO_2)(SeO_3)_2]^{3-}$ anions that are separated by Ba^{2+} ions. Each VO_5 square pyramid is connected to one SeO_3^{2-} anion via edge sharing and another selenite group via corner sharing, resulting in the formation of a 0D $[(VO_2)(SeO_3)_2]^{3-}$ anion. It is interesting to note that both $Ba_3(VO_2)_2(SeO_3)_4$ and $Ba_{2.5}(VO_2)_3(SeO_3)_4{\cdot}3H_2O$ are structurally based on VO_5 and SeO_3 polyhedra, but their structures are quite different. $Ba_{2.5}(VO_2)_3(SeO_3)_4{\cdot}3H_2O$ features a layered structure in which VO_5 polyhedra are interconnected by both bidentate and tridentate SeO_3 groups, forming tunnels of V_4Se_4 8-MRs and V_6Se_6 12-MRs. In $Ba_3(VO_2)_2(SeO_3)_4$, two selenite anions are bidentate chelating whereas the other two are unidentate; hence, the compound displays a much lower dimensionality.

$Ba_2(VO_3)Te_4O_9(OH)$ was obtained by heating a mixture of $Ba(OH)_2{\cdot}8H_2O$ (0.5 mmol), V_2O_5 (0.2 mmol) and TeO_2 (1.0 mmol) at 230°C for 4 days. The structure of $Ba_2(VO_3)Te_4O_9(OH)$ ($P2_1/n$, CS) exhibits a novel 1D $[Te_4O_9(OH)]^{3-}$ chain decorated by VO_4 tetrahedra with the Ba^{2+} located at the interchain space. $Te(2)O_4$ and $Te(4)O_4$ groups form a Te_2O_7 dimer via corner sharing; such dimers are further bridged by $Te(3)O_3$ polyhedra via corner sharing into a 1D tellurium(IV) oxide chain along the *b*-axis. The $Te(1)O_3$ groups are hanging on the same side of the chain through Te(1)–O(3)–Te(2) bridges, resulting in a 1D $[Te_4O_9(OH)]^{3-}$ chain (Scheme 1d). The discrete VO_4 tetrahedra are attached on the $Te(1)O_3$ groups via corner sharing.

$Ba_2V_2O_5(Te_2O_6)$ was obtained by heating a mixture of $Ba(OH)_2{\cdot}8H_2O$ (0.3 mmol), $NaVO_3{\cdot}2H_2O$ (1.0 mmol), and TeO_2 (1.0 mmol) at 230°C for 4 days. The structure of $Ba_2V_2O_5(Te_2O_6)$ ($P2_1/m$, CS) features a 1D vanadium (V) tellurites chain in which the VO_4 tetrahedra are interconnected by the $[Te_2O_6]^{4-}$ dimers with the Ba^{2+} ions acting as the counter ions. A pair of TeO_4 tetrahedra are interconnected into a $[Te_2O_6]^{4-}$ anion via edging sharing. $V(1)O_4$ tetrahedra are bridged by $[Te_2O_6]^{4-}$ anions into a 1D zigzag chain along the *b*-axis. The $V(2)O_4$ tetrahedra are grafted into the chain on the same side. Each $[Te_2O_6]^{4-}$ anion acts as a tridentate ligand and bridges to three $V(1)O_4$ tetrahedra.

These compounds display six different types of anionic structures, including 0D $[(VO_2)(SeO_3)_2]^{3-}$ anion, three different types of 1D vanadium(V) tellurite chains, 2D $[(V_2O_5)_2(TeO_3)_2]^{4-}$ layer, and 3D $[(VO)_3(SeO_3)_5]^{4-}$ (Fig. 20). The richness of

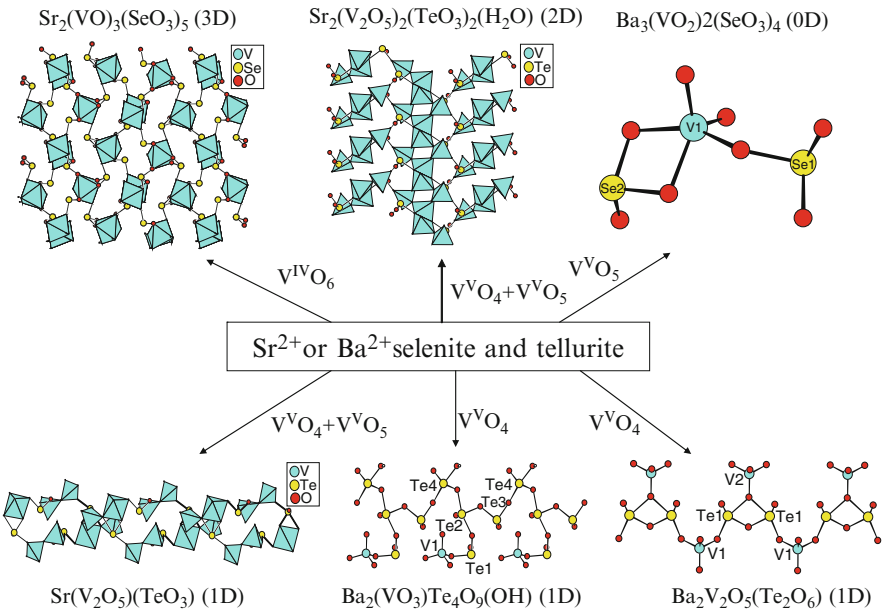

Fig. 20 View of the six different types of anionic structures in Ba^{II}/Sr^{II}–V^{V}/V^{IV}–Se^{IV}/Te^{IV}–O systems

the structure type for the vanadium tellurites or selenites can be attributed to the various coordination geometries available for the vanadium(V) cation and various coordination modes the tellurite and selenite anions can adopt [95].

Reports on A(Ae)–Nb^{5+}(or Ta^{5+})–Se^{4+}(or Te^{4+}) oxides are still rare. Only four types of structures were reported before our group's work, namely, $Na_{1.4}Nb_3Te_{4.9}O_{18}$, $NaNb_3Te_4O_{16}$, $Ba_2M_6Te_2O_{21}$ (M = Nb, Ta), and $BaMTeO_4(PO_4)$ (M = Nb, Ta) [96–98]. Our exploratory efforts in the alkali metal–Nb^V/Ta^V–Se^{IV}/Te^{IV}–O systems afford six new compounds with two different types of structures, namely, $KNb_3O_6(TeO_3)_2$, $KTa_3O_6(TeO_3)_2$, $RbNb_3O_6(TeO_3)_2$, $RbTa_3O_6(TeO_3)_2$, $KNb_3O_6(SeO_3)_2$, and $Cs_3Nb_9O_{18}(TeO_3)_2(TeO_4)_2$ [99]. These compounds were synthesized by standard solid-state reactions of KBr (or Rb_2CO_3 or Cs_2CO_3), Nb_2O_5 (or Ta_2O_5) and TeO_2 (or SeO_2) at 720–840°C for 4–6 days.

$KNb_3O_6(TeO_3)_2$, $KTa_3O_6(TeO_3)_2$, $RbNb_3O_6(TeO_3)_2$, $RbTa_3O_6(TeO_3)_2$, and $KNb_3O_6(SeO_3)_2$ are isostructural. Their structures (*P*bcm, CS) feature a novel 3D anionic network based on 2D layers of the corner-sharing NbO_6 or TaO_6 octahedra further bridged by TeO_3 or SeO_3 polyhedra, forming 1D tunnels of 4- and 6-MRs along the *a*-axis. The lone pair of the Te(IV) or Se(IV) atoms are orientated toward the center of the 4-MR tunnels, whereas the alkali cations are located at the 6-MR tunnels. Let us take $KNb_3O_6(TeO_3)_2$ as a representative to discuss the 3D network in more detail. Nb(2)O_6 octahedra are interconnected via corner sharing into a double chain along the *a*-axis, whereas Nb(1)O_6 octahedra are interconnected via corner sharing into a single chain along the *a*-axis. The above two types of 1D chains are alternate and interconnected via corner sharing along the *c*-axis, resulting in the formation of a corrugated niobium oxide layer parallel to the *ac* plane. Neighboring niobium oxide layers are bridged by TeO_3 groups into a 3D anionic network, forming 1D tunnels of 4- and 6-MRs along the *a*-axis. There are two types of 4-MRs tunnels, based on Te_2Nb_2 rings and Nb_3Te rings, respectively. The 6-MR tunnels are based on solely Nb_4Te_2 rings.

It is interesting to compare the structure of $ANb_3O_6(TeO_3)_2$ (A = K, Rb) with those of $Na_{1.4}Nb_3Te_{4.9}O_{18}$ and $NaNb_3Te_4O_{16}$ [96]. All three structures are based on NbO_6 octahedra connected by TeO_3 groups (or/and TeO_4 groups). Both $Na_{1.4}Nb_3Te_{4.9}O_{18}$ and $NaNb_3Te_4O_{16}$ feature 1D chains of corner sharing NbO_6 octahedra, whereas the structure of $KNb_3O_6(TeO_3)_2$ is based on 2D layers of corner-sharing NbO_6 octahedra. The Te(IV) cations in $KNb_3O_6(TeO_3)_2$ are all in distorted trigonal pyramidal environments, whereas additional TeO_4 groups with a "seesaw" geometry are present in $Na_{1.4}Nb_3Te_{4.9}O_{18}$, and $NaNb_3Te_4O_{16}$.

$Cs_3Nb_9O_{18}(TeO_3)_2(TeO_4)_2$ exhibits a different structure from those of the above five compounds. The structure of $Cs_3Nb_9O_{18}(TeO_3)_2(TeO_4)_2$ (*C*mcm, CS) features a novel 2D Nb–Te–O layer in which layer of corner-sharing NbO_6 octahedra is further decorated by asymmetric TeO_3 groups and 1D chains of corner-sharing TeO_4 polyhedra. Nb(1)O_6 octahedra are interconnected via corner sharing into a 1D chain along the *c*-axis, so are Nb(3)O_6 and Nb(5)O_6 octahedra. Nb(4)O_6 and Nb(2)O_6 octahedra form a linear Nb_4O_{21} tetramer via corner sharing. The above corner-sharing NbO_6 octahedral chains were interconnected by the linear Nb_4O_{21} tetramers via corner sharing into a thick Nb–O layer parallel to the *bc*-plane, forming 1D

tunnels of 6-MRs along the *c*-axis. The thickness of the niobium oxide layer is about 19.3 Å. The TeO_3 polyhedra and the 1D chains of corner-shared TeO_4 groups are grafted on the thick 2D Nb–O layer to form a Nb–Te–O layer, leaving virtually no free interlayer space. The Cs^+ cations are located at the 1D 6-MR tunnels. It is interesting to compare the structure of $Cs_3Nb_9O_{18}(TeO_3)_2(TeO_4)_2$ with that of $BaNbO_4Te(PO_4)$ [98]; both have layered anionic structures. The niobium oxide skeleton in $Cs_3Nb_9O_{18}(TeO_3)_2(TeO_4)_2$ is a 2D, whereas that in $BaNbO_4Te(PO_4)$ is a simple 1D chain.

These results indicate that metal selenites or tellurites containing V^{5+}, Nb^{5+}, or Ta^{5+} also display rich structure chemistry as those of Mo^{6+} and W^{6+}.

3.1.2 Ln-d^0 TM–Se(IV)/Te(IV)–O System

A lot of works have been done in Ln-d^0 TM–Se(IV)/Te(IV)–O system, mainly by the Halasyamani group and our group. The transition metal ions with d^0 electronic configuration used include Mo(VI), W(VI), and V(V) ions. The Halasyamani group reported three compounds, namely, $LaNbTeO_6$ and $La_4M_2Te_6O_{23}$ (M = Nb or Ta) [100]. We systematically explored the lanthanide selenium(IV) or tellurium(IV) oxides with additional transition metal ions with d^0-electronic configuration in our attempts to find new lanthanide SHG materials. Solid-state reactions of lanthanide(III) oxide (or/and lanthanide(III) oxychloride), MoO_3 (or WO_3) and TeO_2 at high temperature led to twelve new compounds with eight different types of structures, namely, $Nd_2MoSe_2O_{10}$, $Gd_2MoSe_3O_{12}$, $La_2MoTe_3O_{12}$, $Nd_2MoTe_3O_{12}$, $Ln_2MoTe_4O_{14}$ (Ln = Pr, Nd), $La_2WTe_6O_{18}$, $Nd_2W_2Te_2O_{13}$, and $Ln_5MTe_7O_{23}Cl_3$ (Ln = Pr, Nd; M = Mo, W) [101, 102]. Hydrothermal reactions of lanthanide(III) oxide (or/and lanthanide(III) chloride), MoO_3 (or V_2O_3) and SeO_2 at 200 or 230°C led to nine new compounds with four different types of structures, namely, $Nd_2(V_2O_4)(SeO_3)_4{\cdot}H_2O$, $Ln(VO_2)(SeO_3)_2$ (Ln = Eu, Gd, Tb), $H_3Ln_4Mo_{9.5}O_{32}(SeO_3)_4(H_2O)_2$ (Ln = La, Nd,), and $Ln_2Mo_3O_{10}(SeO_3)_2(H_2O)$ (Ln = Eu, Dy, Er) [103, 104].

Light purple phase of $Nd_2MoSe_2O_{10}$ was obtained by heating a mixture of Nd_2O_3 (0.6 mmol), MoO_3 (0.6 mmol), and SeO_2 (1.2 mmol) at 700°C for 6 days. $Nd_2MoSe_2O_{10}$ (*P*-1, CS) can also be formulated as $Nd_2(MoO_4)(SeO_3)_2$. Its structure features a 3D network in which the Nd(III) ions are interconnected by SeO_3^{2-} anions and MoO_4 tetrahedra. The interconnection of Nd(1) atoms via bridging selenite groups lead to a ⟨001⟩ layer, whereas Nd(2) atoms are bridged by MoO_4 tetrahedra to form a ⟨002⟩ layer. The above two types of layers are further interconnected via Nd–O–Se bridges into a 3D network. The lone pairs of the selenium(IV) cations are orientated to the cavities of the structure.

When Gd_2O_3 was used instead of Nd_2O_3, light yellow single crystals of $Gd_2MoSe_3O_{12}$ with a different structure were obtained. $Gd_2MoSe_3O_{12}$ (*P*-1, CS) can also be formulated as $Gd_2(MoO_3)(SeO_3)_3$, which can be considered as one O^{2-} anion of $Nd_2MoSe_2O_{10}$ being replaced by the third selenite group. The structure of $Gd_2MoSe_3O_{12}$ features a 3D network of gadolinium(III) selenite with the MoO_6 octahedra occupying the cavities of the network (Fig. 21). Unlike that in

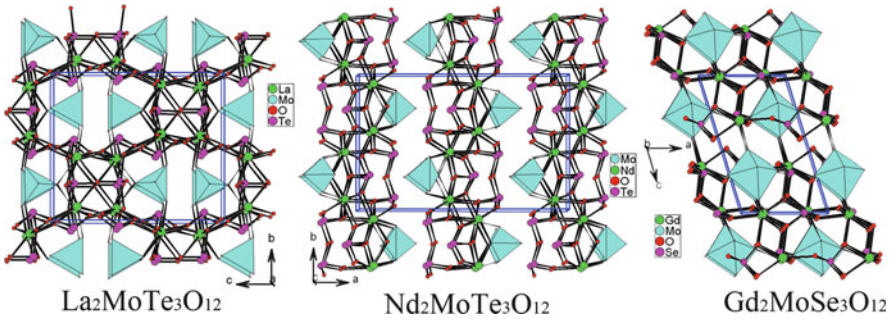

Fig. 21 View of the different structure types of $Ln_2MoTe_3O_{12}$ (Ln = La, Nd, Gd) with a similar formula

$Nd_2MoSe_2O_{10}$, the molybdenum(VI) atom in $Gd_2MoSe_3O_{12}$ is octahedrally coordinated by three oxygen atoms from three selenite groups and three O^{2-} anions. The MoO_6 octahedron is distorted toward a face (local C_3 direction), exhibiting three "long" and three "short" Mo–O bonds. The magnitude of the distortion (Δd) is calculated to be 1.492. The interconnection of the gadolinium(III) ions by selenite groups results in a 3D network with tunnels running along the *b*-axis. The MoO_6 octahedra are located at the tunnels formed by the gadolinium(III) selenite, forming Mo–O–Gd and Mo–O–Se bridges.

Colorless crystals of $La_2MoTe_3O_{12}$ were obtained by solid-state reaction of La_2O_3 (0.3 mmol), MoO_3 (0.6 mmol), and TeO_2 (1.5 mmol) in an evacuated quartz tube at 750°C for 7 days. The structure of $La_2MoTe_3O_{12}$ (*P*nma, CS) is composed of two La^{3+} ions, one MoO_4^{2-} anion, and one $Te_3O_8^{4-}$ anion. It can be considered as two selenite anions in $Nd_2MoSe_2O_{10}$ being replaced by a $Te_3O_8^{4-}$ anion. The trinuclear $Te_3O_8^{4-}$ anion is formed by one TeO_4 group corner sharing with two TeO_3 groups (Scheme 1a). The Mo(VI) cation is in a slightly distorted tetrahedral coordination geometry with the Mo–O distances ranging from 1.754(8) to 1.793(11) Å. The interconnection of the lanthanum(III) by chelating and bridging $Te_3O_8^{4-}$ anions led to a 3D network with 1D tunnels of La_6Te_4 MRs along *a*-axis. The MoO_4 polyhedra filled in the above tunnels and connected with the La^{3+} ions via Mo–O–La bridges (Fig. 21).

Light purple crystals of $Nd_2MoTe_3O_{12}$ were obtained by the solid-state reaction of a mixture of Nd_2O_3 (0.2 mmol), MoO_3 (0.6 mmol), and TeO_2 (1.2 mmol) in an evacuated quartz tube at 700°C for 6 days. $Nd_2MoTe_3O_{12}$ (*P*nma, CS) can be formulated as $Nd_2(MoO_4)(TeO_3)(Te_2O_5)$, it can also be considered as the $Te_3O_8^{4-}$ anion in $La_2MoTe_3O_{12}$ being replaced by a tellurite and a ditellurite anions. The structure of $Nd_2MoTe_3O_{12}$ features a 2D layer built by the lanthanide ions interconnected by tellurite groups and ditellurite groups, with the MoO_4 tetrahedra acting as the interlayer pendant groups (Fig. 21). The interlayer distance is about 8.85 Å [101].

Light green single crystals of $Pr_2MoTe_4O_{14}$ were obtained by the solid-state reaction of a mixture containing Pr_2O_3 (0.25 mmol), MoO_3 (0.25 mmol), and TeO_2

(1.5 mmol) in an evacuated quartz tube at 750°C for 6 days whereas light purple single crystals of $Nd_2MoTe_4O_{14}$ were prepared by heating the mixture of Nd_2O_3 (0.18 mmol), MoO_3 (0.35 mmol) and TeO_2 (1.4 mmol) at 720°C for 6 days. $Ln_2MoTe_4O_{14}$ (Ln = Pr, Nd) (*P*-1, CS) are isostructural and feature a 3D network in which the Ln(III) ions are interconnected by 1D $Te_4O_{10}^{4-}$ chains and MoO_4 tetrahedra. Therefore, $Ln_2MoTe_4O_{14}$ (Ln = Pr, Nd) can also be formulated as $Ln_2(MoO_4)(Te_4O_{10})$ (Ln = Pr, Nd). The TeO_3 and TeO_4 groups are interconnected via corner sharing into a novel 1D $Te_4O_{10}^{4-}$ anionic chain. Te(3)O_4 and Te(4)O_3 groups are interconnected via corner sharing, leading to a linear chain. Te(1)O_3 and Te(2)O_4 groups form a dimer by corner sharing. The dimers are hanging on the same side of the linear chain through corner sharing (Scheme 1e). Such 1D $[Te_4O_{10}]^{4-}$ anionic chain is very different from the 1D $[Te_4O_9(OH)]^{3-}$ anionic chain in $Ba_2(VO_3)Te_4O_9(OH)$ we discussed earlier. It is worthy to compare the structures of $Ln_2MoTe_4O_{14}$ (Ln = Pr, Nd) with those of $La_2MoTe_3O_{12}$ and $Nd_2MoTe_3O_{12}$. All four compounds contain MoO_4 tetrahedra; however, their Te–O architectures are completely different: $La_2MoTe_3O_{12}$ features discrete $Te_3O_8^{4-}$ anions, whereas $Nd_2MoTe_3O_{12}$ contains both TeO_3^{2-} anion and dimeric $Te_2O_5^{2-}$ anions, and 1D $Te_4O_{10}^{4-}$ anions are formed in $Ln_2MoTe_4O_{14}$ (Ln = Pr, Nd). $Nd_2MoTe_3O_{12}$ features a layered structure with MoO_4 tetrahedra hanging between two neighboring layers, whereas the MoO_4 tetrahedra in $La_2MoTe_3O_{12}$ are located at the tunnels of lanthanum (III) tellurium(IV) oxide. In $Ln_2MoTe_4O_{14}$ (Ln = Pr, Nd), the MoO_4 tetrahedron serves as a pillar between two lanthanide(III) tellurium(IV) oxide layers.

Colorless plate-shaped single crystals of $La_2WTe_6O_{18}$ were obtained by solid-state reaction of a mixture of La_2O_3 (0.30 mmol), WO_3 (0.60 mmol), and TeO_2 (1.5 mmol) in an evacuated quartz tube at 750°C for 6 days. $La_2WTe_6O_{18}$ (*P*-3*c*1, CS) can also be formulated as $La_2(WO_4)(Te_3O_7)_2$. The TeO_4 groups are interconnected into a $Te_3O_7^{2-}$ layer via corner sharing. Within the layer, three-member rings and "pear-shaped" six-member rings are found (Scheme 1h). The interconnection of La^{3+} ions by bridging WO_4^{2-} anions led to a 2D $[La_2WO_4]^{4+}$ layer along the *ab* plane. One $[La_2WO_4]^{4+}$ layer is sandwiched by two $Te_3O_7^{2-}$ layers into a thick layer in the *ab* plane via La–O–Te bridges. The thickness of the layer is about 7.65 Å and the width of the interlayer opening is about 3.0 Å. The lone-pair electrons of Te(IV) atoms are orientated toward the interlayer space.

Light purple single crystals of $Nd_2W_2Te_2O_{13}$ was obtained by solid-state reactions of a mixture of Nd_2O_3 (0.25 mmol), WO_3 (0.50 mmol), and TeO_2 (1.25 mmol) in an evacuated quartz tube at 720°C for 6 days. $Nd_2W_2Te_2O_{13}$ (*P*-1, CS) features a 3D network structure in which the W_2O_{10} dimers occupy the large apertures formed by neodymium tellurite. Among two unique Nd^{3+} ions in the asymmetric unit, one is 8-coordinated whereas the other one is 9-coordinated. Unlike that in $La_2WTe_6O_{18}$, both the W(VI) cations in $Nd_2W_2Te_2O_{13}$ are octahedrally coordinated. A pairs of WO_6 octahedra are interconnected via edge sharing into a $W_2O_{10}^{8-}$ dimer. One W atom is distorted toward a face (local C_3 direction) with three "short" and three "long" W–O bonds, whereas W(2) atom is distorted toward an edge (C_2) with two "short," two "normal," and two "long" W–O bonds. The magnitudes of the distortion (Δd) is 1.118 and 0.945 Å, respectively, for W(1)O_6

and $W(2)O_6$. The interconnection of the Nd(III) ions by the tellurite groups resulted in a 3D network with two types of apertures along the *a*-axis. The large apertures with a narrow-long shape are formed by 10-member rings composed of 4 TeO_3 groups and 6 Nd(III) ions, whereas the small ones are formed by four-member rings composed of 2 Nd(1) and two $Te(1)O_3$ groups. The W_2O_{10} dimers are located at the large apertures. In $Nd_2W_2Te_2O_{13}$, each W_2O_{10} dimer connects with two TeO_3 groups (one in a unidentate fashion and the other in a bidentate bridging fashion) to form a $[W_2Te_2O_{13}]^{6-}$ anion. Therefore, the structure of $Nd_2W_2Te_2O_{13}$ also can be viewed as the Nd^{3+} ions being interconnected by $[W_2Te_2O_{13}]^{6-}$ anions via Nd–O–Te and Nd–O–W bridges.

Isostructural $Ln_5MTe_7O_{23}Cl_3$ (Ln = Pr, Nd; M = Mo, W) (*C*2/m, Cs) were obtained by solid-state reactions of a mixture containing LnOCl (Ln = Pr, Nd), WO_3 (or MoO_3), and TeO_2 in an evacuated quartz tube at 750 or 720°C for 6 days. These compounds feature a 3D network of lanthanide(III) molybdenum(VI) tellurium(IV) oxychloride with large apertures occupied by isolated Cl anions and the lone-pair electrons of Te(IV). $Ln_5MTe_7O_{23}Cl_3$ can be also formulated as $Ln_5(MO_4)(Te_5O_{13})(TeO_3)_2Cl_3$. 2 $Te(1)O_3$, 2 $Te(2)O_4$, and 1 $Te(3)O_3$ groups are corner sharing to form a novel $Te_5O_{13}^{6-}$ pentamer in a "semi-cycle" shape (Scheme 1c). The interconnection of Ln(III) ions via $Te_5O_{13}^{6-}$ and TeO_3^{2-} anions resulted in a thick layer parallel to the *ab* plane. Neighboring lanthanide tellurium(IV) oxide layers are bridged by Cl(2) atoms into a complicated 3D network, forming two different types of apertures. The small $Ln_4O_2Cl_2$ ring was capped by the MO_4 polyhedra on both sides, whereas the large apertures formed by eight-member rings are filled by the isolated Cl^- anions and the lone-pair electrons of Te(IV) atoms of the $Te_5O_{13}^{6-}$ groups [102].

The solid-state luminescent properties of $Nd_2MoSe_2O_{10}$, $Nd_2MoTe_3O_{12}$, $Nd_2MoTe_4O_{14}$, and $Nd_2W_2Te_2O_{13}$ were investigated at both room temperature and 10 K, and the solid-state luminescent properties of $Nd_5MoTe_7O_{23}Cl_3$ and $Nd_5WTe_7O_{23}Cl_3$ were studied at room temperature. Under excitation at 514 nm, the room temperature emission spectra for all six Nd(III) compounds display three sets of characteristic emission bands for the Nd(III) ion in the near IR region: $^4F_{3/2} \rightarrow {}^4I_{9/2}$, $^4F_{3/2} \rightarrow {}^4I_{11/2}$, and $^4F_{3/2} \rightarrow {}^4I_{13/2}$. $Nd_2MoTe_3O_{12}$ contains only one independent Nd (III) site, whereas $Nd_2MoSe_2O_{10}$, $Nd_2MoTe_4O_{14}$, and $Nd_2W_2Te_2O_{13}$ each contains two unique Nd(III) sites with C_1 symmetry. Due to the crystal field effect, each transition band was split into several subbands. $Pr_5MoTe_7O_{23}Cl_3$ and $Pr_5WTe_7O_{23}Cl_3$ display four sets of emission bands at 491 nm (very strong, $^3P_0 \rightarrow {}^3H_4$), 534 nm (moderate, $^3P_0 \rightarrow {}^3H_5$), 619 nm (moderate, $^3P_0 \rightarrow {}^3H_6$), 649 nm (strong, $^3P_0 \rightarrow {}^3F_2$) and 735 nm (weak, $^3P_0 \rightarrow {}^3F_4$) under $\lambda_{ex} = 448$ nm. Under the same experimental conditions, the corresponding emission bands for $Pr_2MoTe_4O_{14}$ are much weaker. Due to the so called "crystal field effect" as well as multiple Pr^{3+} sites, a few emission bands were split into several subbands [101, 102].

It is noticed that most of MoO_x ($x = 4$ or 6) polyhedra in the above compounds are not polymerized because of small Mo/Ln (≤ 1) ratios. We deem that these MoO_4 or MoO_6 may polymerize into novel polynuclear clusters or extended structures through corner- or edge sharing if the Mo/Ln ratios are larger (>1).

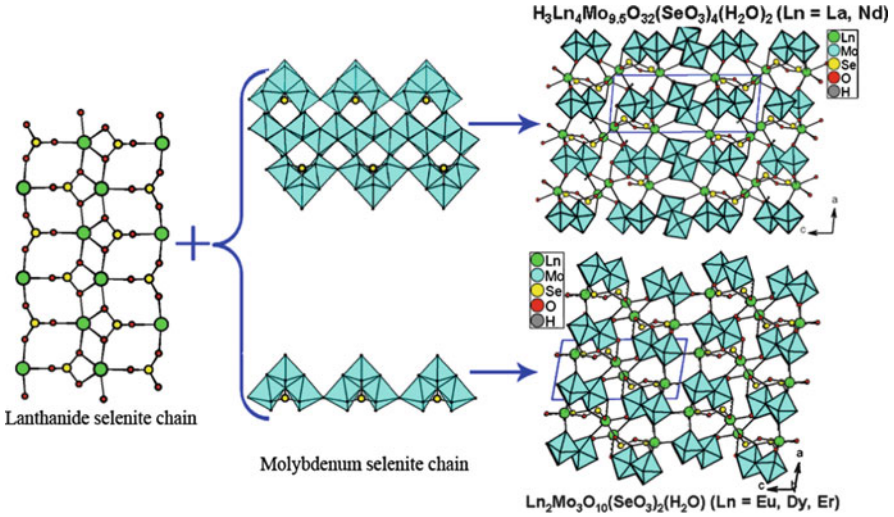

Fig. 22 View of the structure of $H_3Ln_4Mo_{9.5}O_{32}(SeO_3)_4(H_2O)_2$ (Ln = La, Nd) and $Ln_2Mo_3O_{10}(SeO_3)_2(H_2O)$ (Ln = Eu, Dy, Er)

Our explorations of Mo-rich Ln^{III}–Mo^{VI}–Se^{VI}–O phases led to five new lanthanide selenites containing MoO_6 octahedra, namely, $H_3Ln_4Mo_{9.5}O_{32}(SeO_3)_4(H_2O)_2$ (Ln = La, Nd,) and $Ln_2Mo_3O_{10}(SeO_3)_2(H_2O)$ (Ln = Eu, Dy, Er) [103]. The MoO_6 octahedra in the above two classes of compounds are interconnected into two types of novel molybdenum oxide chains.

The above five compounds were initially synthesized by the hydrothermal reactions of a mixture of lanthanide oxide (0.1 mmol), molybdenum oxide (0.5 mmol), and selenium dioxide (1.0 mmol) in 5 mL of distilled water at 230°C for 4 days. $H_3Ln_4Mo_{9.5}O_{32}(SeO_3)_4(H_2O)_2$ (Ln = La, Nd,) (*P*-1, CS) features a complicated 3D network in which the molybdenum selenite chains are further interconnected by lanthanide selenite chains (Fig. 22). The interconnection of La (1) and La(2) ions by bridging SeO_3^{2-} groups resulted in a lanthanide selenite chain along the *b*-axis. $Mo(1)O_6$, $Mo(2)O_6$, and $Mo(3)O_6$ octahedra are interconnected by edge-sharing bonds forming a $[Mo_3O_{14}]^{10-}$ trimer. The $Se(2)O_3^{2-}$ group capped on the trimer via Se–O–Mo bridges to form a $[Mo_3SeO_{14}]^{6-}$ unit. Such units are further condensed into a molybdenum selenite chain of $[Mo_3SeO_{13}]^{4-}$ via corner sharing along the *b*-axis. A pair of $Mo(4)O_6$ octahedra are edge shared into a $[Mo(4)_{1.5}O_{11}]^{13-}$ dimer; so are pairs of $Mo(5)O_6$ octahedra. The interconnection of $[Mo(4)_{1.5}O_{11}]^{13-}$ and $[Mo(5)_2O_{11}]^{10-}$ via edge sharing resulted in a double strand polymer of $[Mo_{1.75}O_8]^{5.5-}$. A pair of $[Mo_3SeO_{13}]^{4-}$ chains are sandwiched by two $[Mo_{1.75}O_8]^{5.5-}$ chains into a thick 1D slab of $[Mo_{4.75}SeO_{19}]^{5.5-}$ through Mo–O–Mo bridges.

$Ln_2Mo_3O_{10}(SeO_3)_2(H_2O)$ (Ln = Eu, Dy, Er) ($P2_1/m$, CS) with lower Ln/Mo molar ratio was obtained for the heavier lanthanide elements. Their structures feature a 3D framework also constructed by the intergrowth of the molybdenum selenite

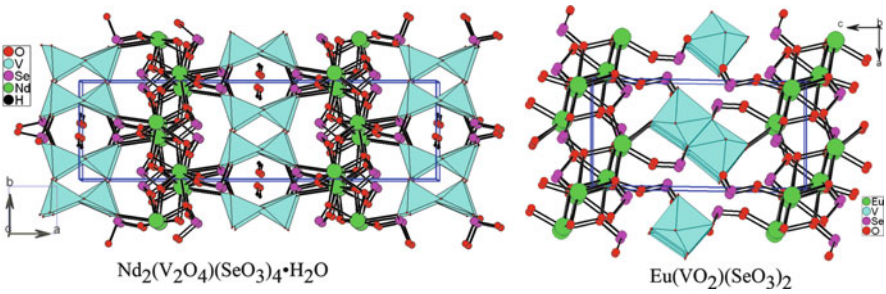

Fig. 23 View of the different structure types of $Nd_2(V_2O_4)(SeO_3)_4{\cdot}H_2O$ and $Eu(VO_2)(SeO_3)_2$

chains and the lanthanide selenites chains (Fig. 22). The interconnection of $Ln(1)^{3+}$ and $Ln(2)^{3+}$ ions through bridging $Se(1)O_3^{2-}$ and $Se(2)O_3^{2-}$ groups led to a lanthanide selenite chain along the *b*-axis. Two $Mo(1)O_6$ and one $Mo(2)O_6$ octahedra are interconnected by edge sharing into a $[Mo_3O_{14}]^{10-}$ trimer. This $[Mo_3O_{14}]^{10-}$ trimer is further capped by Se(2) atoms into a $[Mo_3SeO_{14}]^{6-}$ unit. Neighboring $[Mo_3SeO_{14}]^{6-}$ units are further interconnected via corner sharing into a molybdenum selenite chain as in $H_3Ln_4Mo_{9.5}O_{32}(SeO_3)_4(H_2O)_2$ (Ln = La, Nd,). The interconnection of the alternating lanthanide selenite and molybdenum selenite chains along the *a*-axis via Mo–O–Ln bridges resulted in a novel 3D network.

We had also isolated four lanthanide vanadium selenites with two types of structures, namely, $Nd_2(V_2O_4)(SeO_3)_4{\cdot}H_2O$ and $Ln(VO_2)(SeO_3)_2$ (Ln = Eu, Gd, Tb) [104]. They were hydrothermally synthesized by reactions of a mixture of $LnCl_3{\cdot}6H_2O$ (Ln = Nd, Eu, Gd, Tb), V_2O_3, and selenium dioxide in 5.0 or 8.0 mL of distilled water at 200°C for 4 days. During the reactions, V^{3+} ion has been oxidized to V^{5+}.

The structure of compound $Nd_2(V_2O_4)(SeO_3)_4{\cdot}H_2O$ features a 3D network composed of the 2D layers of $[Nd(SeO_3)]^+$ that are bridged by 1D $[V_2O_4(SeO_3)_2]^{2-}$ chains with the lattice water molecules located at the small 6-membered ring tunnels thus formed (Fig. 23). The two VO_5 tetragonal pyramids are interconnected by edge sharing to form a $[V_2O_8]^{6-}$ binuclear cluster unit. The $[V_2O_8]^{6-}$ dinuclear cluster units are further bridged by $Se(2)O_3^{2-}$ groups via corner sharing into a 1D chain along the *c*-axis. The Nd^{3+} ions are interconnected by bridging $Se(1)O_3$ groups into a neodymium(III) selenites layer parallel to the *bc* plane. The above two building units are further interconnected via Nd–O–Se(2) –O–V bridges into a 3D architecture with two types of narrow-long shaped 6-MR and 10-MR tunnels along the *c*-axis. The lattice water molecules are located at 6-MR tunnels composed of four VO_5 and two SeO_3 groups. The lattice water molecules also form a few hydrogen bonds with oxoanion and selenite oxygen atoms, which further increases the stability of the 3D structure. The structure of $Ln(VO_2)(SeO_3)_2$ (Ln = Eu, Gd, Tb) ($P2_1/m$, CS) also features a 3D network composed of 2D $[Ln(SeO_3)]^+$ layers which are bridged by 1D $[(VO_2)(SeO_3)]^-$ chains (Fig. 23). The two VO_6 octahedra are interconnected by edge sharing to form a $[V_2O_{10}]^{10-}$ dimer. These dimers are further interconnected though the corner sharing oxoanions into a double chain along the *b*-axis, $Se(1)O_3$ groups are grafted on both sides of the double chain in a bidentate bridging fashion, whereas

$Se(3)O_3$ groups capped on V_4 rings of the 1D chain. The Ln(III) ions are bridged by $Se(2)O_3$ and $Se(4)O_3$ groups into a double layer perpendicular to the *c*-axis. The above two building units are further interconnected via Ln–O–Se–O–V bridges into a 3D architecture with narrow-long shaped 10-MR tunnels along the *b*-axis.

It should be mentioned that these lanthanide selenites and tellurites containing V^{5+}, Mo^{6+}, and W^{6+} are not SHG active since they are all structurally centrosymmetric. This is very different from the corresponding metal iodates some of which are SHG active, as discussed earlier.

3.1.3 TM-d^0 TM–Se(IV)/Te(IV)–O System

A number of compounds in the translation metal (TM)-d^0 TM–Te(IV)/Se(IV)–O systems have been reported, a few of which exhibit moderate SHG efficiency (Table 2).

Four new transition metal vanadium selenites or tellurites with different types of structures were isolated by our group, namely, $ZnVSe_2O_7$, $Cd_6V_2Se_5O_{21}$, $Zn_3V_2TeO_{10}$, and $Cd_4V_2Te_3O_{15}$ [61, 105].

Dark-cyan crystals of $ZnVSe_2O_7$ was prepared by hydrothermal reactions of a mixture of $Zn(CH_3COO)_2{\cdot}2H_2O$ (0.84 mmol), V_2O_5 (0.28 mmol), SeO_2 (1.08 mmol), and H_2O (5 mL) at 200°C for 4 days. V^{5+} ion was reduced to V^{4+} ion during the reactions. The structure of $ZnVSe_2O_7$ ($P2_1/n$, CS) features a 3D network composed of 3D anionic framework of $[VSe_2O_7]^{2-}$ with the zinc(II) cations located at the six MR tunnels along *a*-axis. $ZnVSe_2O_7$ can also be formulated as $Zn(VO)(SeO_3)_2$. The VO_6 octahedra are interconnected via corner sharing into a 1D vanadium oxide chain along the $\langle 101 \rangle$ direction. These chains are further bridged by $Se(1)O_3$ groups into a 2D layer parallel to the *ac* plane. Such 2D layers are further interconnected by bridging $Se(2)O_3$ groups into pillar layers $[VSe_2O_7]^{2-}$ with two types of 6-MRs tunnels along the *a*-axis. Both 6-MRs are composed of four VO_6 octahedra and two SeO_3 groups, one is wider whereas the other is narrower. The lone pairs of the selenium(IV) point toward the center of the narrow ones, whereas the zinc(II) cations are located at the wider tunnels.

Red needle-shaped single crystals of $Cd_6V_2Se_5O_{21}$ were obtained by the solid-state reaction of a mixture of CdO, V_2O_5, and SeO_2 in a molar ratio of 2:1:1 or 1:1:1 at 680°C for 6 days. $Cd_6V_2Se_5O_{21}$ can also be formulated as $Cd_6(V_2O_6)(SeO_3)_5$. The structure of $Cd_6V_2Se_5O_{21}$ ($P2_1/c$, CS) features a novel 3D network composed 3D $\{Cd_6(SeO_3)_5\}^{2+}$ with 1D 16-MR tunnels along the *b*-axis, 1D $\{V_2O_6\}^{2-}$ anionic chains are located at the big tunnels and form Cd–O–V bridges. There are six unique cadmium(II) ions, two vanadium(V) cations, and five selenites in its asymmetric unit. The cadmium(II) ions are interconnected by bridging and chelating selenite groups into a 3D framework of $\{Cd_6(SeO_3)_5\}^{2+}$ with 1D 16-MRs tunnels along the *b*-axis. The size of the tunnel is estimated to be 3.0×12.0 Å^2 based on the structural data (the atomic radii of the ring atoms have been deducted). The 16-MRs tunnels are constructed by six SeO_3 groups and ten cadmium atoms. The lone pairs of the selenite anions are pointing toward the center of the tunnels. $V(1)O_4$ and

$V(2)O_4$ tetrahedra are interconnected alternately via corner sharing into a 1D $\{V_2O_6\}^{2-}$ anionic chain along the *b*-axis. These vanadium oxide chains are inserted in the above tunnels of the cadmium(II) selenite and interact with the main skeleton via V–O–Cd bridges [105].

Solid-state reactions of zinc(II) or cadmium(II) oxide, V_2O_5, and TeO_2 at high temperature led to two novel quaternary compounds, namely, $Zn_3V_2TeO_{10}$ and $Cd_4V_2Te_3O_{15}$ [61].

$Zn_3V_2TeO_{10}$ ($P2_1/c$, CS) features a novel 3D network composed of 2D zinc tellurite layers bridged by $V(1)O_4$ tetrahedra with 8-MRs tunnels along the *c*-axis, and the $V(2)O_4$ tetrahedra are located at the above tunnels. In the structure, $Zn(1)O_6$ and $Zn(2)O_5$ polyhedra are interconnected via edge- and corner sharing into a 1D chain along the *a*-axis. $Zn(3)O_5$ polyhedra are interconnected via edge sharing to form a 1D chain along the *c*-axis. The two types of 1D chains are further interconnected via corner sharing into a zinc(II) oxide layer parallel to the *ac* plane. The TeO_4 groups are grafted into the layers through Te–O–Zn bridges to form a thick zinc(II) tellurite layer with 8-MRs tunnels along the *c*-axis. Neighboring such layers are bridged by $V(1)O_4$ tetrahedra via corner sharing along the *b*-axis into a 3D architecture. The $V(2)O_4$ tetrahedra are located at the eight-membered ring tunnels formed by two tellurite groups and six zinc atoms.

$Cd_4V_2Te_3O_{15}$ crystallizes in the NCS space group $P2_12_12_1$. Its structure features a 3D network composed of 2D cadmium tellurite layers bridged by discrete VO_4 tetrahedra and 1D vanadium oxide helical chains (Fig. 24). There are four Cd(II) ions, two V(V), and three tellurite groups in the asymmetric unit of $Cd_4V_2Te_3O_{15}$. It can also be formulated as $Cd_4(VO_3)_2(TeO_3)_3$. All four unique cadmium(II) ions are octahedrally coordinated by six oxygen atoms, and both vanadium(V) ions are in the tetrahedral geometry. $V(1)O_4$ tetrahedra are interconnected into a 1D right-handed helical chain via corner sharing, whereas the $V(2)O_4$ tetrahedra remain "isolated." The CdO_6 octahedra are interconnected into a 2D cadmium(II) oxide layer via corner- and edge sharing. The tellurite (TeO_3) anions capped on both sides

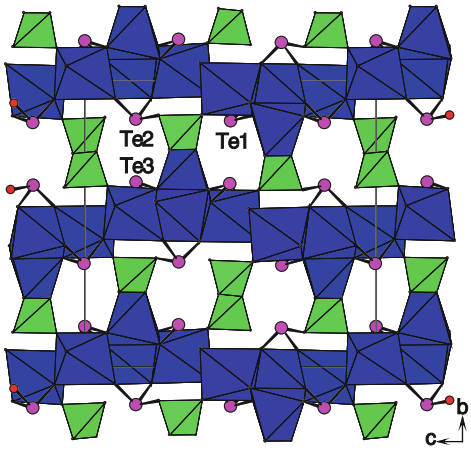

Fig. 24 View of the structure of $Cd_4V_2Te_3O_{15}$ down the *a*-axis. The CdO_6 and VO_4 polyhedra are shaded in *blue* and *green*, respectively. Te and O atoms are drawn as *pink* and *red circles*, respectively

of the cadmium(II) oxide layer to form a novel cadmium(II) tellurite layer parallel to the *ac* plane. Neighboring cadmium(II) tellurite layers are further bridged by the "isolated" $V(2)O_4$ tetrahedra and the V(1) oxide helical chains into a 3D architecture with two types of left-handed helical tunnels along the *a*-axis. The larger ones are formed by eight-membered rings composed of four cadmium(II) atoms, three vanadium(V) atoms, and a tellurium(IV) atom, whereas the smaller ones are based on six-membered rings containing four cadmium(II) and two vanadium(V) atoms. The lone-pair electrons of the tellurium(IV) atoms are orientated toward the tunnels above [61]. SHG measurements revealed that $Cd_4V_2Te_3O_{15}$ displays a moderately strong SHG signal about 1.4 times that of KDP. This SHG response could be attributed to both the lone pairs of the tellurite anions and the 1D vanadium(V) oxide helical chain. The DTA studies indicate that $Cd_4V_2Te_3O_{15}$ exhibits an endothermic peak at 751°C in the heating curve and an exothermic peak at 695°C in the cooling curve; hence, $Cd_4V_2Te_3O_{15}$ may melt congruently at about 751°C. This suggests that $Cd_4V_2Te_3O_{15}$ is a congruently melting compound, which was also confirmed by powder XRD studies under different temperatures. Therefore, in principle, large single crystals could be grown from the stoichiometric melts.

A large number of transition metal molybdenum(VI) (or tungsten(VI)) selenites or tellerites have been reported, some of them are SHG active [58, 62, 66, 106].

Polar $Zn_2(MoO_4)(QO_3)$ (Q = Se, Te) was reported by the Halasyamani group very recently [62]. Crystals of $Zn_2(MoO_4)(TeO_3)$ were grown by hydrothermal reactions of ZnO (2.0 mmol), TeO_2 (1.0 mmol), MoO_3 (1.00 mmol), and NH_4Cl/NH_3 1 M buffer solution (3 mL) at 230°C for 2 days, whereas Bulk polycrystalline and crystals of $Zn_2(MoO_4)(SeO_3)$ were prepared by solid-state reactions of a mixture of ZnO (2.0 mmol), SeO_2 (1.0 mmol), and MoO_3 (1.0 mmol) at 550°C for 48 h. $Zn_2(MoO_4)(QO_3)$ (Q = Se, Te) are isostructural and both crystallized in a polar space group $P2_1$. Their structures feature a 3D network composed of 2D zinc selenites (or tellurites) layers further bridged by MoO_4 tetrahedra. The ZnO_n ($n = 4$, 6) polyhedra are interconnected into a wave-like 2D layer via corner sharing with the SeO_3 (or TeO_3) groups capping from both sides of the layer. These zinc selenites (or tellurites) layers are further interconnected by the MoO_4 tetrahedra to a 3D framework via corner sharing. The polarities come mainly from the lone-pair cations since MoO_4 tetrahedra cannot undergo SOJT distortion. Powder SHG measurements using 1,064 nm radiation indicate the compounds exhibit moderate SHG efficiencies of 100 and 80 × α-SiO_2 for $Zn_2(MoO_4)(SeO_3)$ and $Zn_2(MoO_4)(TeO_3)$, respectively. Both of them are nonphase-matching materials [62].

Three new phases in Ag^{I}–Mo^{VI}/W^{VI}–Te^{IV}–O system, namely, $Ag_2Mo_3Te_3O_{16}$, $Ag_2MoTe_4O_{12}$, and $Ag_6W_3Te_4O_{20}$, were prepared by our group [58]. They were synthesized hydrothermally from a stoichiometric mixture of Ag_2O, TeO_2, MoO_3 or WO_3, and 10 mL of H_2O at 230°C. The loaded compositions are: Ag_2O (0.1 mmol), TeO_2 (0.3 mmol), and MoO_3 (0.3 mmol) for $Ag_2Mo_3Te_3O_{16}$; Ag_2O (0.1 mmol), TeO_2 (0.4 mmol), and MoO_3 (0.1 mmol) for $Ag_2MoTe_4O_{12}$; Ag_2O (0.3 mmol), TeO_2 (0.4 mmol), and WO_3 (0.3 mmol) for $Ag_6W_3Te_4O_{20}$.

$Ag_2Mo_3Te_3O_{16}$ is isostructural to $Na_2Mo_3Te_3O_{16}$ and crystallized in a polar space group *I*2 [57]. Its structure features a 1D $[Mo_3Te_3O_{16}]^{2-}$ anionic chain

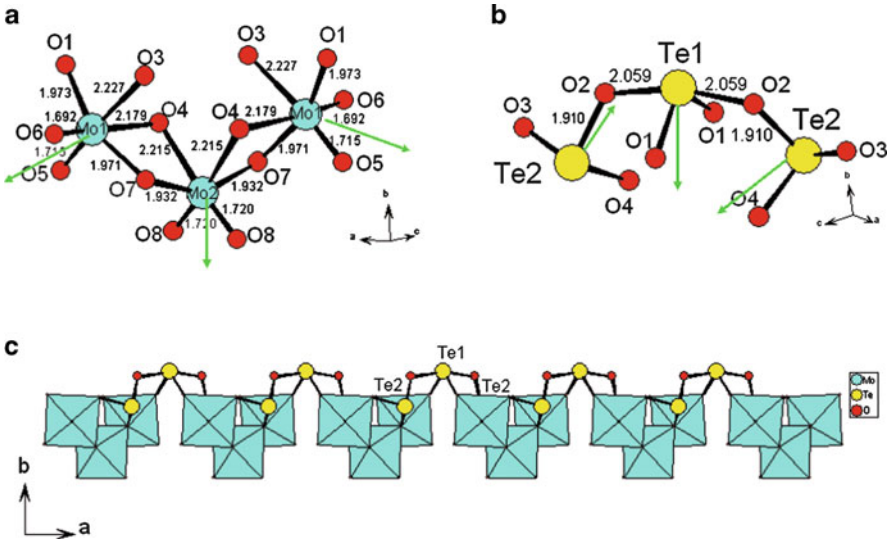

Fig. 25 The $[Mo_3O_{14}]^{12-}$ cluster (**a**), the $[Te_3O_8]^{4-}$ cluster (**b**) and a 1D $[Mo_3Te_3O_{16}]^{2-}$ anion (**c**) in $Ag_2Mo_3Te_3O_{16}$. The *green arrows* indicate the directions of the polarization of the cations

composed of $[Mo_3O_{14}]^{10-}$ clusters bridged by $[Te_3O_8]^{4-}$ anions via corner sharing. Neighboring chains are further bridged by the Ag^+ ions into a condensed 3D network. The $[Mo_3O_{14}]^{10-}$ cluster is formed by three edge-shared MoO_6 octahedra in which the Mo^{6+} cations are distorted toward an edge (local C_2 direction), resulting in two short, two normal, and two long Mo–O bonds. The magnitude of the distortion (Δd) was calculated to be 1.52 and 1.02 for Mo(1) and Mo(2), respectively. The $[Te_3O_8]^{4-}$ anion composes of one Te(1)O_4 and two Te(2)O_3 groups interconnected by corner sharing (Scheme 1a). In the molybdenum tellurite chains, the lone pairs of the TeO_3 groups are aligned on the same side to produce a large macroscopic dipole moment in the compound (Fig. 25). SHG measurements revealed that $Ag_2Mo_3Te_3O_{16}$ displays a large SHG response of about 8 × KDP. From Fig. 25, we can see that the polarization of the two Mo(1)O_6 octahedra in the $[Mo_3O_{14}]^{10-}$ cluster are almost cancelled out whereas the polarization of the central Mo(2)O_6 octahedron is approximately along the *b*-axis. As for the $[Te_3O_8]^{4-}$ anion, the contributions from Te(2)O_3 groups almost cancelled each other, and that of the Te(1)O_4 group is polarized along the *b*-axis. Hence, the polarizations of both types of asymmetric polyhedra within the 1D $[Mo_3Te_3O_{16}]^{2-}$ anionic chain are "constructive" add. Therefore, the molybdenum tellurite chains are polar.

$Ag_2MoTe_4O_{12}$ (*C*2/c, CS) is isostructural with $Na_2MTe_4O_{12}$ (M = Mo, W), and its structure features a 3D anionic $[MoTe_4O_{12}]^{2-}$ network with Ag^+ ions filling the cavities of the structure. The Te(1)O_5 and Te(2)O_3 groups are interconnected into a 2D $[Te_4O_{10}]^{4-}$ anionic double layer perpendicular to the *a*-axis via corner- and

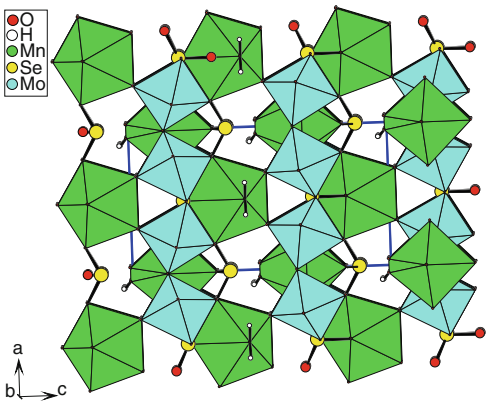

Fig. 26 View the structure of $Mn(MoO_3)(SeO_3)(H_2O)$ down the *b*-axis

edge sharing. These double layers are bridged by MoO_6 octahedra into a 3D anionic $[MoTe_4O_{12}]^{2-}$ network.

The structure of $Ag_6W_3Te_4O_{20}$ (*C*2/c, CS) exhibits a 3D anionic network composed of 2D W(2)–Te(1)–O layers being bridged by 1D W(1)–Te(2)–O chains with the silver(I) ions located at the cavities of the structure. Neighboring $W(1)O_6$ octahedra are bridged by pairs of $Te(2)O_4$ groups via corner sharing into a 1D anionic chain along the *c*-axis. Two $Te(1)O_4$ groups are interconnected to a Te_2O_6 dimer via edge sharing. $W(2)O_6$ octahedra are bridged by Te_2O_6 dimers to form a 2D layer parallel to the *bc* plane. The W(2)–Te(1)–O layers were further connected by the 1D W(1)–Te(2)–O chains to a 3D framework via Te(2)–O–W(2) bridges [58].

Our systematic explorations of new SHG materials in the divalent transition metal-Mo(VI)–Se(IV)/Te(IV)–O systems afforded seven new compounds, namely, $TM(MoO_3)(SeO_3)(H_2O)$ (TM = Mn, Co), $Fe_2(Mo_2O_7)(SeO_3)_2(H_2O)$, $Cu_2(MoO_4)(SeO_3)$, $Ni_3(MoO_4)(TeO_3)_2$, and $Ni_3(Mo_2O_8)(XO_3)$ (X = Se, Te) [66, 106].

Yellow brick-shaped crystals of $Mn(MoO_3)(SeO_3)(H_2O)$ were isolated by heating a mixture of 0.4 mmol MoO_3, 0.4 mmol $MnCO_3$, 1.2 mmol SeO_2, and 5 mL H_2O at 210°C. The structure of $Mn(MoO_3)(SeO_3)(H_2O)$ ($Pmc2_1$, NCS) features a complicated 3D network composed of MnO_7 polyhedra, MoO_6 octahedra, and SeO_3 polyhedra (Fig. 26). Its asymmetric unit contains two unique Mn atoms lying on mirror planes, one Mo in the general site, and two Se atoms sitting on mirror planes. Both Mn(1) and Mn(2) are seven coordinated by three selenite oxygens, one aqua ligand, and four oxoanions in a pentagonal bipyramid geometry. Mo(1) is octahedrally coordinated by two selenite oxygens, two terminal, and two bridging oxoanions. The MoO_6 octahedron is distorted toward an edge (local C_2 direction) with two "short," two "normal," and two "long" Mo–O bonds, and the magnitude of the distortion (Δd) was calculated to be 0.98. The MoO_6 octahedra are corner shared into a 1D Mo–O chain along the *a*-axis. MnO_7 polyhedra and SeO_3 groups are interconnected into a ladder-shaped 1D chain along the *a*-axis. The above two types of chains are further interconnected and alternating along *b* and *c*-axis, forming a complicated 3D network with 1D tunnels of Mn_2Mo_2Se 5-MRs and small tunnels of $MnMo_2$ 3-MR along the *b*-axis.

SHG measurements revealed that $Mn(MoO_3)(SeO_3)(H_2O)$ displays a moderate SHG signal of about three times of KDP [66].

Brown plate-shaped crystals of $Co(MoO_3)(SeO_3)(H_2O)$ were obtained by heating a mixture of 0.4 mmol MoO_3, 0.4 mmol $CoCl_2$, 1.2 mmol SeO_2, and H_2O (5 mL) at 210°C. Although $Co(MoO_3)(SeO_3)(H_2O)$ and $Mn(MoO_3)(SeO_3)(H_2O)$ have a similar formula, they display totally different structures. The structure of $Co(MoO_3)(SeO_3)(H_2O)$ (*P*-1, CS) features a 3D network composed of 1D molybdenum(VI) selenite chains bridged by CoO_6 octahedra with 1D 8-MR tunnels along the *a*-axis. The asymmetric unit of $Co(MoO_3)(SeO_3)(H_2O)$ is composed of two Co(II) atoms on inversion centers, one Mo(VI), one SeO_3^{2-} anion, and an aqua ligand on general sites. Both Co(1) and Co(2) are octahedrally coordinated by six oxygen atoms which is different from the seven-coordinated Mn(II) atoms in the $Mn(MoO_3)(SeO_3)(H_2O)$. The Mo(1) atom is octahedrally coordinated by two selenite oxygens, two terminal and two bridging oxoanions with three "short" and three "long" Mo–O bonds. Hence, the Mo(VI) cation is distorted toward a face (local C_3 direction) and the magnitude of the distortion (Δd) was calculated to be 1.248. The MoO_6 octahedra are interconnected into a 1D Mo–O chain along the *a*-axis via edge sharing, and the selenite anions are hanging on both sides of the chain. Within the molybdenum(VI) selenite chain, the polarization directions of the neighboring MoO_6 octahedra are opposite each other and the polarizations of the selenites are cancelled out. These centrosymmetric molybdenum(VI) selenite chains are further bridged by the CoO_6 octahedra into a 3D network with 1D 8-MR tunnels along the *a*-axis. The long narrow 8-MR tunnels are composed of 2 MoO_6 octahedra, 4 CoO_6 octahedra, and 2 selenites. The lone-pair electrons of the Se(IV) cations are orientated toward the center of the tunnels.

Red brick-shaped crystals of $Fe_2(Mo_2O_7)(SeO_3)_2(H_2O)$ were isolated by heating a mixture of 0.4 mmol MoO_3, 0.4 mmol Fe_2O_3, 1.2 mmol SeO_2, and H_2O (5 mL) at 230°C for 4 days. The structure of $Fe_2(Mo_2O_7)(SeO_3)_2(H_2O)$ (*C*2/c, CS) features a 3D architecture composed of iron(III) selenite layers interconnected by Mo_2O_{10} dimers. The asymmetric unit of $Fe_2(Mo_2O_7)(SeO_3)_2(H_2O)$ contains one FeO_6 octahedra, one MoO_6 octahedra, and one selenite anion. The MoO_6 octahedron is distorted toward an edge (local C_2 direction), displaying two "short," two "normal," and two "long" Mo–O bonds. The magnitude of the distortion (Δd) is calculated to be 1.45. Each pair of FeO_6 octahedra form a Fe_2O_{10} dimer via edge sharing, and such dimers are further bridged by selenite anions into a $\langle 100 \rangle$ layer. Two MoO_6 octahedra form a Mo_2O_{10} dimer by edge sharing. The above iron(III) selenite layers are further interconnected by the Mo_2O_{10} dimers via Mo–O–Fe bridges into a 3D framework with 1D 8-MR tunnels along the *b*-axis. The 8-MR is composed of 2 SeO_3, 2 FeO_6, and 4 MoO_6 groups. The lone pairs of the selenite groups are orientated toward the centers of the above tunnels.

$Cu_2(MoO_4)(SeO_3)$ was obtained by heating a mixture of 0.4 mmol MoO_3, 0.4 mmol CuO, 0.4 mmol SeO_2, and H_2O (5 mL) at 210°C for 4 days. The structure of $Cu_2(MoO_4)(SeO_3)$ ($P2_1/c$, CS) exhibits a 2D layer composed of 1D copper(II) oxide chains that are further bridged by SeO_3 groups and MoO_4 tetrahedra. Its asymmetric unit contains two CuO_5 square pyramids, one MoO_4 tetrahedron, and

one SeO_3 group. Two $Cu(2)O_5$ square pyramids are edge shared to $Cu(2)_2O_8$ dimers, and the latter are further bridged by the $Cu(1)O_5$ square pyramids to form a copper(II) oxide chain along the *c*-axis. Neighboring copper oxide chains are further bridged by SeO_3 anions and MoO_4 tetrahedra via corner sharing into a 2D layer parallel to the *bc* plane with 1D 5-MR tunnels along the *c*-axis. The unusual odd member ring is composed of 1 $Cu(1)O_5$ square pyramid, 2 $Cu(2)O_5$ square pyramids, 1 MoO_4 tetrahedron, and 1 SeO_3 group. The lone-pair electrons of the Se(IV) atoms are orientated toward the interlayer space. The interlayer *d*-spacing is about 8.15 Å [66].

Red prism-shaped crystals of $Ni_3(MoO_4)(TeO_3)_2$ were synthesized by solid-state reactions at 720°C: $3NiO + MoO_3 + 2TeO_2 \rightarrow Ni_3(MoO_4)(TeO_3)_2$. $Ni_3(MoO_4)(TeO_3)_2$ crystallizes in the NCS space group $P2_12_12_1$. Its structure features a novel 3D network of nickel(II) oxide with lager 1D tunnels along *a*-axis, the MoO_4 tetrahedra, and TeO_3 groups capped on walls of the tunnels. Among three unique nickel(II) ions in the asymmetric unit, Ni(1) and Ni(2) are octahedrally coordinated, whereas Ni(3) is in a square pyramidal geometry. $Ni(1)O_6$ and $Ni(2)O_6$ octahedra are alternately interconnected into a 2D layer parallel to the *ab* plane by edge sharing, whereas $Ni(3)O_5$ square pyramids are corner sharing into a 1D right-hand helical chain along the *a*-axis. The above 2D layers and the 1D chains are further interconnected via Ni(1)–O(4)–Ni(3) and Ni(2)–O(9)–Ni(3) bridges into a 3D network with large 12-MR tunnels along the *a*-axis. The tunnels are based on Ni_{12} rings. The MoO_4 tetrahedra and TeO_3 groups capped on walls of the tunnels [106]. SHG measurements indicate that the SHG signal of $Ni_3(MoO_4)(TeO_3)_2$ is much weaker than that of KDP. This is due to the fact that the Mo^{6+} in a tetrahedral geometry is not subject to SOJT distortion and the polarizations of the tellurite groups which capped on the walls of the large 12-MR tunnels have been mostly cancelled out.

Green brick-shaped crystals of $Ni_3(Mo_2O_8)(SeO_3)$ were initially prepared by the solid-state reaction of a mixture of Nd_2O_3 (0.35 mmol), MoO_3 (0.35 mmol), $NiCl_2$ (0.35 mmol), and SeO_2 (1.4 mmol) at 700°C for 5 days. Although Nd(III) is not present in the product, the addition of Nd_2O_3 helped the crystallization of $Ni_3(Mo_2O_8)(SeO_3)$, and the quality of the crystals is very poor when the synthesis was carried out in the absence of Nd_2O_3. The structure of $Ni_3(Mo_2O_8)(SeO_3)$ (*P*-1, CS) features a 3D network composed of $[Ni_6O_{22}]^{32-}$ cluster units that are interconnected by $[Mo_4O_{16}]^{8-}$ clusters and SeO_3^{2-} anions. There are three NiO_6 octahedra, two MoO_6 octahedra, and one SeO_3 group in the asymmetric unit. The Mo(VI) cations are distorted toward an edge (local C_2 direction) with two "short," two "normal," and two "long" Mo–O bonds. The magnitudes of the distortions (Δd) are calculated to be 1.18 and 1.29, respectively, for Mo(1) and Mo(2). Four MoO_6 octahedra are interconnected by edge sharing to form a cyclic $[Mo_4O_{16}]^{8-}$ tetranuclear cluster unit. Six NiO_6 octahedra are interconnected into ahexanuclear $[Ni_6O_{22}]^{32-}$ cluster unit through edge sharing. The $[Ni_6O_{22}]^{32-}$ cluster units are bridged by SeO_3^{2-} groups to form a 2D nickel selenite layer parallel to the *ab* plane. Neighboring nickel selenite layers are further interconnected by the $[Mo_4O_{16}]^{8-}$ clusters via Mo–O–Ni bridges into a 3D network structure. The lone pairs of the selenium(IV) atoms are orientated to the cavities of the structure.

Green brick-shaped crystals of $Ni_3(Mo_2O_8)(TeO_3)$ were prepared by the solid-state reaction of a mixture containing NiO (0.5 mmol), MoO_3 (0.5 mmol), and TeO_2 (1.5 mmol) at 720°C for 6 days. The structure of $Ni_3(Mo_2O_8)(TeO_3)$ is different from that of $Ni_3(Mo_2O_8)(SeO_3)$, although their chemical formulae are comparable. $Ni_3(Mo_2O_8)(TeO_3)$ (*C*2/m, CS) features a 3D structure in which the corrugated nickel-oxide anionic chains are bridged by $[Mo_4O_{16}]^{8-}$ cluster units and TeO_3^{2-} anions. As in $Ni_3(Mo_2O_8)(SeO_3)$, the Ni(II) and Mo(VI) cations are octahedrally coordinated by six oxygens. Similar to that in $Ni_3(Mo_2O_8)(SeO_3)$, the four MoO_6 octahedra in $Ni_3(Mo_2O_8)(TeO_3)$ are interconnected via edge sharing to form a $[Mo_4O_{16}]^{8-}$ tetranuclear cluster unit. Different is two $Ni(1)O_6$ and one $Ni(2)O_6$ octahedra are interconnected via edge sharing into a $[Ni_3O_{13}]^{20-}$ trinuclear unit. Neighboring such trinuclear units are further interconnected through edge sharing into a corrugated $[Ni_3O_{11}]^{16-}$ anionic chain along *b*-axis. This nickel oxide chain can also be viewed as $Ni(2)O_6$ octahedra being grafted onto the corrugated chain of $Ni(1)O_6$ through edge sharing. It is interesting to note that $[Ni_6O_{22}]^{32-}$ clusters are formed in $Ni_3(Mo_2O_8)(SeO_3)$, whereas corrugated $[Ni_3O_{11}]^{16-}$ anionic chains are observed in $Ni_3(Mo_2O_8)(TeO_3)$. Both nickel-oxide building units are based on Ni_3O triangles. The Ni_3O triangles in $[Ni_6O_{22}]^{32-}$ clusters are condensed via sharing Ni···Ni edges, whereas those in $[Ni_3O_{11}]^{16-}$ anionic chains are interconnected through pairs of Ni–O–Ni bridges. These different nickel(II) oxide architectures may result from the different coordination modes of the selenite and tellurite groups as well as the different ionic radii of Se(IV) and Te(IV). Neighboring corrugated nickel(II) oxide chains are bridged by TeO_3^{2-} anions to form a thick nickel(II) tellurite layer parallel to the *ab* plane. The thickness of the layer is about 12.1 Å. Such layers are further interconnected by the $[Mo_4O_{16}]^{8-}$ clusters via Mo–O–Ni bridges into a 3D network structure. The lone-pair electrons of the tellurium(IV) atoms are orientated to the tunnels of the structure [106].

3.1.4 p-Block Elements-d^0 TM–Se(IV)/Te(IV)–O System

The Tl^+, Pb^{2+}, and Bi^{3+} cations may also have stereoactive lone-pair electrons and can form asymmetric coordination environments. As for Ga^{3+}/In^{3+}, the cations of group IIIA, have an oxidation state of +3 as lanthanide(III) ions but their coordination geometries are more closer to those of transition metal ions. Thus, we deemed that these p-block main group cations in combinations with two other different kinds of SOJT cations may result in new compounds with new types of structures as well as different optical properties. So far such compounds are still rare.

Two NCS quaternary oxides, namely, $TlMVO_5$ (M = Se^{4+} or Te^{4+}) have been synthesized by hydrothermal techniques [63]. $TlMVO_5$ (M = Se^{4+} or Te^{4+}) crystallize in a polar space group $Pna2_1$, their structures feature a 3D framework composed of corner-shared VO_6 octahedra connected by asymmetric SeO_3 (or TeO_4) and TlO_8 polyhedra. Powder SHG measurements using 1,064 nm radiation revealed that $TlMVO_5$ (M = Se^{4+} or Te^{4+}) have SHG efficiencies of approximately 40 times of α-SiO_2, but they are nonphase matchable.

Four such tellurites, namely, $Bi_2WTe_2O_{10}$, $Bi_2W_3Te_2O_{16}$, $BiNbTe_2O_8$, $Pb_4M_{10}Te_6O_{41}$ (M = Nb^{5+} or Ta^{5+}) were reported in the Pb^{2+}/Bi^{3+}-d^0 TM–Se^{4+}/Te^{4+}–O systems [37, 107–109]. $Bi_2WTe_2O_{10}$ features 1D chains of $[WO_4(TeO_3)_2]^{4-}$ anions that are further interconnected by Bi^{3+} ions [107], whereas $Bi_2W_3Te_2O_{16}$ features triple-decker chains of $[W_3O_{10}(TeO_3)_2]^{4-}$, which are further interconnected by Bi^{3+} ions [108]. $BiNbTe_2O_8$ can be described as layers of corner-shared NbO_6 octahedra and fluorite-like sheets of BiO_8 distorted cubes capped by TeO_4 groups are further interconnected by TeO_3 pyramids via Nb–O–Te–O–Bi bridges [109]. $Pb_4M_{10}Te_6O_{41}$ (M = Nb^{5+} or Ta^{5+}) exhibits a 3D framework consisting of layers of corner-shared NbO_6 octahedra being further interconnected by TeO_3 and PbO_6 polyhedra [37].

Two new quaternary mixed metal oxide materials, namely, $InVTe_2O_8$ and $InVSe_2O_8$, have been synthesized by standard solid-state reactions in In^{3+}–V^{5+}–Se^{4+}/Te^{4+}–O systems [64]. $InVTe_2O_8$ crystallized in the centrosymmetric space group $P2_1/n$. Its structure is a 2D layer consisting of 1D chains of corner-shared InO_6 octahedra being further bridged by Te_4O_{12} tetramers and VO_4 tetrahedra. $InVSe_2O_8$ exhibits a totally different structure type although its formula is similar to that of $InVTe_2O_8$. $InVSe_2O_8$ crystallized in NCS polar space group *P*m, its structure is a 3D framework composed of 1D edge-shared InO_6 chains and 1D corner-shared VO_5 chains that are bridged by the SeO_3 anions. Powder SHG measurements, using 1,064-nm radiation, indicated that $InVSe_2O_8$ has a SHG efficiency ~30 times that of α-SiO_2 and it is nonphase matchable. The origin of the polarization in $InVSe_2O_8$ is thought to be from the local moments of the VO_5 square pyramids which were partly cancelled by the selenite groups [64].

Nine new quaternary phases in the p-block elements-d^0 TM–Se(IV)/Te(IV)–O systems, namely, $Pb_2V_2^{V}Se_2O_{11}$, $Pb_2V_3^{IV}Se_5O_{18}$, $Pb_2Nb_2^{V}Se_4O_{15}$, $Bi_2V_2^{V}Se_4O_{16}$, and $Bi_2Mo_2^{VI}Se_2O_{13}$, [110], and $Ga_2MoQ_2O_{10}$ (Q = Se, Te), $In_2Mo_2Se_2O_{13}(H_2O)$, and $In_2MoTe_2O_{10}$ [111], were isolated by our group. They exhibit eight different types of anionic structures.

$Pb_2V_2^{V}Se_2O_{11}$, $Pb_2V_3^{IV}Se_5O_{18}$, $Pb_2Nb_2^{V}Se_4O_{15}$, $Bi_2V_2^{V}Se_4O_{16}$, and $Bi_2Mo_2^{VI}Se_2O_{13}$ were hydrothermally synthesized by reactions of a mixture of PbO (or Bi_2O_3), V_2O_3 (or Nb_2O_5, MoO_3), and SeO_2 in 5–8 mL of distilled water, at 200 or 230°C for 4–5 days. It should be mentioned that the two vanadium(V) phases were formed through the oxidation of the V^{3+} ion. These compounds cannot be prepared by directly using the V_2O_5 as the V sources.

All five compounds contain three types of asymmetric building blocks: two types of cations with a lone pair and a distorted MO_6 (M = V, Nb, Mo) octahedron. Their structures belong to five different types. The structure of $Pb_2V_2^{V}Se_2O_{11}$ (*P*-1, CS) features 1D $[V_2O_5(SeO_3)_2]^{4-}$ chains that are further bridged by the Pb^{2+} cations into a 3D network. There are two PbO_5 square pyramids, two VO_6 octahedra, and two selenite anions in the asymmetric unit of $Pb_2V_2^{V}Se_2O_{11}$; hence, $Pb_2V_2^{V}Se_2O_{11}$ can also be formulated as $Pb_2V_2^{V}O_5(SeO_3)_2$. A pair of $V(1)O_6$ octahedra are interconnected by edge sharing to a $V(1)_2O_{10}$ dimer. Two $V(2)O_6$ octahedra are capping on the $V(1)_2O_{10}$ dimer to form a cyclic $[V_4O_{16}]^{12-}$ tetranuclear cluster unit. Neighboring $[V_4O_{16}]^{12-}$ tetranuclear cluster units are further interconnected by

$Se(2)O_3^{2-}$ groups via corner sharing into a 1D anionic chain of $[V_2O_5(SeO_3)_2]^{4-}$ along the *b*-axis, and the $Se(1)O_3^{2-}$ groups are hanging on both sides of the chain. Neighboring such chains are further bridged by lead(II) ions into a 3D network.

The structure of $Pb_2V_3^{IV}Se_5O_{18}$ (*P*nma, CS) features a 3D anionic framework of $[V_3Se_5O_{18}]^{4-}$ with the lead(II) cations being located at the 1D 8-MR tunnels along *b*-axis. There are two lead(II) ions located on the mirror plane, two V^{5+} ions with V(1) at a mirror plane and three selenite anions with Se(1) at a mirror plane in the asymmetric unit of $Pb_2V_3^{IV}Se_5O_{18}$; hence, $Pb_2V_3^{IV}Se_5O_{18}$ can also be formulated as $Pb_2(V^{IV}O)_3(SeO_3)_5$. The VO_6 octahedra are bridged by SeO_3 groups via corner sharing into a 3D anionic framework with two types of 1D 8-MR tunnels along the *b*-axis. One type of 1D 8-MR tunnel is based on 2 $V(1)O_6$ octahedra, 2 $V(2)O_6$ octahedra, 2 $Se(1)O_3$, and 2 $Se(3)O_3$ groups and the lone pairs of $Se(1)O_3$ and $Se(3)O_3$ groups are oriented toward its center. The other type of 1D 8-MR tunnel is based on 1 $V(1)O_6$ octahedra, 3 $V(2)O_6$ octahedra, 2 $Se(2)O_3$, 1 $Se(1)O_3$, and 1 $Se(3)O_3$ groups; the lone pair of $Se(2)O_3$ is oriented toward the center of the tunnel. The lead (II) ions are also located at the second type of 1D 8-MR tunnels.

The structure of $Pb_2Nb_2^{V}Se_4O_{15}$ (*C*2/c, CS) features novel niobium(V) oxy-selenite chains of $[Nb_2O_3(SeO_3)_4]^{4-}$ that are bridged by Pb^{2+} cations into a 3D network. The asymmetric unit of $Pb_2Nb_2^{V}Se_4O_{15}$ contains one severely distorted PbO_5 square pyramid, one NbO_6 octahedron, and two selenite anions. The NbO_6 octahedra are interconnected via corner sharing into a ladder-like double chain along the *c*-axis; $Se(2)O_3$ and $Se(1)O_3$ groups are grafted into the chain in a bidentate bridging and a unidentate fashion, respectively. The PbO_5 square pyramids are interconnected into a 2D layer parallel to the *bc* plane via corner- and edge sharing. The above two types of building units are further interconnected via Pb–O–Se–O–Nb bridges into a complicated 3D network with 1D tunnels of 8-MR along *c*-axis. The 1D 8-MR tunnels are based on 4 NbO_6 octahedra and 4 $Se(2)O_3$ groups, the lone pairs of the Se(2) atoms are oriented toward the center of the tunnel.

The structure of $Bi_2V_2^{V}Se_4O_{16}$ ($P2_1$/c, CS) features a 3D network composed of the 2D layer of $[Bi_2(SeO_3)_2]^{2+}$ and the 1D $[(VO_2)_2(SeO_3)_2]^{2-}$ chains. Its asymmetric unit contains two BiO_7 polyhedra, two VO_6 octahedra, and four selenite anions; hence, $Bi_2V_2^{V}Se_4O_{16}$ can also be formulated as $Bi_2(V^{V}O_2)_2(SeO_3)_4$. Neighboring $V(1)O_6$ and $V(2)O_6$ octahedra are interconnected via corner sharing into a 1D chain and a pair of such chains are further interconnected via edge sharing into a 1D double chain along the *b*-axis, $Se(3)O_3$, and $Se(4)O_3$ groups are grafted into the double chain in a bidentate bridging fashion. The BiO_7 polyhedra are interconnected to a 2D layer parallel to the *ac* plane via edge- and face sharing, $Se(1)O_3$ and $Se(2)O_3$ groups are capping on the both sides of the bismuth(II) oxide layer. The above two building units are further interconnected via Bi–O–Se bridges into a 3D architecture with narrow-long-shaped 10-MR tunnels along the *b*-axis.

$Bi_2Mo_2^{VI}Se_2O_{13}$ is isostructural to $Nd_2W_2Te_2O_{13}$ mentioned earlier [102], in which the two Nd^{3+} ions have been replaced by two Bi^{3+} ions and W^{6+} cations by Mo^{6+} cations. The structure of $Bi_2Mo_2^{VI}Se_2O_{13}$ (*P*-1, CS) features a 3D network of 3D bismuth selenite with the 10-MR tunnels along *a*-axis occupied by the Mo_2O_{10} clusters [110].

It should be mentioned that although the above compounds contain two types of lone-pair cations as well as d^0 transition metal ions, they are not SHG active due to their centrosymmetric structures.

Systematic explorations of new phases in the Ga^{III}/In^{III}–Mo^{VI}–Se^{IV}/Te^{IV}–O systems by hydrothermal reactions or solid-state reactions at high temperature led to four new quaternary compounds, namely, $Ga_2MoQ_2O_{10}$ (Q = Se, Te), $In_2Mo_2Se_2O_{13}(H_2O)$, and $In_2MoTe_2O_{10}$ [111].

$Ga_2MoQ_2O_{10}$ (Q = Se, Te) were obtained by heating a mixture of Ga_2O_3, MoO_3, SeO_2, (or TeO_2) at 200 or 230°C for 4 days. $Ga_2MoQ_2O_{10}$ (Q = Se, Te) (*P*nma, CS) are isostructural, and their features a novel 3D network in which 1D chains of the edge-shared GaO_6 octahedra are further interconnected by bridging QO_3^{2-} (Q = Se, Te) anions and MoO_6 octahedra. There are one GaO_6 octahedron, one MoO_6 octahedron and two QO_3 groups in the asymmetric unit. The GaO_6 octahedra are interconnected into a 1D chain along *b*-axis via edge sharing. Neighboring gallium oxide chains are further bridged by MoO_6 octahedra into a corrugated 2D layer passing through about 1/3 *c* and 2/3 *c* with $Q(2)O_3$ groups capping on the cavities of the layer. It should be noted that MoO_6 octahedra are bridged by $Q(2)O_3$ groups into a molybdenum tellurite chain parallel to *b*-axis via corner sharing. Hence, the corrugated 2D structure can also be described as a layer formed by gallium oxide chains and molybdenum tellurite chains that are alternating along *a*-axis. The above Ga–Mo–Te–O layers are further bridged by $Q(1)O_3$ groups into a 3D network with large 1D tunnels of $Ga_6Mo_2Q_4$ 12-member rings and small tunnels of Ga_2Q_2 four-member rings both along the *b*-axis. The lone pairs of the Q^{4+} cations are orientated toward the center of the large tunnels. Although the chemical compositions of $Ga_2MoQ_2O_{10}$ and $Nd_2MoSe_2O_{10}$ are comparable, their structures are quite different. In $Nd_2MoSe_2O_{10}$, the Nd^{3+} ions are eight-coordinated and the Mo^{6+} cation is tetrahedrally coordinated. $Nd_2MoSe_2O_{10}$ features a 3D network composed of alternating neodymium(III) selenite layers and neodymium(III) molybdate layers.

When the indium(III) oxide was used instead of gallium(III) oxide, $In_2Mo_2Se_2O_{13}(H_2O)$ and $In_2MoTe_2O_{10}$ were isolated. Rose-pink prism-shaped crystals of $In_2Mo_2Se_2O_{13}(H_2O)$ were obtained by heating a mixture of MoO_3 (0.5 mmol), In_2O_3 (0.5 mmol), SeO_2 (1.2 mmol), and H_2O (6 mL) at 200°C for 5 days. The structure of $In_2Mo_2Se_2O_{13}(H_2O)$ is isostructural to $Fe_2Mo_2Se_2O_{13}(H_2O)$ [66]. $In_2Mo_2Se_2O_{13}(H_2O)$ (*C*2/c, CS) can also be formulated as $In_2\{Mo_2O_7(H_2O)\}(SeO_3)_2$. Its structure features a pillared-layered structure in which the indium selenite layers are bridged by $Mo_2O_9(H_2O)$ dimers. Colorless prism-shaped crystals of $In_2MoTe_2O_{10}$ were obtained by heating a mixture of MoO_3 (0.3 mmol), In_2O_3 (0.25 mmol), TeO_2 (0.58 mmol), and H_2O (8 mL) at 230°C for 7 days. It should be note that the single phase powder sample of $In_2MoTe_2O_{10}$ was obtained by solid-state reaction of a mixture composed of MoO_3, In_2O_3, and TeO_2 in a molar ratio of 1:1:2. $In_2MoTe_2O_{10}$ ($P2_1/n$, CS) can also be formulated to be $In_2(MoO_4)(TeO_3)_2$ as in $Nd_2(MoO_4)(SeO_3)_2$. However, their structures are quite different. $In_2MoTe_2O_{10}$ features a 2D layered structure, which is built from indium oxide layers with MoO_4 and TeO_n ($n = 4, 5$) polyhedra hanging on both sides of the layer. The structure is composed of InO_7, InO_6, and MoO_6 octahedra as

well as TeO_3 groups. $In(1)O_7$ and $In(2)O_6$ polyhedra are interconnected via edge sharing into a dimer, such dimers are further interconnected via corner sharing into a indium(III) oxide layer. The MoO_4 and TeO_n ($n = 4, 5$) groups capped on both sides of the indium oxide layer. The lone pairs of the Te^{4+} cation are orientated toward the interlayer space. The interlayer distance is about 9.0 Å. There are also weak interlayer Te–O bonds (2.512(8) Å). It is interesting to note that the $Te(1)O_4$ group is "isolated," whereas $Te(2)O_5$ groups are interconnected via corner sharing into 1D tellurium(IV) oxide "zigzag chain" along *b*-axis.

These four compounds are also not SHG active since they are structurally centrosymmetric; hence, polarizations of asymmetric MoO_6 octahedra and selenite or tellurite groups have been completely cancelled out.

3.2 Metal Selenites or Tellurites Containing Halogen Anions

It is reported that the transition metal selenites or tellurites containing halogen anions can display many types of novel structures and interesting magnetic properties such as low dimensional magnets, etc. Transition metal Te(IV) or Se(IV) oxyhalides can be regarded as so-called "chemical scissors" [112, 113]. The later transition metal cations form bonds to both oxygen and halide, whereas lone-pair cations tend to form bonds only to oxygen anions. Such chemical difference can be utilized to prepare low dimensional transition metal materials with interesting magnetic properties [112, 113]. Furthermore, it is well known that the introduction of halogen anions can widen the transparency of NLO materials in the UV region as in $KBe_2BO_3F_2$ (KBBF) [114]. Recent studies also show that the introduction of the halogen anions into the lead(II) borates can significantly enhance the SHG efficiency of the inorganic compounds [115]. So far, a few of compounds in metal Te(IV) or Se(IV) oxyhalides have been reported, some of which exhibit NCS structures. For example, $Bi_4Te_2O_9Br_2$ crystallizes in the polar space group *P*mm2, and it also displays pyroelectric property. Its structure features a 2D layer of $[Bi_4Te_2O_9]^{2+}$ separated by bromine anions [116]. $BaCu_2Te_2O_6Cl_2$ crystallized in the polar space group $P2_1$, its structure is a 3D network composed of edge-shared $Cu(1)Cl_2O_3$ and $Cu(2)ClO_4$ square pyramidal dimers bridged by $Te(1)O_3$ and $Te(2)O_4$ groups with the Ba^{2+} cations being located at the cavities of the structure [117].

Based on above reasons, we have performed systematic explorations in the transition metal or lanthanide transition metal Te(IV) or Se(IV) oxyhalide systems, 12 new compounds were isolated by solid-state reactions at high temperatures, including $\{Cd_2(Te_6O_{13})\}\{Cd_2Cl_6\}$, $Cd_7Cl_8(Te_7O_{17})$ [118], $Ni_5(SeO_3)_4Cl_2$, $Ni_5(SeO_3)_4Br_2$, $Ni_7(TeO_3)_6Cl_2$, $Ni_{11}(TeO_3)_{10}Cl_2$, [119, 120], $DyCuTe_2O_6Cl$, $ErCuTe_2O_6Cl$, $ErCuTe_2O_6Br$, $Sm_2Mn(Te5O_{13})Cl_2$, $Dy_2Cu(Te_5O_{13})Br_2$, and $Nd_4Cu(TeO_3)_5Cl_3$ [121]. Among these compounds, $Cd_7Cl_8(Te_7O_{17})$ and $Nd_4Cu(TeO_3)_5Cl_3$ crystallized in polar space group.

$[Cd_2(Te_6O_{13})][Cd_2Cl_6]$ was obtained quantitatively by the reaction of a mixture of $CdO/CdCl_2/TeO_2$ in a molar ratio of 1: 3: 6 at 670°C for 6 days. The structure of $[Cd_2(Te_6O_{13})][Cd_2Cl_6]$ (*P*-1) features cationic cadmium(II) tellurium(IV) oxide layers parallel to *ab* plane and "isolated" anionic cadmium(II) chloride double chains along the *a*-axis. The $[Cd_2Cl_6]^{2-}$ double chain passing through the cell edge is formed by edge-shared $Cd(3)Cl_6$ and $Cd(4)Cl_6$ octahedra. The cadmium (II) tellurium(IV) oxide layer in $[Cd_2(Te_6O_{13})][Cd_2Cl_6]$ is formed by novel 1D slabs of $Te_6O_{13}^{2-}$ anions interconnected by Cd–O double chains. $Te(1)O_4$, $Te(2)O_4$, and $Te(3)O_4$ groups are interconnected via corner- and edge sharing into a trinuclear unit, and neighboring units are corner shared into a 1D chain along the *a*-axis. Two $Te(5)O_5$ and two $Te(6)O_3$ groups form a tetranuclear unit via corner- and edge sharing. The above 1D chains and tetranuclear units are bridged by $Te(4)O_4$ groups, through corner sharing, into a 1D $Te_6O_{13}^{2-}$ slab, forming six- and seven-member polyhedral rings (Scheme 1f). The width of the slab is about 14.6 Å. The lone-pair electrons of the Te(IV) atoms are oriented toward the open space between the cadmium chloride chains and cadmium tellurium(IV) oxide layers.

Colorless crystalline sample of $Cd_7Cl_8(Te_7O_{17})$ was then obtained quantitatively by the reaction of a mixture of $CdO/CdCl_2/TeO_2$ in a molar ratio of 3/4/7 at 720°C for 6 days. $Cd_7Cl_8(Te_7O_{17})$ crystallized in a polar space group $Pca2_1$, its structure features a 3D network composed of different tellurium(IV) oxide and cadmium chloride substructures with long narrow tunnels along the *b*-axis. The two structural building blocks are 1D $[Te_7O_{17}]^{6-}$ anions and unusual corrugated $[Cd_7Cl_8]^{6+}$ layers based on cyclohexane-type Cd_3Cl_3 rings. The $Te_7O_{17}^{6-}$ anion features a 1D architecture different from that of the $Te_6O_{13}^{2-}$ anion in $[Cd_2(Te_6O_{13})][Cd_2Cl_6]$. Only two types of tellurium(IV) oxide polyhedra are found: TeO_3 for Te(7) and TeO_4 for the remaining six tellurium atoms. TeO_3 and TeO_4 groups are interconnected via corner sharing into another type of 1D slab, forming two types of six-member polyhedral rings and one type of three-member polyhedral ring (Scheme 1g). The three-member ring is composed of three TeO_4 groups. One type of the six-member ring is formed by solely TeO_4 groups in a "pear" shape, whereas the other type is made of two TeO_3 and four TeO_4 groups. The width of this 1D slab is 12.1 Å, which is slightly narrower than that of the $Te_6O_{13}^{2-}$ anion in $[Cd_2(Te_6O_{13})][Cd_2Cl_6]$. In contrast to those in $[Cd_2(Te_6O_{13})][Cd_2Cl_6]$, the Cd and Cl atoms in $Cd_7Cl_8(Te_7O_{17})$ are interconnected to a novel corrugated 2D layer parallel to the *bc* plane. The layer is based on distorted cyclohexane-type Cd_3Cl_3 rings. These 2D layers can be viewed as the result of removing 1/8 of Cd(II) ions from a perfect "Cd_8Cl_8" 2D layer leaving vacant Cd_6Cl_6 rings. The above two types of building units are interconnected via Te–O–Cd bridges into a 3D network with long narrow tunnels along the *b*-axis. The stereoactive lone pairs of the Te(IV) atoms are oriented toward the narrow tunnels [118]. The polarization directions of tellurite groups are almost opposite, resulting in mostly cancellation of the local dipole moments, which is also confirmed by a very weak SHG response we measured recently.

When Ni(II) halide was used instead of Cd(II) halide, four different structures with a general formula of $Ni_{n+1}(QO_3)_nX_2$ (Q = Se, X = Cl, Br, $n = 4$; Q = Te, X = Cl, $n = 6$, 10) were isolated.

$Ni_5(SeO_3)_4Cl_2$ was prepared by solid-state reaction of 0.4 mmol of $NiCl_2$, 0.8 mmol of Ni_2O_3, and 1.6 mmol of SeO_2 at 700°C for 6 days. $Ni_5(SeO_3)_4Cl_2$ (*P*-1, CS) features a 3D network formed by the interconnection of nickel(II) octahedra via corner-, edge- and face sharing with Se^{4+} ions capping on its cavities. Such a structure is different from $Ni_5(TeO_3)_4Cl_2$ with a similar formula. $Ni_5(TeO_3)_4Cl_2$ exhibits a layered structure composed of corner-, edge- and face shared 2D Ni(II) octahedral layer capped by TeO_3 groups on the both sides [119].

Red brick-shaped single crystals of $Ni_5(SeO_3)_4Br_2$ were prepared by the solid-state reaction of a mixture containing Ni_2O_3 (1.2 mmol), $NiBr_2$ (0.6 mmol), and SeO_2 (2.4 mmol) at 670°C for 6 days. $Ni_5(SeO_3)_4Br_2$ (*P*-1, CS) features a 3D network different from that of $Ni_5(SeO_3)_4Cl_2$. Its 3D structure can be viewed as nickel(II) oxy-bromide layers that are bridged by Se(IV) and additional Ni(II) ions. $Ni(1)O_5Br$ and $Ni(3)O_5Br$ octahedra are interconnected via edge sharing into a 1D chain, and neighboring chains are further interconnected via corner sharing into a layered architecture. The above 2D nickel oxybromide layers are further interconnected by Ni(2) and Se(IV) atoms into a condensed 3D network. Such a 3D network can also be viewed as a pillared layered structure in which Ni(2) and selenite groups act as pillars [120].

Green brick single crystals of $Ni_7(TeO_3)_6Cl_2$ and orange plates of $Ni_{11}(TeO_3)_{10}Cl_2$ were obtained from a same solid-state reaction of a mixture of NiO (2.4 mmol), $NiCl_2$ (0.6 mmol), and TeO_2 (1.8 mmol) at 710°C for 6 days. The structure of $Ni_7(TeO_3)_6Cl_2$ (*R*-3, CS) features a novel 3D network based on Ni_4ClO_3 cubane-like clusters with Te atoms located at the cavities of the network. Three $Ni(1)O_5Cl$ moieties and one $Ni(2)O_6$ unit forms a Ni_4ClO_3 cubane-like cluster via O···O and O···Cl edge sharing. The four nickel(II) ions within the Ni_4ClO_3 cluster displays a slightly distorted tetrahedron. Each pair of cubanes are condensed into a dimeric unit by sharing a Ni(2) atom. Along the *ab* plane, the Ni_4ClO_3 cubanes are interconnected via edge sharing into a novel 2D cluster layer, forming 12-member polyhedral rings. Each ring is composed of six Ni_4ClO_3 cubanes; hence, such cubane cluster layers are to some extent similar to those of graphite. Neighboring 2D layers are interconnected by sharing Ni(2) atoms into a 3D network with small long-narrow-shaped tunnels along the *a*-axis. The Te atoms are located at the above tunnels and connected to the cubanes via Te–O–Ni bridges. It should be pointed out that such stacking of the cluster layers eliminates the large tunnels along *c*-axis created by 12-member rings.

The structure of $Ni_{11}(TeO_3)_{10}Cl_2$ (*P*-1, CS) features a very complicated 3D network. There are six unique nickel(II) ions, five tellurite groups, and one chloride anion in its asymmetric unit. The interconnection of NiO_5Cl, NiO_6, and NiO_5 polyhedra via corner- and edge sharing led to a complex 3D network of nickel oxychloride. The Te(IV) atoms are located at the voids of the network and also connect with the framework through Ni–O–Te bridges. The 3D nickel oxychloride network can also be considered as a pillared layered architecture based on the nickel oxide layers composed of Ni(2), Ni(3), Ni(4), and Ni(5). Each pair of $Ni(1)O_5Cl$ octahedra form a dimeric unit via edge sharing; these dimers act as pillars between two neighboring nickel oxide layers.

It is interesting to note that the four nickel(II) compounds can be generally formulated as $Ni_{n+1}(QO_3)_nX_2$, where Q and X represent Se(or Te) and halide anion, respectively. Also, the nickel sites may be partially occupied when *n* is large such as in $Ni_{11}(TeO_3)_{10}Cl_2$. It is also noted that change of halide anion or change of selenite anion by tellurite anion may lead to complete different structural types even though their compounds have similar chemical formulae.

When lanthanide(III) ion was introduced into transition metal Te(IV) or Se(IV) oxyhalides, six new lanthanide transition metal tellurium(IV) oxyhalides were obtained, namely, $DyCuTe_2O_6Cl$, $ErCuTe_2O_6Cl$, $ErCuTe_2O_6Br$, $Sm_2Mn(Te_5O_{13})Cl_2$, $Dy_2Cu(Te_5O_{13})Br_2$, and $Nd_4Cu(TeO_3)_5Cl_3$. They form three different structural types [121].

$DyCuTe_2O_6Cl$, $ErCuTe_2O_6Cl$, and $ErCuTe_2O_6Br$ ($P2_1/c$, CS) are isostructural. They were prepared by the solid-state reaction of a mixture of Dy_2O_3 (or Er_2O_3), CuO, $CuCl_2$ (or $CuBr_2$), and TeO_2 at 750 or 720°C. They feature a 3D network structure. LnO_8 polyhedra are interconnected via edge sharing into a 1D lanthanide (III) oxide chain along the *a*-axis. Each pair of CuO_4Cl polyhedra is bridged by a pair of tellurite groups to form a 1D chain along the *a*-axis. The interconnection of LnO_8 and CuO_4Cl polyhedra via bridging tellurite groups led to a 3D network with apertures running along the *a*-axis. These apertures are formed by ten polyhedral rings composed of 4 Dy, 4 Cu, and 2 tellurite anions. The halide anions and the lone pairs of the tellurium(IV) atoms are orientated toward the above apertures.

Single crystals of $Sm_2MnTe_5O_{13}Cl_2$ and $Dy_2CuTe_5O_{13}Br_2$ were obtained from the solid-state reactions of a mixture containing Sm_2O_3 (or Dy_2O_3), MnO_2 (or CuO), $MnCl_2$ (or $CuBr_2$), and TeO_2 at 750°C for 6 days. $Sm_2MnTe_5O_{13}Cl_2$ and $Dy_2CuTe_5O_{13}Br_2$ ($P2_1/n$, CS) are isostructural and their structures feature a 3D network of lanthanide transition metal tellurite with long, narrow-shaped tunnels occupied by the isolated halides. TeO_3 and TeO_4 polyhedra are interconnected via corner- and edge sharing to form two different tellurium(IV) oxide anions: $Te_3O_8^{4-}$ and $Te_4O_{10}^{4-}$. In $Te_4O_{10}^{4-}$, two TeO_4 form a dimeric unit by edge sharing, and the dimer further corner shares with two TeO_3 groups. $Te_3O_8^{4-}$ is composed of three corner-sharing TeO_3 groups. The interconnection of the Sm^{III} (or Dy^{III}) ions and Mn^{II} (or Cu^{II}) ions by $Te_3O_8^{4-}$ and $Te_4O_{10}^{4-}$ anions results in a 3D network with tunnels running along the *b*-axis. The halide anions remain isolated and are located at the above tunnels. The lone-pair electrons of the tellurium(IV) atoms are also oriented toward the tunnels.

$Nd_4Cu(TeO_3)_5Cl_3$ was obtained as a single phase by the following reactions at 650°C: $2NdOCl + Nd_2O_3 + CuCl + 5TeO_2 \rightarrow Nd_4CuTe_5O_{15}Cl_3$. $Nd_4Cu(TeO_3)_5Cl_3$ crystallizes in the polar space group *I*2, its structure features a 3D network of neodymium(III) tellurite with large tunnels in which 1D chains of copper(I) chloride are inserted. The interconnection of Nd(III) ions by bridging and chelating tellurite groups led to a 3D network with large tunnels along the *b*-axis. The tunnels are formed by 16-membered polyhedral rings composed of 8 TeO_3 and 8 Nd atoms. The lone-pair electrons of the tellurite groups are located at the above tunnels. Neighboring $CuCl_4$ tetrahedra are interconnected via corner sharing into a 1D two-unit repeating (zweier) chain along the *b*-axis. These copper(I) chloride chains are inserted in the centers of the above tunnels and form Cu–Cl–Nd bridges.

In this structure, the polarizations of $Te(2)O_3$, $Te(3)O_3$, $Te(4)O_3$, and $Te(5)O_3$ groups are mostly cancelled out but the polarizations of $Te(1)O_3$ groups are aligned in the same direction to produce a moderate net dipole moment along the *b*-axis [121]. Unfortunately, no SHG measurements for this compound have been made.

3.3 *Metal Tellurites and Selenites Containing Tetrahedral Groups of Main Group Elements*

Tetrahedral groups of main group elements, such as PO_4, BO_4, SiO_4, may also be SHG active and induce the formation of the NCS structures. Hence, metal tellurites and selenites containing additional tetrahedral groups may lead to the formation of new NCS structures with excellent SHG properties. So far such compounds are still rare and mainly focused on tellurite phosphates, namely, $Te_2O_3(HPO_4)$, $Te_8O_{10}(PO_4)_4$, $Te_3O_3(PO_4)_2$, $Te_2O(PO_4)_2$, $Ba_2TeO(PO_4)_2$, $BaTeMO_4(PO_4)$ ($M = Nb^{5+}$ or Ta^{5+}), and $A_2TeMo_2O_6(PO_4)_2$ ($A = K$, Rb, Cs, or Tl) [65, 122–127]. In these compounds, only $Te_2O_3(HPO_4)$ ($Pca2_1$, NCS) and $Te_2O(PO_4)_2$ (Cc, NCS) crystallized in polar space groups. The structure of $Te_2O_3(HPO_4)$ features a 3D framework composed of 2D $Te_2O_3^{2+}$ cationic layer bridged by PO_4 tetrahedra. In this structure, the polarizations of $Te(2)O_4$ groups are toward almost opposite directions, whereas the polarizations of $Te(1)O_4$ groups are align in the same direction; hence, a net dipole moment is produced [122]. $Te_2O(PO_4)_2$ shows a 3D framework structure composed of slightly distorted TeO_5 square pyramids and PO_4 tetrahedra. The polarization directions of $Te(1)O_5$ and $Te(2)O_5$ groups are almost opposite, resulting the cancellation of most of their local dipole moments. SHG measurements reveal that $Te_2O(PO_4)_2$ displays a weak SHG efficiency of approximately 50 × α-SiO_2 [65].

Our explorations in such systems by solid-state reactions and hydrothermal syntheses afford four new compounds with different structures, namely, two novel lanthanum(III) tellurites with additional SiO_4 or GeO_4 tetrahedra ($La_4(Si_{5.2}Ge_{2.8}O_{18})(TeO_3)_4$ and $La_2(Si_6O_{13})(TeO_3)_2$) [128], one selenite with BO_4 tetrahedra ($B_2Se_2O_7$) [14] and one tellurite with GaO_4 tetraheda ($Ga_2Te_3O_9$) [67]. Both $B_2Se_2O_7$ and $Ga_2Te_3O_9$ crystallized in NCS structure and are SHG active.

$La_4(Si_{5.2}Ge_{2.8}O_{18})(TeO_3)_4$ was initially obtained by solid-state reaction of La_2O_3 (0.4 mmol), GeO_2 (0.4 mmol), TeO_2 (1.2 mmol), with 0.4 mmol of CsCl as flux in an evacuated quartz tube at 800°C for 6 days. Si element came from the silica tube. The structure of $La_4(Si_{5.2}Ge_{2.8}O_{18})(TeO_3)_4$ (P-1, CS) features a 3D network composed of the $[(Ge_{2.82}Si_{5.18})O_{18}]^{4-}$ layers and the $[La_4(TeO_3)_4]^{4+}$ layers that alternating along *b*-axis. The germanate-silicate layer consists of corner-shared XO_4 ($X = Si/Ge$) tetrahedra, forming four- and six-member rings. The 2D $[La_4(TeO_3)_4]^{4+}$ layer is formed by lanthanide(III) ions bridged by TeO_3 groups.

$La_2(Si_6O_{13})(TeO_3)_2$ was prepared by solid-state reaction of La_2O_3 (0.4 mmol), SiO_2 (1.6 mmol), and TeO_2 (0.8 mmol) at 960°C for 6 days. The structure of $La_2(Si_6O_{13})(TeO_3)_2$ ($P2_1/c$, CS) is a 3D network composed of the $[Si_6O_{13}]^{2-}$ double layers and the $[La_2(TeO_3)_2]^{2+}$ layers that alternate along *a*-axis. The $[Si_6O_{13}]^{2-}$ double layer is built by corner sharing SiO_4 tetrahedra, forming four-, five-, and eight-member rings. The $[La_2(TeO_3)_2]^{2+}$ layer perpendicular to the *a*-axis is similar to that in $La_4(Si_{5.2}Ge_{2.8}O_{18})(TeO_3)_4$. The TeO_3^{2-} anions in both compounds are only involved in the coordination with the La^{3+} ions to form a lanthanum(III) tellurite layer [128].

Compounds containing both borate anion and selenium(IV) may also possess good SHG properties due to the presence of two types of SHG active groups. So far, $B_2Se_2O_7$, prepared by our group is the only such example. Single crystals of $Se_2B_2O_7$ were isolated quantitatively by the solid-state reaction of B_2O_3 (1.2 mmol) and SeO_2 (2.4 mmol) at 320°C in an evacuated quartz tube. The structure of $Se_2B_2O_7$ ($P2_12_12_1$, NCS) features a 3D network in which B_2O_7 dimers composed of two corner sharing BO_4 tetrahedra are bridged by SeO_3 groups (Fig. 27). The open framework of $Se_2B_2O_7$ can also be described as an interesting mixed (3,4)-connected net of the B and Se (linked by –O– bridges). Right-handed helical tunnels along *c*-axis are formed. These tunnels are based on B_6Se_4 10-member rings. The lone pairs of the Se^{IV} cations are orientated toward the above tunnels. $B_2Se_2O_7$ exhibits a moderate strong SHG efficiency of about 2.2 times of KDP [14].

Many efforts were tried to prepare $Te_2B_2O_7$, the analog of $Se_2B_2O_7$, but were unsuccessful. Probably it is due to too large difference between the distance of Te–O and B–O bonds. We therefore tried to prepare the gallium tellurites. Two isomeric gallium(III) tellurites, namely, α-$Ga_2(TeO_3)_3$ and β-$Ga_2(TeO_3)_3$ were isolated [67].

The two compounds were hydrothermally synthesized by reactions of a mixture of Ga_2O_3 (0.2 mmol), TeO_2 (0.6 mmol), and Li_2CO_3 (0.10 mmol for α-$Ga_2(TeO_3)_3$ or 0.25 mmol for β-$Ga_2(TeO_3)_3$) in 6 mL of distilled water at 230°C for 7 days. It is found

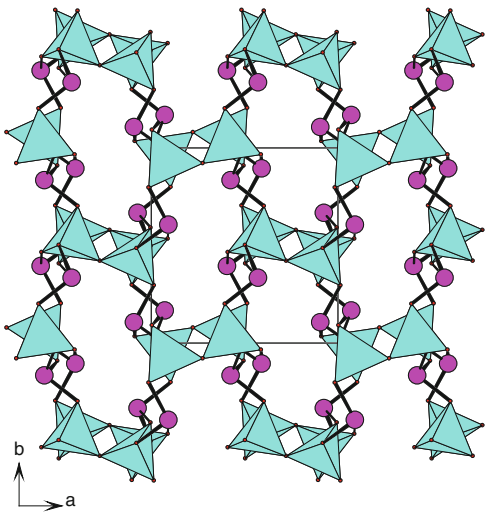

Fig. 27 View of the structure of $Se_2B_2O_7$ down the *b*-axis. BO_4 tetrahedra are shaded in *cyan*. Se, B and O atoms are drawn as *pink*, *cyan* and *red circles*, respectively

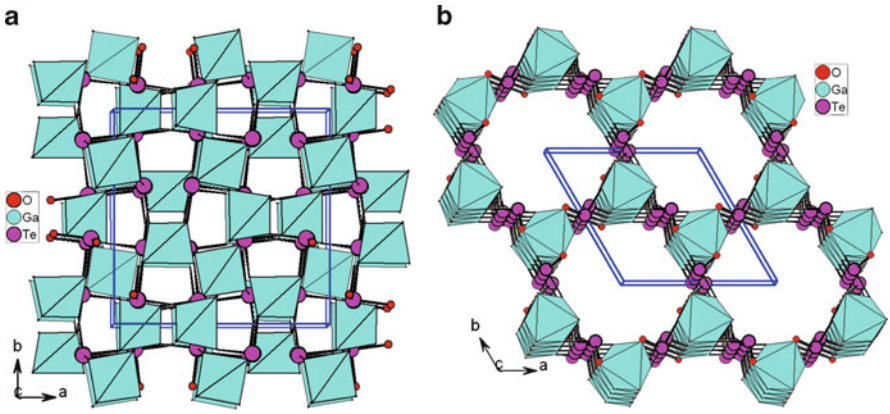

Fig. 28 View of the structure of α-$Ga_2(TeO_3)_3$ (**a**) and β-$Ga_2(TeO_3)_3$ (**b**) down the *c*-axis

that the amount of Li_2CO_3 added is very important to the chemical compositions and structures of the products formed. If 0.10 mmol Li_2CO_3 was used, the noncentrosymmetric α-$Ga_2(TeO_3)_3$ was isolated. When the amount of Li_2CO_3 used was increased to 0.25 mmol, centrosymmetric β-$Ga_2(TeO_3)_3$ was isolated in a very low yield. The structure of acentric α-$Ga_2(TeO_3)_3$ (*I*-43d) features a close packing 3D network with alternatively linkage of GaO_4 tetrahedra and TeO_3 trigonal pyramids via corner sharing (Fig. 28a). The structure of centrosymmetric β-$Ga_2(TeO_3)_3$ ($P6_3/m$) features a 3D open framework with 1D 12-MR tunnels along the *c*-axis. Different from the α phase, the gallium(III) ion in the β phase is octahedrally coordinated. Two GaO_6 octahedra are interconnected to a Ga_2O_9 dimer via face sharing, and such dimers are bridged by the TeO_3 groups into a 1D gallium tellurite chain along the *c*-axis. The above chains are further linked by additional TeO_3 groups into a 3D open framework with 1D 12-MR tunnels along the *c*-axis (Fig. 28b). The internal diameter of the channel is 7.983 Å (about 0.8 nm). SHG measurements on a Q-switched Nd:YAG laser with the sieved powder samples revealed that α-$Ga_2(TeO_3)_3$ displays a moderate-strong SHG response about that of KDP [67].

4 Conclusions and Outlook

In summary, the syntheses, structures, and SHG properties of metal iodates, selenites, and tellurites with lone-pair electrons containing d^0 TM cations, other lone pairs and tetrahedral groups were reviewed. Combination of two or more types of asymmetric units into a same compound not only can gives rise to a rich structural chemistry but also may afford many *NCS* compounds with excellent SHG properties. As for the direction of the out-of-center distortion, it was found that V^{5+} and Nb^{5+} usually displace toward an edge or corner, whereas Mo^{6+} and

W^{6+} are more likely distorted toward an edge or face. V^{5+} cation may adopt the square pyramidal geometry beside tetrahedron and octahedron, whereas Mo^{6+} and W^{6+} are usually tetrahedrally or octahedrally coordinated. Furthermore, V^{5+} cation is not as stable as other d^0 TM cations, and on some occasions it can be reduced to V^{4+} during the reaction. The bond polarization follows the following order of I (V) > Te(IV) > Se(IV), and $Mo^{6+} > V^{5+} > W^{6+} > Nb^{5+} > Ta^{5+}$. Furthermore, the counterions also have dramatic effects on the structural topologies and the SHG properties of the compounds formed. The slight change of the ionic radius of the cation such as A(I) or lanthanide(III) ion could lead to a completely different structure as exampled by $A_2W_3TeO_{12}$ ($A = K^+$, Rb^+, and Cs^+) and $Ln_2MoTe_3O_{12}$ (Ln = La, Nd). $A(VO)_2O_2(IO_3)_3$ ($A = K^+$, Rb^+, Cs^+, NH_4^+) are isostructural but their SHG responses follow a sequence as below, K > Rb > Cs > NH_4. The isostructural compounds of $Ln_3Pb_3(IO_3)_{13}(\mu^3\text{-}O)$ (Ln = La, Pr, Nd) display SHG signals that about 2.0, 1.0, and 0.8 times of KDP, respectively, whereas the SHG signal for the cerium compound is very weak. With respect to synthesis, molar ratios of the starting materials, synthetic methods, and reaction temperatures are also very important to the chemical compositions, structures, and physical properties of materials formed. For example, the amount of Li_2CO_3 controlled whether noncentrosymmetric cubic phase α-$Ga_2(TeO_3)_3$ or centrosymmetric hexagonal phase β-$Ga_2(TeO_3)_3$ is isolated.

As for the different anions, it is worthy to mention that I(V) mainly appears as IO_3 group, but polymeric anionic clusters such as $I_3O_8^-$ in NaI_3O_8 and layered $I_4O_{11}^{2-}$ anion in $Cs_2I_4O_{11}$ are also possible. The Se(IV) cation mainly exists as SeO_3 group (in some cases as the diselenite group), whereas Te(IV) can be 3-, 4-, or 5-coordinated, and the most amazing aspect is that these TeO_x (x = 3–5) polyhedra can be polymerized into many types of polynuclear clusters or extended skeletons (Scheme 1) besides ditellurite anion. Inorganic solids with various polymeric tellurium(IV) oxide anions include $Te_3O_8^{4-}$ trimer in $La_2MoTe_3O_{12}$, $Te_4O_{11}^{6-}$ tetramer in $Er_2Te_4O_{11}$,[29] $Te_5O_{13}^{6-}$ pentamer in $Ln_5MTe_7O_{23}Cl_3$ (Ln = Pr, Nd; M = Mo, W), 1D $Te_4O_{10}^{4-}$ in $Ln_2MoTe_4O_{14}$ (Ln = Pr, Nd), 1D $Te_6O_{13}^{2-}$ in $\{Cd_2(Te_6O_{13})\}\{Cd_2Cl_6\}$ and 1D $Te_7O_{17}^{6-}$ in $Cd_7Cl_8(Te_7O_{17})$, layered $Te_3O_7^{2-}$ in $La_2WTe_6O_{18}$, 1D $[Te_4O_9(OH)]^{3-}$ in $Ba_2(VO_3)Te_4O_9(OH)$, 1D TeO_3^{2-} in $Cs_3Nb_9O_{18}(TeO_3)_2(TeO_4)_2$, 2D $Te_4O_9^{2-}$ in $K_2Te_4O_9{\cdot}3.2H_2O$ and 2D $Te_2O_5^{2-}$ in $Ln(Te_2O_5)X$ (Ln = Nd, X = Cl, Br; Ln = Gd, X = Cl) [14], etc. Certainly more such examples will be discovered in the future and extensive theoretical studies are needed to understand its origin.

Based on this review, several opportunities and challenges are apparent. For d^0 TM–I(V)–O system, no metal iodates containing W(VI) or Ta(V) cation has been reported because of the synthetic difficulties, and only one Nb(V) iodate is reported. For the metal iodates containing other lone pairs, there is no metal iodates with lone pair-containing Sb(III), Sn(II), Se(IV), or Te(IV) reported, and little is known about the bismuth iodates except two centrosymmetric $Bi(IO_3)_3$ and $Bi(IO_3)_3(H_2O)_2$. With respect to metal selenites or tellurites, the combination of lone pair Te(IV) or Se(IV) with borate is quite promising in searching for new SHG materials. Very recently, a series of alkali metal boroselenites were synthesized by solid-state reactions in our group, some of which crystallized in NCS structures and display

excellent SHG properties due to the polarizations from both B–O polyhedra and SeO_3 groups. Furthermore, metal Te(IV) or Se(IV) oxyhalides are mainly focused on low dimensional magnets before, and their SHG properties have been somewhat overlooked. Some metal Te(IV) oxyhalides reported crystallized in polar structures but their NLO properties have not been studied.

Also the crystal growth for the compounds with excellent SHG properties is also very important for practical applications. Large single crystals of $BaMo_2TeO_9$, $Na_2W_2TeO_9$, and $Cs_2Mo_3TeO_{12}$ have been obtained and their physical properties studied in more details; however, large single crystals for other SHG compounds remain to be grown and their physical properties studied more deeply. To fully address these problems, strong interactions between synthetic and theoretical chemists as well as materials chemists are necessary.

Acknowledgments This work was supported by the National Natural Science Foundation of China (Grants Nos. 20731006, 20825104, 21001107, and 20821061), NSF of Fujian Province (Grant 2011J05037) and Key Laboratory of Optoelectronic Materials Chemistry and Physics, Chinese Academy of Sciences (Grant No 2008DP173016).

References

1. Chen CT, Liu G (1986) Annu Rev Mater Sci 16:203–243
2. Halasyamani PS, Poeppelmeier KR (1998) Chem Mater 10:2753–2769
3. Wickleder MS (2002) Chem Rev 102:2011–2087
4. Becker P (1998) Adv Mater 10:979–992
5. Chen CT, Wang YB, Wu BC, Wu KC, Zeng WL, Yu LH (1995) Nature 373:322–324
6. Chen CT, Wu BC, Jiang AD, You GM (1985) Sci Sin Ser B 28:235–243
7. Hagerman ME, Poeppelmeier KR (1995) Chem Mater 7:602–621
8. Bera TK, Jang JI, Song JH, Malliakas CD, Freeman AJ, Ketterson JB, Kanatzidis MG (2010) J Am Chem Soc 132:3484–3495
9. Dmitriev VG, Gurzadyan GG, Nikogosyan DN (1991) Handbook of nonlinear optical crystals. Springer, Berlin
10. Phanon D, Gautier-Luneau I (2007) Angew Chem Int Ed 46:8488–8491
11. Pan SL, Smit JP, Watkins B, Marvel MR, Stern CL, Poeppelmeier KR (2006) J Am Chem Soc 128:11631–11634
12. Zhang WL, Cheng WD, Zhang H, Geng L, Lin CS, He ZZ (2010) J Am Chem Soc 132:1508–1509
13. Kong F, Huang SP, Sun ZM, Mao JG, Cheng WD (2006) J Am Chem Soc 128:7750–7751
14. Mao JG, Jiang HL, Kong F (2008) Inorg Chem 47:8498–8510
15. Wang SC, Ye N, Li W, Zhao D (2010) J Am Chem Soc 132:8779–8786
16. Halasyamani PS (2004) Chem Mater 16:3586–3592
17. Sun CF, Yang BP, Mao JG (2011) Sci China Ser B Chem 54:911–922
18. Ok KM, Halasyamani PS (2006) Chem Mater 18:3176–3183
19. Ok KM, Halasyamani PS (2004) Angew Chem Int Ed 43:5489–5491
20. Phanon D, Gautier-Luneau I (2007) J Mater Chem 17:1123–1130
21. Kim SH, Yeon J, Halasyamani PS (2009) Chem Mater 21:5335–5342
22. Wu BC, Tang DY, Ye N, Chen CT (1996) Opt Mater 5:105–109
23. Sykora RE, Ok KM, Halasyamani PS (2002) J Am Chem Soc 124:1951–1957

24. Sykora RE, Ok KM, Halasyamani PS, Wells DM, Albrecht-Schmitt TE (2002) Chem Mater 14:2741–2749
25. Shehee TC, Sykora RE, Ok KM, Halasyamani PS, Albrecht-Schmitt TE (2003) Inorg Chem 42:457–462
26. Chang HY, Kim SH, Halasyamani PS, Ok KM (2009) J Am Chem Soc 131:2426–2427
27. Chang HY, Kim SH, Ok KM, Halasyamani PS (2009) J Am Chem Soc 131:6865–6873
28. Sun CF, Hu CL, Xu X, Ling JB, Hu T, Kong F, Long XF, Mao JG (2009) J Am Chem Soc 131:9486–9487
29. Yang BP, Hu CL, Xu X, Sun CF, Zhang JH, Mao JG (2010) Chem Mater 22:1545–1550
30. Sun CF, Hu CL, Xu X, Yang BP, Mao JG (2011) J Am Chem Soc 133:5561–5572
31. Porter Y, Bhuvanesh NSP, Halasyamani PS (2001) Inorg Chem 40:1172–1175
32. Porter Y, Ok KM, Bhuvanesh NSP, Halasyamani PS (2001) Chem Mater 13:1910–1915
33. Ok KM, Bhuvanesh NSP, Halasyamani PS (2001) Inorg Chem 40:1978–1980
34. Ra HS, Ok KM, Halasyamani PS (2003) J Am Chem Soc 125:7764–7765
35. Zhang WG, Tao XT, Zhang CQ, Gao ZL, Yu WT, Cheng XF, Liu XS, Jiang MH (2008) Cryst Growth Des 8:304–307
36. Zhang WG, Tao XT, Zhang CQ, Zhang HJ, Jiang MH (2009) Cryst Growth Des 9:2633–2636
37. Ok KM, Halasyamani PS (2004) Inorg Chem 43:4248–4253
38. Hart RT, Ok KM, Halasyamani PS, Zwanziger JW (2004) Appl Phys Lett 85:938–939
39. Goodey J, Broussard J, Halasyamani PS (2002) Chem Mater 14:3174–3180
40. Johnston MG, Harrison WTA (2001) Inorg Chem 40:6518–6520
41. Balraj V, Vidyasagar K (1999) Inorg Chem 38:5809–5813
42. Ok KM, Halasyamani PS (2005) Inorg Chem 44:9353–9359
43. Li PX, Hu CL, Xu X, Wang RY, Sun CF, Mao JG (2010) Inorg Chem 49:4599–4605
44. Liu XM, Li GH, Hu YW, Yang M, Kong XG, Shi Z, Feng SH (2008) Cryst Growth Des 8:2453–2457
45. Sun CF, Hu CL, Xu X, Mao JG (2010) Inorg Chem 49:9581–9589
46. Hu T, Qin L, Kong F, Zhou Y, Mao JG (2009) Inorg Chem 48:2193–2199
47. Sun CF, Hu T, Xu X, Mao JG (2010) Dalton Trans 39:7960–7967
48. Sullens TA, Almond PM, Byrd JA, Beitz JV, Bray TH, Albrecht-Schmitt TE (2006) J Solid State Chem 179:1192–1201
49. Chen XA, Zhang L, Chang X, Xue HP, Zang HG, Xiao WQ, Song XM, Yan H (2007) J Alloy Compd 428:54–58
50. Chang HY, Kim SW, Halasyamani PS (2010) Chem Mater 22:3241–3250
51. Chang HY, Kim SH, Ok KM, Halasyamani PS (2009) Chem Mater 21:1654–1662
52. Harrison WTA, Buttery JHN (2000) Z Anorg Allg Chem 626:867–870
53. Harrison WTA, Dussack LL, Jacobson AJ (1994) Inorg Chem 33:6043–6049
54. Balraj V, Vidyasagar K (1998) Inorg Chem 37:4764–4774
55. Harrison WTA, Dussack LL, Vogt T, Jacobson AJ (1995) J Solid State Chem 120:112–120
56. Goodey J, Ok KM, Broussard J, Hofmann C, Escobedo FV, Halasyamani PS (2003) J Solid State Chem 175:3–12
57. Chi EO, Ok KM, Porter Y, Halasyamani PS (2006) Chem Mater 18:2070–2074
58. Zhou Y, Hu CL, Hu T, Kong F, Mao JG (2009) Dalton Trans 38:5747–5754
59. Kim JH, Baek J, Halasyamani PS (2007) Chem Mater 19:5637–5641
60. Porter Y, Halasyamani PS (2003) J Solid State Chem 174:441–449
61. Jiang HL, Huang SP, Fan Y, Mao JG (2008) Chem Eur J 14:1972–1981
62. Nguyen SD, Kim SH, Halasyamani PS (2011) Inorg Chem 50:5215–5222
63. Sivakumar T, Chang HY, Baek J, Halasyamani PS (2007) Chem Mater 19:4710–4715
64. Lee DW, Oh SJ, Halasyamani PS, Ok KM (2011) Inorg Chem 50:4473–4480
65. Kim MK, Kim SH, Chang HY, Halasyamani PS, Ok KM (2010) Inorg Chem 49:7028–7034
66. Zhang SY, Jiang HL, Sun CF, Mao JG (2009) Inorg Chem 48:11809–11820
67. Kong F, Xu X, Mao JG (2010) Inorg Chem 49:11573–11580
68. Sun CF, Hu CL, Kong F, Yang BP, Mao JG (2010) Dalton Trans 39:1473–1479

69. Sykora RE, Wells DM, Albrecht-Schmitt TE (2002) J Solid State Chem 166:442–448
70. Shehee TC, Pehler SF, Albrecht-Schmitt TE (2005) J Alloy Compd 388:225–229
71. Ok KM, Halasyamani PS (2005) Inorg Chem 44:2263–2271
72. Sykora RE, Wells DM, Albrecht-Schmitt TE (2002) Inorg Chem 41:2697–2703
73. Chen XA, Chang X, Zang HG, Wang Q, Xiao WQ (2005) J Alloy Compd 396:255–259
74. Chen XA, Zhang L, Chang X, Zang HG, Xiao WQ (2006) Acta Crystallogr Sect C 62:i76–i78
75. Loefgren P (1967) Acta Chem Scand 21:2781–2791
76. Bergman JG, Wood JS (1987) Acta Crystallogr C 43:1831–1832
77. Yeon J, Kim SH, Halasyamani PS (2009) J Solid State Chem 182:3269–3274
78. Bentria B, Benbertal D, Bagieu-Beucher M, Masse R, Mosset A (2003) J Chem Crystallogr 33:867–873
79. Phanon D, Gautier-Luneau I (2006) Z Kristallogr 221:243–244
80. Kellersohn T, Alici E, Esser D, Lutz HD (1993) Z Kristallogr 203:225–233
81. Belokoneva EL, Dimitrova OV (2010) Kristallografiya 55:24–27
82. Bindi L, Welch MD, Bonazzi P, Pratesi G, Menchetti S (2008) Mineral Mag 72:771–783
83. Yang BP, Sun CF, Hu CL, Mao JG (2011) Dalton Trans 40:1055–1060
84. Ling J, Albrecht-Schmitt TE (2007) Eur J Inorg Chem 5:652–655
85. Zhang JJ, Tao XT, Sun YX, Zhang ZH, Zhang CQ, Gao ZL, Xia HB, Xia SQ (2011) Cryst Growth Des 11:1863–1868
86. Zhang WG, Li F, Kim SH, Halasyamani PS (2010) Cryst Growth Des 10:4091–4095
87. Kortz U, Savelieff MG, Ghali FYA, Khalil LM, Maalouf SA, Sinno DI (2002) Angew Chem Int Ed 41:4070–4073
88. Harrison WTA, Dussack LL, Jacobson AJ (1996) J Solid State Chem 125:234–242
89. Vaughey JT, Harrison WTA, Dussack LL, Jacobson AJ (1994) Inorg Chem 33:4370–4375
90. Kwon YU, Lee KS, Kim YH (1996) Inorg Chem 35:1161–1167
91. Lee KS, Kwon YU, Namgung H, Kim SW (1995) Inorg Chem 34:4178–4181
92. Hou JY, Huang CC, Zhang HH, Yang QY, Chen YP, Xu JF (2005) Acta Crystallogr Sect C 61:i59–i60
93. Sivakumar T, Ok KM, Halasyamani PS (2006) Inorg Chem 45:3602–3605
94. Harrison WTA, Vaughey JT, Goshorn JW (1995) J Solid State Chem 116:77–86
95. Zhang SY, Hu CL, Sun CF, Mao JG (2010) Inorg Chem 49:11627–11636
96. Ok KM, Halasyamani PS (2005) Inorg Chem 44:3919–3925
97. Muller-Buschbaum H, Wedel B (1996) Z Naturforsch B51:1411–1414
98. Ok KM, Orzechowski J, Halasyamani PS (2004) Inorg Chem 43:964–968
99. Gu QH, Hu CL, Zhang JH, Mao JG (2011) Dalton Trans 40:2562–2569
100. Ok KM, Zhang L, Halasyamani PS (2003) J Solid State Chem 175:264–271
101. Shen YL, Jiang HL, Xu J, Mao JG, Cheah KW (2005) Inorg Chem 44:9314–9321
102. Jiang HL, Ma E, Mao JG (2007) Inorg Chem 46:7012–7023
103. Zhang SY, Mao JG (2011) Inorg Chem 50:4934–4943
104. Li PX, Zhang SY, Mao JG (2010) Dalton Trans 39:11560–11567
105. Jiang HL, Kong F, Fan Y, Mao JG (2008) Inorg Chem 47:7430–7437
106. Jiang HL, Xie Z, Mao JG (2007) Inorg Chem 46:6495–6501
107. Champarnaud-Mesjard JC, Frit B, Chagraoui A, Tairi A (1996) Z Anorg Allg Chem 622:1907–1912
108. Champarnaud-Mesjard JC, Frit B, Chagraoui A, Tairi A (1996) J Solid State Chem 127:248–255
109. Blanchandin S, Champarnaud-Mesjard JC, Thomas P, Frit B (2000) Solid State Sci 2:223–228
110. Li PX, Kong F, Hu CL, Zhao Na, Mao JG (2010) Inorg Chem 49:5943–5952
111. Kong F, Hu CL, Hu T, Zhou Y, Mao JG (2009) Dalton Trans 38:4962–4970
112. Johnsson M, Törnroos KW, Mila F, Millet P (2000) Chem Mater 12:2853–2857
113. Johnsson M, Lidin S, Törnroos KW, Bürgi HB, Millet P (2004) Angew Chem Int Ed 43:4292–4295

114. Wu HQ, Pan SL, Poeppelmeier KR, Li HY, Jia DZ, Chen ZH, Fan XY, Yang Y, Rondinelli JM, Luo HS (2011) J Am Chem Soc 133:7786–7790
115. Huang YZ, Wu LM, Wu XT, Li LH, Chen L, Zhang YF (2010) J Am Chem Soc 132:12788–12789
116. Kholodkovskaya LN, Dolgikh VA, Popovkin BA (1995) J Solid State Chem 116:406–408
117. Feger CR, Kolis JW (1998) Inorg Chem 37:4046–4051
118. Jiang HL, Mao JG (2006) Inorg Chem 45:717–721
119. Shen YL, Mao JG, Jiang HL (2005) J Solid State Chem 178:2949–2953
120. Jiang HL, Mao JG (2006) Inorg Chem 45:7593–7599
121. Shen YL, Mao JG (2005) Inorg Chem 44:5328–5335
122. Mayer H (1975) Z Kristallogr 141:354–362
123. Mayer H, Weil M (2003) Z Anorg Allg Chem 629:1068–1072
124. Alcock NW, Harrison WD (1982) Acta Crystallogr B38:1809–1811
125. Mayer H, Pupp G (1977) Z Kristallogr 145:321–333
126. Ok KM, Halasyamani PS (2006) J Solid State Chem 179:1345–1350
127. Guesdon A, Raveau B (2000) Chem Mater 12:2239–2243
128. Kong F, Jiang HL, Mao JG (2008) J Solid State Chem 181:263–268

http://www.springer.com/978-3-642-29617-8

Structure-Property Relationships in Non-Linear Optical Crystals I
The UV-Vis Region
Wu, X.-T.; Chen, L. (Eds.)
2012, XIII, 236 p., Hardcover
ISBN: 978-3-642-29617-8